THE EFFECTS OF RADIATION ON THE EXTRACELLULAR MATRIX

Angela Diana

St. Catherine's College

Thesis submitted to the Medical Sciences Division of the University of Oxford in partial fulfilment of the requirements for the degree of Doctor of Philosophy

CRUK/MRC Oxford Institute for Radiation Oncology

Department of Oncology

University of Oxford

Trinity 2019

Word count: 21150

Table of Contents

Abstract

The extracellular matrix (ECM) is a complex meshwork of insoluble fibrillary proteins and signalling factors interacting together to provide architectural and instructional cues to surrounding cells. Alterations in ECM organisation or composition and excessive ECM deposition have been observed in diseases such as fibrosis, cardiovascular diseases and cancer. Due to its complexity, ECM involvement in cancer is still poorly understood, and its role in ionising radiation response is unknown.

We used subcutaneous mouse models of colorectal and pancreatic cancer to investigate the effects of ionising radiation (IR) on tumour microenvironment. In particular, we looked at the effects of radiation on Col5a1, a regulatory fibril-forming collagen that forms heterotypic fibrils with Col1a1. Immunostainings showed that Col5a1 protein expression decreased in irradiated tumours compared with the non-irradiated controls, whereas Col1a1 expression did not change. This result was confirmed by RT-PCR and Western Blot analysis. Using picrosirius red staining, we found that collagen deposition was significantly altered by irradiation. Besides, five collagen structural parameters (alignment, density, width, length and straightness) were analysed using second harmonic generation imaging, a highly specific technology for detection of collagen fibres. Our data indicated a significant decrease in collagen width after irradiation in a pancreatic cancer model, whereas all parameters were significantly changed in the colorectal cancer model. *Col5a1* gene knock-down significantly decreased cell survival upon IR and cell migration as assessed using colony formation assays and 3D-spheroid imaging

To confirm our data, we generated a knockout *Col5a1* KPC cell line and injected it subcutaneously *in vivo* in C57/BL6 mice. The lack of *Col5a1* in the *in vivo* tumour led to a reduction in tumour growth; however, radiation seemed to activate a compensatory effect which refrained the irradiation inhibition effect on tumour growth. *In vitro* migration assay and cell growth assay, results showed a similar pattern.

Col5a1 knock-down and knockout significantly inhibited cell proliferation, inhibited cell migration *in vitro* and inhibited tumour growth *in vivo*. Our data, therefore, present Col5a1 as a possible novel prognostic marker and a potential therapeutic target.

To my family

Acknowledgement

Firstly, I would like to thank my supervisors, Profs. Ruth Muschel and Anderson Ryan and my former supervisor Prof. Emmanouil Fokas for their guidance and support. I am grateful for the valuable opportunity they have given me. It has been a long journey filled with challenges and inspirations. Thanks to them, I grew up both scientifically and personally, learning lessons that will guide and help me in my future career.

I want to thank all the members of Muschel's lab and former Fokas's lab for their scientific help and support during these four years, and for creating a pleasant working environment. In particular, I want to thank those who supported me during dark times, and I now consider more friends than colleagues: Ceren, JianZhou, Jakob and Serena.

I also want to thank the Department and the students of Oncology, being the student representative for one year allowed me to get to know the majority of them and to create some real friendships. In particular, I want to thank Mina and Ioanna for being, together with Giovanna, the first friendly faces in the Department. In the same way, I also want to thank St. Catherine's College and the Catz MCR, which became a second home in Oxford and filled my experience in this city with unforgettable memories.

My love and gratitude also goes to the 'CS': Giovanna, Andrea, Mattia, Virginia and Martin: my family far from home. Having you by my side made a real difference in my daily life, your constant support and your incredible energy and affection just made me go through the darkest times of this PhD. Thanks to you, I never felt alone. In particular, I want to thank Giovanna for being my real 'mate' during these years, without you everything in these four years would have been

merely more miserable. Furthermore, of course, I want to thank Martin for just being exactly who he is, one of the best people I ever met in my life. I am sure we all have a bright future in front of us, and we will never be torn apart.

My gratitude also goes to my family: my mom, my dad and my brother Enzo. I know how difficult it has been for them to let me go. I sincerely appreciate that I never received any kind of pressure or disapproval in any of my life choices. I love you immensely. I also want to thank my old friends who are in Milan or spread around the world, thanks for representing home wherever you are and every time I see you.

Lastly, all of these would not have happened without the funding support from CRUK and the Marie Curie scholarships. In particular, being part of the Marie Curie network enhanced the preciousness of this PhD. I will be forever grateful for the opportunity I had, the memories I made and the people I met thanks to the Radiate network.

Specific Acknowledgement

All works presented in this thesis were completed by the candidate with help for specific procedures from the following colleagues:

Dr Yunhong Cao for CRISPR plasmid cloning

Dr Jianzhou Chen for obtaining *Col5a1* CRISPR knock out cell line

Dr Bostjan Markelc and Dr Jianzhu Chen for tumour inoculation in mice

Prof. Nils Cordes and Dr Wei-Chun Lee from the OncoRay Institute in Dresden, Germany for 3D cell culture techniques.

1 Introduction

1.1 The Extracellular Matrix

The extracellular matrix (ECM) is a complex meshwork of cross-linked proteins that provides the physical scaffolding required to maintain tissue morphology[1]. Together with its structural role, the ECM is of fundamental importance in tissue morphogenesis, differentiation and homeostasis. The composition of the ECM composition is tissue-specific, although the main constituents are water, proteins and polysaccharides. The ECM topology and composition is a result of dynamic and reciprocal dialogue between the various cellular components (e.g. fibroblast, epithelial, adipocyte, endothelial elements)[2]. ECM composition is also markedly heterogeneous (**figure 1**[3]), being composed by fibrillar components, such as collagens, fibronectin and elastin, and non-fibrillar components such as hyaluronan, proteoglycans and glycoproteins including matricellular proteins immersed in the ground substance, an amorphous substance which fills the space between cells and filaments[2].

Different cells, including fibroblasts, epithelial cells, immune cells, endothelial cells, and pericytes, are interconnected by complex networks between the macromolecular components of the ECM and cell surface receptors and matrix effectors. ECM receptors, such as integrins, discoidin domain receptors (DDRs) and syndecans mediate cell adhesion to the ECM[4]. Cell migration through the ECM can be mediated by cytoskeletal coupling to the ECM. By interacting with cell surface-receptors and by binding and sequestration of growth-factors (GFs), the ECM directs fundamental morphological and physiological function to induce signalling pathway activation and modulate gene transcription[5].

ECM is continuously being remodelled, either enzymatically or not enzymatically[6] in a delicate balance between synthesis and degradation. Its molecular components are subjected to several post-translational modifications[2]. ECM remodelling happens in normal conditions in healing wounds. Given the importance of ECM in keeping tissue homeostasis and the complexity of its role, any dysregulation in ECM structure, composition and function can lead to a diseased state such as cancer of fibrosis[7].

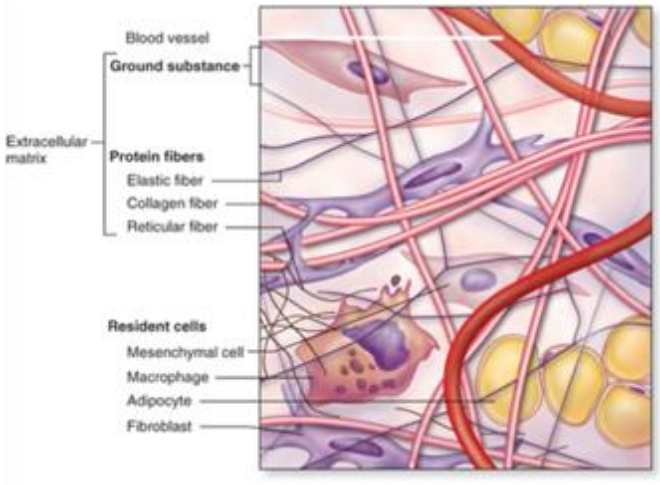

Figure 1: Components of a typical connective tissue. The tissue is composed of cells supported in a mesh-like structure of ECM filled in with ground substance (Copyright McGraw-Hill education[3])

1.1.1 The Extracellular Matrix and TGF-β

Transforming growth factor-β is a member of the transforming growth factor superfamily of cytokines. It has a critical role in many cellular functions including cellular response, cell growth, cell proliferation, cell differentiation and apoptosis. It is also considered a pro-fibrotic factor[8] and regulates the ECM

synthesis. TGF-β is released from platelets and secreted from cells in a biologically inactive and latent form. Before it can bind to its receptor, TGF-β must be first activated[9].

ECM and TGF-β signalling processes are strictly interconnected. The ECM provides storage for latent TGF-β[10]. ECM-mediated signalling is reciprocally influenced by TGF-β[11]. Cellular exposure to TGF-β affects integrin activation and expression; at the same time, TGF-β activation and cellular response is regulated by ECM signalling through integrins[11].

TGF-β expression had been studied in different tumour types, resulting either in a tumour suppressor or tumour promoter. In healthy cells or early-stage tumour types, TGF-β acts to block cell proliferation through SMAD-dependent inhibition of MYC as well as activation of cyclin-dependent kinase inhibitors[12]. In premalignant cells, TGF-β can induce cell apoptosis. In advanced tumours instead, TGF-β-dependent cytotoxic effects are suppressed and EMT-associated cell invasion and metastasis become dominant[13]. In addition, TGF-β can induce a variety of different anti- and pro-tumourigenic effects by acting on stromal cells and stimulating matrix deposition in the cancer microenvironment[14]. The switch between the pro- and anti-tumourigenic phenotype is not well understood yet. TGF-β signalling has been shown to be associated, both in genetically engineered mouse cancer models and endogenously in human disease, with substantial changes in tumour stroma[15,16], as well as with the induction of a mesenchymal phenotype for epithelial cells. In invasive breast cancer, TGF-β expression correlates with an increase in ECM deposition, as long as with other cancer markers such as metastasis and immune cells infiltration[15].

TGF-β signalling forms a complicated network in cancer cells[17].

1.1.1.1 TGF-β and Fibrosis

TGF-β is a leading player in fibrosis. TGF-β is believed to regulate tissue fibrosis as a consequence of pathological ECM accumulation[18]. Carcinomas that overexpress TGF-β commonly display a desmoplastic stromal environment[15,19,20]. TGF-β had been shown to induce myofibroblast differentiation in fibroblasts, which resulted in an increased collagen deposition and ECM remodelling. Transient overexpression of active TGF-β1 using a viral expression alone is sufficient to cause persistent fibrosis in multiple organs, including skin[21], lung[22], and intestine[23]. Hence, TGF-β1 is not only deposited into the ECM but is also perceived by specialized cell receptors as an authentic ECM protein[24]. A significant number of studies have established that integrin binding is the main prerequisite for latent TGF-β1 activation, in particular in conditions of inflammation and fibrosis[25].

1.1.2 The Extracellular Matrix as a Cancer hallmark

The concept that the tumour microenvironment plays a remarkable role in fostering or restraining tumours is now prevalent, but for many years researcher focused on the intrinsic effects of cancer cells, ignoring their surroundings. Immune cells, angiogenesis, oxygen tension, interstitial pressure, ECM remodelling and tumour metabolite components of the TME have received recent attention as essential determinants of cancer cell behaviour and disease progression. A significant component of the TME is the ECM. The ECM is tightly regulated during embryonic development and tissue homeostasis but is commonly disorganised in cancer[26]. The ECM regulates cancer progression both

directly, by promoting cellular transformation and metastasis, and indirectly by promoting the generation of a tumorigenic environment through deregulation of stromal cells behaviour and facilitating tumour-associated angiogenesis and inflammation[27].

Within the tumour stroma, different cell types, including both cancer cells and resident fibroblasts, which differentiate in CAFs, have a role in modifying the ECM[28]. It is well recognised that fibroblasts are the primary source of most of the structural collagens in the ECM, whereas tumour cells synthesize many of the proteoglycans and other linking proteins such as laminins and fibronectin.

In 2012 *Hynes et al*[28] confirmed that both tumour and stromal cells contribute to the composition of the ECM of tumours using a proteomics-based analysis paired with a bioinformatic definition of the 'matrisome' (ECM and ECM-associated proteins) to analyse the protein composition of lung and colon both in cancer, metastasis and normal tissue *in vivo* xenografts by determining which proteins were murine and which human. The analysis of over a hundred ECM proteins showed that the matrisome components secreted by tumour cells vary significantly accordingly with the metastatic potential of the analysed cell line[28,29]. Another study identified the tumour microenvironment molecular signature in normal breast tissue and invasive breast cancer by analysing the differences in gene expression between stromal and epithelial cells was performed by *Casey et al*[30]. Then suggested that aggressive and metastatic cancer cell lines produced ECM components such as collagens, fibronectin, laminin, and so on[30].

Cancer cells can modify the environment secreting ECM components and ECM-modifying enzymes. LOX gene encoding is induced by intra-tumoral

hypoxia and LOX-mediated collagen and elastin cross-linking leads to ECM stiffening, which may enhance tumour migration in hypoxic conditions[31].

Activated fibroblasts in the tumour microenvironment, also called CAFs (cancer cell associated fibroblasts), constitutes the majority of the tumour stroma together with macrophages. Cancer cells drive CAFs to produce and deposit an abnormal amount of ECM components altering the ECM composition, both qualitatively and quantitatively. As a consequence, the ECM of the primary tumour site changes dramatically compared to physiological conditions. Cancer cells hijack fibroblast functions usually associated with wound healing to promote disease progression. Tumour cell accumulation within the tissue can trigger a chronic wound healing response from normal fibroblasts, starting a process which leads to a desmoplastic tissue environment due to ECM aberrant remodelling and increased stiffness [32]. Other important key players in mediation of cancer cell plasticity are Tumour-associated macrophages (TAMs), Tumour-associated neutrophils (TANs), Cancer-associated adipocytes (CAAs) and Tumour-infiltrating lymphocytes (TILs).

Deregulated ECM dynamics such as increased tissue stiffness and desmoplasia, as well as breaching the basement membrane are hallmarks of cancer[33].

1.1.3 The ECM role in colorectal cancer

Colorectal cancer is a major cause of death in Western countries with an average five years survival rate of 67%[34]. Early detection and prevention led to a steady decrease in the number of deaths due to colorectal cancer in the last two decades. Despite this relatively high survival rate, because of the high frequency of colon cancer, many deaths result. There is a high risk of death in the later

stages, especially in the event of metastasis to the liver in which the majority of patients fail to respond to treatment[35]. Growing interest is now on the role played by the tumour microenvironment in cancer progression, to tackle the problem of failure to treat metastasis. In 2014, *Fang et al*[29] pointed out how ECM, collagen, in particular, is involved in tumour progression and can play both a positive or negative role, either inhibiting or promoting cancer progression at different stages of cancer development. The ECM could either behave as a barrier to drug delivery, conferring chemoresistance to cancer [29] or act as a protective factor for survival in patient with colorectal carcinoma[36].

During cancer cell growth, many cancers exhibit different grades of desmoplasia. With this term is indicated the unorganised production of fibrous or connective tissue composed mainly of myofibroblasts and collagen fibres. Similarly, in colon cancer, during tumour progression, collagen fibres become thicker and disaligned[37,38]. The presence of more dense and ordered collagen fibres in the colon tumour samples suggests that collagen has a pivotal role in malignant transformation[38].

1.1.4 **The ECM role in pancreatic cancer**

Pancreatic ductal adenocarcinoma (PDAC) is the fourth cause of cancer death worldwide and is predicted to become the second cause of death related to cancer by 2030[39]. PDAC is characterized by a five years survival rate of 5%. Despite advances in cancer therapy, treatment outcome for PDAC patients remains unsatisfactory.

Pancreatic cancers progress with a desmoplastic reaction characterized by an excessive ECM deposition and recruitment and activation of CAFs, associated with altered immune-surveillance and depleted vasculature. This

stromal remodelling alter the interactions between tumour cells and stromal compartments, which could promote disease progression. In addition, PDAC fibrosis compromises drug delivery increasing resistance to therapy. Nevertheless, benefit from anti-stromal therapies remains uncertain. *In vivo* experiments targeting the SHH pathway were shown to significantly reduce fibrosis and increase drug uptake transiently stabilizing the disease[40].

Similarly, it was shown that using hyaluronidase to reduce the abundance of hyaluronan in tumour stroma and reduce tissue tension in a xenograft human pancreatic cancer with an angiotensin inhibitor reduce tissue tension facilitating drug delivery. Unfortunately, the attempted translation of these findings into phase 2 clinical trials targeting fibrosis did not increase patient survival[41]. Data from mouse models of PDAC revealed that, even after reduction in fibrosis by depletion of proliferating α-sma positive stromal cells, there was no improvement on mortality, while the vasculature remained abnormal and tumours remained hypoxic and even less differentiated[41]. Another study targeting fibrosis through inhibition or genetic ablation of SHH resulted in a less differentiated and more aggressive tumour. These data imply that the stroma can both promote and restrain tumour progression. It was recently shown that ECM remodelling does not occur evenly throughout the tumour, but that it was heterogenous and spatially defined within pancreatic tumours[42].

Stromal cells such as CAFs are predominantly mediating ECM remodelling. However, cancer cells can activate signalling pathways that regulate survival and metastasis in pancreatic cancer[43]. Similarly, increase stiffening of the ECM could promote the epithelial to mesenchymal transition in pancreatic tumour, and reduce pancreatic cancer response to chemotherapy[39].

1.1.5 Collagen

1.1.5.1 Collagen Structure:

Collagens constitute the main structural element of the ECM and are the most abundant fibrous proteins within the interstitial ECM constituting up to 30% of total protein mass of a multicellular animal.

Collagen consists of three polypeptide chains named α-chains. Size of these α-chains can vary from 662 (human α1(X)) to 3152 (human α3 (VI)). They can be either be identical to form homotrimers (e.g. Collagen II, III, VII, VIII, X) or different to form heterotrimers (e.g. Collagen I, IV, V, VI, IX and XI)[44]. The α-chains contain a rod-like domain of varying length with a glycine each third residue. The three α-chains of fibril forming collagens are twisted in a triple helix with a one-residue stagger between adjacent α-chains. The triple helix is the common structure motif in collagen molecules and is also called Collagen domain (COL).

At this time, the collagen family comprises 28 members numbered with Roman numerals in vertebrates (I-XXVIII). There are several isoforms for the same collagen type (e.g. Collagen IV and VI) and hybrid isoforms comprised of α-chains belonging to two different collagen types (e.g. Collagen Va1/XI).

1.1.5.2 Collagen binding receptors:

Collagens regulate cell adhesion, provide tensile strength, support chemotaxis and migration, and direct tissue development through the binding of their cell receptors[5]. Several collagens such as Collagen 5a1, referred to as ‘minor’ collagens, have been proved to be crucial for tissue integrity despite being of low abundance.

In order to fulfil its biological role, collagen interacts with different molecules. In their review *An et al*[45] schematised the classes of molecules the three major fibrillar Collagens (type I, II and III) interact with in an interactome-type network diagram (**Figure 2**), including different cell-surface receptors and other ECM proteins.

There are three main collagen receptor families: collagen-binding integrins[46], collagen-binding immune receptors and discoidin domain receptors[47] (DDR1 and DDR2). The largest family of receptors involved in mediating cell adhesion to fibronectin, laminins and collagens are the integrins. Integrins are heterodimeric transmembrane glycoprotein receptors. Collagen binding integrins are $\alpha1\beta1$, $\alpha2\beta1$, $\alpha10\beta1$ and $\alpha11\beta1$[46].

Under pathological conditions, such as inflammation, tissue regeneration and tumours, this class of integrins play a prominent role. Integrin $\alpha1\beta1$ and $\alpha2\beta1$ are involved in the innate immune response[48]. Recent data suggest that $\alpha11\beta$ is an important collagen receptor for collagen remodelling on activated fibroblasts in wound healing, fibrosis and in tumour stroma[49].

DDRs are kinase receptors which bind the main collagens (I, II and III) and upon binding to collagen, DDRs are involved in cell adhesion, proliferation, differentiation and matrix remodelling[46,47,50].

Among the collagen-binding immune-receptors, Glycoprotein VI regulates platelets during thrombosis[51]. Another important receptor is LAIR-1 which works as inhibition signal for most of the immune cells. The binding with collagen inhibits LAIR-1 function[52,53].

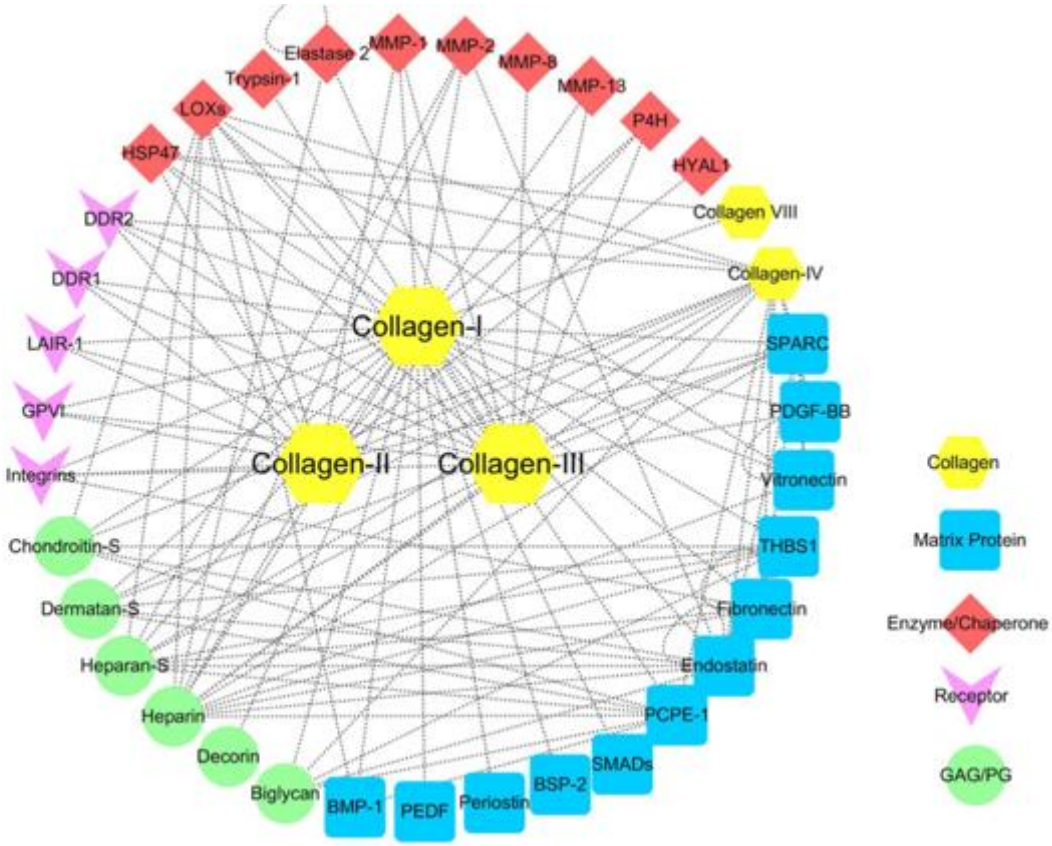

Figure 2: *An et al*[45] representation of the three major fibrillar collagens interaction network. Representative examples of each class collagens interacts with are plotted with Cytoscape 3.2.1 based on multiple sources including MatrixDB.

1.1.5.3 Collagen biosynthesis:

Collagen is synthetized and assembled according to the canonical normal pathway for a secreted protein. Collagen chains are synthetized as long chains called pro-collagens, and subsequently they are co-translationally transported into the lumen of the rough endoplasmic reticulum (ER). Here and in the Golgi complex, the procollagen chain is glycosylated. Glucose and galactose residues are added to hydroxylysine residues and at the same time oligosaccharides are added to asparagine residue in the C-terminal propeptide, a segment of the

procollagen molecule that is absent in the mature collagen. Next specific proline and lysine residues are hydroxylated. Finally, before the triple helix forms, the three chains are aligned using disulphide bonds between the terminal N- and C-propeptide sequences. The triple helix is now formed[54].

The tropocollagen molecule is then secreted into the extracellular space. N-terminal and C-terminal pro-peptides are removed by the procollagen peptidases during or following exocytosis. The protein now consists almost entirely of a triple-stranded helix. The excision of the pro-peptides allows the collagen molecules to polymerize into collagen fibrils in the extracellular space[54].

Stromal fibroblasts transcribe and secret the bulk of interstitial collagen. Collagen fibrils are organized into sheets and cables by fibroblasts exerting tension on the matrix[55].

1.1.5.4 Collagen degradation:

Collagen degradation is tightly regulated in physiological conditions and represents a very important process in development, morphogenesis, tissue remodelling and repair. Its dysregulation is involved in different diseases such as cancer, fibrosis, chronic ulcers, rheumatoid arthritis, nephritis. One major class of proteases involved in collagen degradation are the metalloproteinase (MMPs). MMPs can be categorized into five main subgroups based on their substrate specificity and structure: collagenases (MMP-1, MMP-8 and MMP-13), gelatinases (MMP-2 and MMP-9), stromelysins (MMP-3, MMP-10 and MMP-11), matrilysins (MMP-7 and MMP-26) and MT-MMPs (MMP-14, MMP-15 and MMP-16)[56]. Of interest for us are gelatinases MMP-2 and MMP-9 since they are able to digest a number of ECM components such as collagen type I, IV and V[56,57]. Furthermore these two proteases have been found upregulated in fibrosis and

their upregulation has been associated with tumour aggressiveness, metastatic potential and poor prognosis.

MMP-2 is considered to play an important role in metastasis. Among the various stimuli which stimulate MMP-2 synthesis and secretion there are cytokines. Produced during tumour invasion, atherosclerosis and inflammation. Enhanced expression of MMP-2 in cancer cells has been found in relation with a lower survival of patients with CRC[58].

MMP9 is also associated with metastasis and widely expressed in various tumours and associated with poor disease prognosis in oral and gastric cancer, breast cancer, non-small lung cancer, colorectal cancer and osteosarcoma[59].

1.1.6 **Collagen in tumours**

Collagen in the tumour microenvironment produce biochemical signals which are sensed both by cancer and stromal cells, triggering a cascade of biological events. As we already discussed the ECM goes under structural changes during tumour invasion. Remodelling of the ECM includes morphological changes characterized by linearization of collagens fibres at the tumour invasion front, with significant impacts on tumour cell biology including gene expression, cell differentiation, proliferation, migration and responses to treatments. Studies conducted on breast cancer showed a correlation between breast density and breast cancer risk[60,61]. In normal conditions, collagen fibres were typically curly and smooth in the epithelial breast tissue. When tumour progressed the fibres thickened, linearized and stiffened, promoting the cell invasion in the ECM and metastasis. Intravital imaging showed that collagen fibres linearized were used as ‘highways’ from breast cancer cells and leucocytes to rapidly migrate[62].

In the appropriate context, the ECM is enough to restrain malignant tumour progression. At the same time, ECM can also promote tumour progression. For example, Collagen IV overexpression can enhance cell survival and metastatic potential for lung cancer cells in liver[63].

1.1.7 Collagen 5a1 is a minor constituent of the ECM

Collagen 5a1 is a relative minor member of the ECM and a component of the fibril subclass of collagens[64]. It is involved in the regulation of fibril assembly[65,66]. It co-assembles with type I collagen and regulates the assembly and lateral growth of the type I collagen fibrils. In 2004, Wenstrup et al[65] generated a *Col5a1* knockout mouse model. The mouse model with homozygous *Col5a1* gene target deletion was embryonic lethal; it did not develop past early organogenesis and mice were characterised by a virtual absence of collagen fibrils. Interestingly mice with a Col5a1-/+ genotype survived normally but phenotypically resembled people with the Ehlers/Syndrome[67] and these mice have half the number of fibrils than their wild type littermates[65]. Collagen type I gene expression was not affected by *Col5a1* deletion. These data suggested that collagen 5a1 has an essential role in collagen fibril initiation. These observations have been confirmed using a conditional *col5a1* gene knock out model by *Sun et al*[66].

Several isoforms of Collagen 5a1 exist, which differ in the type and ratio of constituent chains. The most widely distributed and more abundant are α1(V) and α2(V), forming heterotypic fibrils with Collagen I[64]. Collagen 5a1 is normally present in the ECM of tissues that express Collagen I. Different studies investigating how changes in the Collagen 5a1/1a1 ratio regulates fibril formation *in vitro* fibril assembly experiments[68], *in vivo*[69] and in patients[70], have led to the hypothesis that Col5a1 serves as a negative regulator of collagen fibril diameter,

but is critical for fibre formation. Collagen 5a1 distribution, similar to other collagens, is tissue-specific, possibly related to the tissue functions. It is present in most connective tissue matrices, especially tendons, skins and cornea, and is multifunctional in health, disease, and fibrosis[64].

The role of 5a1 collagen in the organization and biological properties of collagen ECM is still poorly understood.

1.1.8 **Collagen 5a1 in Cancer and Fibrosis**

Although is a minor constituent of the ECM in healthy humans, COL5A1 is highly expressed in cancer, wound repair, chronic inflammation, and fibrogenesis.

The induction of skin tumours, by the tumour promoter 12-O-tetradecanoyl-phorbol-13 acetate (TPA), in mice is associated with an increase of the relative content of Collagen 5a1 in the dermis and a lack of change in the levels of Collagen I and III[71]. This led to the hypothesis that Col5 disturbed the interactions between the dermis and epidermis facilitating tumour development.

In pancreatic ductal adenocarcinoma, Collagen 5a1 expressed by pancreatic stellate cells affects the malignant phenotype of several pancreatic cancer cell lines promoting adhesion, migration and viability. The inhibition of β1-integrin, a component of a Collagen 5a1 receptor abolished Collagen 5a1-induced effects on pancreatic cancer cells, identifying the B1-integrin/FAK signalling pathway as an important mediator of Collagen 5 effects on tumour cells[72].

In colorectal cancer, a study showed upregulation of collagen 5a1, as well as of Col1a1 and Col4a1 *in vivo*. *In vitro* studies showed that direct cell-cell contact between fibroblasts and colorectal cancer cells leads to an increase in

ECM density, composed of unorganised collagens, including Col5a1, and proteoglycans[73].

Furthermore, *COL5A1* has been identified as a biomarker of human gastric cancer using gene expression profiling[74] and RNA-sequencing has revealed that it is associated with the ECM degradation pathways in papillary thyroid carcinoma[75]. However, the possible role of *Col5a1* in radiation responses has not been studied.

1.2 Radiotherapy

Radiotherapy is one of the most common treatments in cancer therapy. It is used to treat up to 50% of all cancer patients and as an adjuvant treatment in 40% of the patients who undergo surgery.

The essential principle of cancer radiotherapy is to kill cancer cells sparing normal tissues. It is important because IR has a double nature: given at high doses is able to kill tumours or stop or slow tumour growth but can impair tissues such as the intestine, liver, lungs and haematopoetic tissue of the bone marrow. Long term there is a small chance that it could increase an individual's risk of developing cancer. The use of radiation therapy in the clinic is designed to target the tumour while sparing the normal tissue. Giving the tumour the highest dose while reducing the dose to the surrounding tissues is achieved partly by taking into account the IR physical properties and using available techniques which direct an elevated IR dose to a limited area sparing the surrounding tissues to a large extent. Modern RT techniques deliver radical or high IR doses to tumour target in precise and accurate doses, while reducing IR doses to the surrounding

normal tissues. This has led to significant reduction of radiation-induced toxicities and improvement on local-regional tumour control in some cancer types[76].

Exposure of cells to IR induces DNA damage with double-strand breaks being the main lethal lesion. This DNA damage activates DNA damage - induced stress response. Target proteins, which primary function is to facilitate DNA repair and prevent the proliferation of damaged cells (checkpoint blockade) are activated or repressed after IR[77]. Similarly, IR activates a damage response at the tissue level. Multicellular programmes are activated and executed by soluble signals such as chemokines, cytokines and growth factors, which modulate cell behaviour.

To sum up cancer is a leading cause of death globally, radiotherapy plays an important role in cancer treatment. Owing to the development of radiation physics and imaging techniques, modern RT has made a significant progress in tumour treatment and normal tissue preservation. Anyhow, there are still emerging and unmet needs including the role of tumour microenvironment in the radiation response in order to further improve radiotherapy efficiency. Emerging data suggests that tumour microenvironment has a fundamental role in modulating radiation response both locally and systemically[78]. A better understand of the tumour microenvironment role in radiation therapy may help improve the therapeutic efficiency of RT. Very little is known about the immediate, such as within one week, response of the ECM to radiation.

1.2.1 **The effects of radiation on the ECM**

Radiotherapy is widely used in cancer therapy as a method to cause cell death through DNA damage. At times considerably distant from the radiation, many months to years, extensive pathological fibrosis may occur especially noted

in the heart, skin, lungs, kidneys, gastrointestinal tract and liver[79] leading to impaired organ function.

Radiation cytotoxic effects are thought to be exerted through DNA damage and direct induction of ROS, but it has been demonstrated that the radiation effect on a single cell can be propagated to neighbour cells that have not been exposed to irradiation. This effect can be observed both in adjacent cells[80] or in cells located up to 1 mm distance[81]. In addition, radiation damage may be transmitted through culture medium from an irradiated cell population to a separated unirradiated one, suggesting that the damage signal is diffusable[82]. This effect is called bystander effect and is highly dependent on cell type and radiation rate exposure, therefore the biological outcome is variable.

Giannopolou et al.[83] used a CAM model to show that 48 hours after irradiation the gene expression of the majority of the studied ECM proteins, increased. Using this model they speculated that X-rays induced an early apoptosis of CAM cells through angiogenesis-related ECM proteins synthesis modulation and deposition regulated by tumour cells[83]. These findings confirmed previous studies showing that radiation increased the gene expression, as well as the turn-over and cross-linking of collagens[84].

Radiation can also modulate cancer cell response and inhibition of Integrin-ECM interactions. Inhibition of integrin signalling induces selective apoptosis in malignant cells enhancing the radiation tumouricidal effect[85]. Integrin-ECM signalling is an important component of radiation response both *in vitro* and *in vivo*[86]. The mechanism is not fully understood, however it is thought that radiation induces changes in integrin signalling predisposing cells to metastasis in recurrent diseases[87].

In 2018, *Miller et al*[88] described the effects of ionizing radiation on ECM stiffness. Interestingly, they discovered that ionizing radiation can reduce stiffness of a 3D collagen matrix without collagen denaturation but through the cleavage of C-C and C-N peptide bones in the backbone of the collagen protein. Reduction in stiffness of a 3D collagen matrix through radiation also alter cell behaviour, causing a decreased adhesion, spreading and migration[88]. They did not find any difference between fractionated and single dose, suggesting that the effects on ECM stiffness are dose but not rate dependent.

1.2.2 **Fibrosis**

Fibrosis is a pathological condition generated by an excessive ECM production and deposition. It may follow chronic or severe tissue injuries, and it represents one of the main side effects in radiation therapy treatment[89]. Pathological fibrosis can lead to organ failure and it has also been reported to increase the risk of cancer. For example in breast an increased mammographic density, which represents the amount of collagen in breast, is correlated with a high risk of developing breast cancer[90]. Interestingly, *Parker et al* showed that a fibrotic ECM can induce fibroblasts to further increase ECM production[91]. Isolated ECM from patients with or without idiopathic pulmonary fibrosis (IPF) was co-cultured with both IPF and non-IPF fibroblasts *in vitro*. intriguingly the IPF derived ECM promoted ECM production in both IPF and non-IPF fibroblasts, by downregulating miR-29, which regulates the expression of many ECM genes[91]. This experiment suggests that the ECM origin had a greater effect on gene expression than the fibroblast origin.

1.2.2.1 Radiation-induced fibrosis

Radiation-induced fibrosis (RIF) is usually a late effect of radiotherapy and may be seen in skin[92], the lungs[93–95], the gastrointestinal[96–98] and genitourinary tracts, muscle and other organs. It can cause functional impairment which can lead to death or to a significant decrease in the quality of life. There may be a genetic component for predisposition to RIF. Radiation tissue injury triggers the inflammation and induces the transformation from fibroblasts to myofibroblasts. These myofibroblasts proliferate excessively, and at the same time produce abnormal amounts of collagen and other ECM components. TGF-β is a major mediator of fibrosis[99].

Overall, these studies show that the ECM actively participates in stimulating further ECM synthesis and therefore in the fibrotic process development. A better understanding of the radiation effects on ECM composition and function before fibrosis arises could be helpful in improve radiotherapy efficiency.

1.2.2.2 Fibrosis Animal Model

The use of different scoring systems for radiation induced fibrosis limits comparability among different studies. However, it is difficult to establish a fixed radiation dose since RIF depends from different factors such as radiation dose, irradiated organ, origin of injected tumour cells, and so on as illustrated in figure 3.

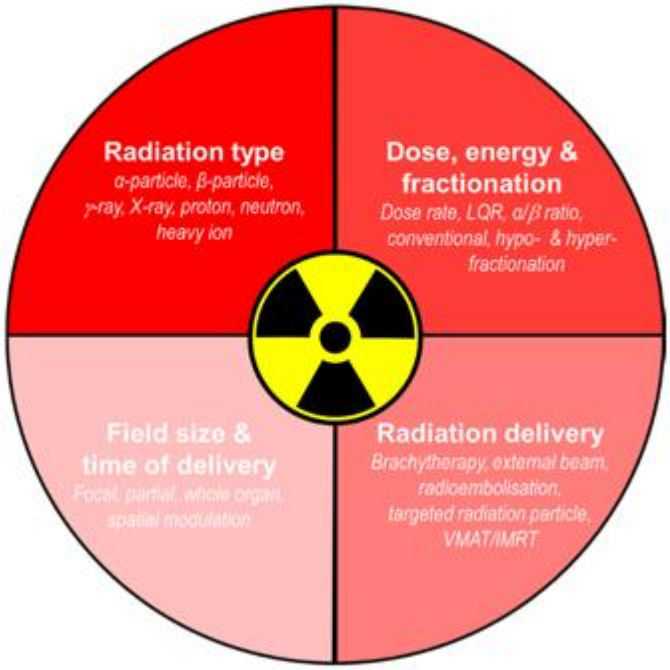

Figure 3: *McKelvey et al*[100] Aspects of radiation delivery that modulate the inflammatory/ immune response including fibrosis.

Different methods have been proposed in different cancer models in the study of fibrosis. For example *Pan et al*, established a pulmonary fibrotic model exposing C57BL/6 mice to a single dose of 17 Gy on the right side of the thorax and lung fibrosis was evaluated 3 weeks after the radiation treatment[101]. *Groves et al* instead exposed C57BL/6 mice to a single thoracic radiation dose of 12.5 Gy, and noticed fibrosis 6 weeks after irradiation[102].

Recently, *Bull et al* suggested a new model for radiation induced fibrosis in the gut. Mice were irradiated form 2 up to 4 fractions dose of 6 Gy or 8 Gy per day. They were culled 6 weeks post irradiation and all showed fibrosis[103]. However, they were able to reduce the number of irradiation doses thanks to a precise irradiator which hit precisely a radiation field of 3 x 3 cm^2.

In summary, all RIF mouse models in literature are characterised by an administration of high doses of radiation, with a minimum of 12.5 Gy, and a post irradiation phase of at least 3 weeks. Fibrosis is evaluated on morphological parameters and ECM protein abundancy.

1.3 Research objectives:

This project consist of two parts. The first part aimed to investigate the effects of irradiation on the ECM with a particular attention to Collagen 5a1 expression and changes in collagen deposition (Chapter 3). The second part focused on determining the role of Collagen 5a1 on cell migration, radio-resistance, collagen deposition and organisation (Chapter 4).

It is well established Col5a1 has a key role in tumour progression and in fibrosis. However, there are some critical questions that need to be addressed, including its role in radiation response.

To study the effects of radiation on Col5a1 expression we used a subcutaneous tumour animal model. Tumours were irradiated when they reached a volume of 100 mm^3. We then analysed the effects of radiation on Col5a1, Col1a1 and a-sma expression mainly by immunohistochemistry. In order to understand what led to the decrease of Col5a1 we investigated the gene regulation both *in vivo* and *in vitro* through RT-PCR and the presence or activation of two matrix-metallo proteinases, MMP2 and MMP9, known to cleave and degrade Col5a1.

We observed the effects of radiation on collagen organisation using Red Picrosirius Staining and SHG imaging. Using the software Ct-fire we were able to quantify collagen parameters, such as length, width, angle and alignment.

We subsequently tried to understand the role of Col5a1 in tumour progression and radiation-response by partially, siRNA, or completely, CRISPR/Cas9, downregulating Col5a1 expression in KPC tumour cells.

We investigated the effects of downregulated Col5a1 *in vitro* using 3D and 2D techniques. We looked at the effects that partial or complete downregulation

of Col5a1 had on migration through a spheroid migration assay, tumour growth through sphere assay, MTT analysis and cell counting, radio-resistance through CFA.

We injected Col5a1 KO KPC cells, obtained through CRISPR/Cas9, subcutaneously in mice. We subsequently evaluated the effects of radiation on Col5a1 expression and collagen organisation *in vivo* using immunohistochemistry, red picrosirius staining and SHG.

2 MATERIALS AND METHODS

2.1 Cell lines and cell culture

MC38 (murine colon cancer), KPC (murine pancreatic adenocarcinoma), and PANC-1 (human pancreatic carcinoma) cell lines were originally obtained from American Type Culture Collection (ATCC).

MC38, KPC and PANC-1 were cultured in DMEM with 10% fetal bovine serum (FBS) and Penicillin/Streptomycin (100 I.U./mL).

All cells were grown in a sterile incubator (Blinder) with 5% CO_2 at 37°C. Cells were used at 80% of confluency and kept for no more than 10 passages.

All cell culture experiments were performed under sterile conditions in a laminar flood hood.

2.2 Reagents

2.2.1 Antibodies

Table 1: Primary and Secondary antibodies in immunoblotting and staining

Antibody	Clonality	Supplier	Catalog Number	Dilution W.B.	Dilution IF
Rabbit anti-mouse Col5-α1	Polyclonal	Santa Cruz	Sc-20648	1:500	1:100
Rabbit anti-mouse Col5-α1	Polyclonal	Invitrogen	PA5-23989	/	1:100
Rabbit anti-mouse Col1-α1	Polyclonal	Abcam	Ab43710	/	1:100
Goat anti-mouse MMP-9	Polyclonal	R&D System	AF909	1:100	/
Rabbit anti-mouse α-SMA	Polyclonal	Abcam	Ab-5694	/	1:100
Rabbit anti-mouse β-actin	Monoclonal	Abcam	4970s	1:1000	/
Goat anti-rabbit Alexa Fluor 488	Polyclonal	Life Technologies	A-11008	/	1:1000
Rabbit IgG	Polyclonal	Abcam	Ab172730	/	1:100
Goat anti-rabbit IgG HRP	Polyclonal	Invitrogen	#31466	1:5000	/
Donkey anti-goat IgG HRP	Polyclonal	Invitrogen	#A15999	1:1000	/

2.3 Irradiation in tissue culture

Cells were seeded in 6-well plates with a density of 0.5-5 x 10_4 cells/cm_2 and maintained at 37°C with 5% of CO_2. Four hours later, cells were treated with gamma-rays at indicated time points. Gamma-rays treatment was delivered using a 137Cs-laboratory Irradiator (IBL 637, CIS bio International, Saclay, France) which produces gamma-rays (0.662 MeV) at a dose rate of 0.81 Gy/minute.

2.4 Transient gene knock down using siRNA

To knock down Col5a1 we utilized scrambled or Col5-a1-siRNAs obtained from Sigma. Transfection was carried out using Lipofectamin 3000 (Invitrogen). Cells were seeded in a 6 well plate. When the cultured cells reached a density of 40-50%, they were treated with siRNA/lipofectamin 3000 complexes (20 nM) in 800 μL of Opti-MEM (Invitrogen) without serum for 48 hours, after this period cells were used for the experiments. Three different siRNAs were tested, and the most efficient was selected.

The knock down efficiency was tested by Real-Time PCR.

Table 2: siRNA list

		Targeted exon	**siRNA location**	**Species**
COL5A1	A	3	693	Mouse
COL5A1	B	2	306	Mouse
COL5A1	C	7	1269	Mouse
Nt-COL5A1	nt	Non targeting		Mouse

2.5 Generation of knock out cell line using CRISPR

2.5.1 CRISPR Plasmid Cloning

Gene knock out cell lines were generated using the CRISPR technique.

gRNA primers were designed using Feng Zhang lab's[104] CRISPR design (http://crispr.mit.edu/) and cloned into plasmid PX701 and PX702 by Dr Yun Hong Cao respectively according to a published protocol. Briefly, plasmids were digested with BpiI (ThermoFisher) and purified using GFX™ PCR DNA and Gel Band Purification Kit (GE Healthcare, Chicago, USA). The pair of gRNA oligos were phosphorylated, annealed and ligated with the digested plasmids. The ligation reaction was then treated with Plasmid-safe ATP-Dependent DNase (Cambio Ltd, Cambridge, UK) to prevent recombination products. The plasmid cloning was verified by sequencing.

2.5.2 Plasmid Transfection and Generation of Single Cell Clones

We used the transfection protocol of Dr Jianzhou Chen. Briefly, cells were transfected with PX701-gRNA-1 and PX702-gRNA-2 plasmids simultaneously using Lipofectamine® 3000 Transfection Reagent (ThermoFisher). A total number of $0.5x10^5$ cancer cells were seeded in 12-well plate and maintained in the incubator. After twenty-four hours, the following reagents mixture were prepared: (1) Lipofectamine 3000 dilution: Opti-MEM medium (ThermoFisher) 150 μL + Lipofectamin 3000 4 μL; (2) Master mix of DNA: Opti-MEM medium 150 μL + PX701-gRNA-1 1 μg + PX702-gRNA-2 1 μg + p3000 reagent 4 μL. After mixing well, the master mix of DNA was added to diluted Lipofectamin 3000 reagent and incubated at room temperature for 15 minutes. The DNA-lipofectamin complex was added to the cells and returned to the incubator for 24

hours. Following transfection, cells were washed with PBS and cultured with medium containing 1.5 μg/mL of puromycin for 24-48 hours to select transfected cells. Cells which remained alive after selection were proceeded to generate single clones via serial dilution (0.5 cells per well in 96-well plates). Single cell clones with gene knock out were selected and validated using RT-PCR.

2.6 RT-qPCR

2.6.1 RNA Isolation

RNA was extracted from cells and tissues using Trizol (Sigma-Aldrich). All RNA were dissolved in RNAase-free water and stored at -80C.

In general, a total amount of 5-50 ug of RNA was yielded from each sample in this study. Their quality and quantity were measured using a NanoDrop 2000 microvolume spectrophotometer (Thermo Fisher). RNA samples with the ratio of absorbance at 260 and 280 nm (A260/280) > 1.8 and A260/230 > 2.0 were proceeded to subsequent analysis.

2.6.2 DNase treatment and cDNA synthesis

All RNAs were treated with DNAse prior to the cDNA synthesis using Turbo DNA-freeTM Kit (Life technologies). Approximately 2 μg of RNA for each sample was transcribed into cDNA using the High-Capacity cDNA Reverse Transcription Kit (Thermo Fisher).

2.6.3 qPCR

qPCR was performed using SYBR-GREEN (Invitrogen) with specific primers. Reactions were run on a Mx3005p (Agilent Technologies, Santa Clara,

CA, USA) in a final volume of 25 μL with cDNA equivalent of 10 ng RNA and 2 μmol/L of primers. The cycling conditions were as follow: 95 C for 15s, followed by 40 cycles of 95°C for 5 s and 60 °C for 30 s.

Following amplification, the threshold cycle (Ct) values for target genes and reference genes were recorded. The fold induction was calculated using the ΔΔCt method. Firstly, difference of Ct values, ΔCt, between the target gene and reference gene was calculated. Then, the difference of ΔCt (ΔΔCt) between the experimental sample and control sample was calculated. The mRNA fold induction of the target gene in the experimental sample and control sample was calculated. The mRNA fold induction of the target gene in the experimental samples was then equal to $2^{(-\Delta\Delta Ct)}$.

2.6.4 **Quality Control of qPCR**

The following controls were used in this study: non-enzyme control (excluding reverse transcriptase in the step of cDNA synthesis) for each sample and non-target control (excluding cDNA in the step of PCR reaction) for each pair of primers. The Ct values of all controls in this study were > 35. All genes we investigated in this study displayed single peak on melting curve analysis after the amplification of qPCR. Their specificity were further validated by gel electrophoresis of qPCR products.

Table 3: Primers for RT-qPCR

Oligo Name		Sequence (5'-3')	Base Count	Annealing Temperature	Species
mCol5a1#F	Forward	CTTCGCCGCTACTCCTGTTC	20	66.10	Mouse
mCol5a1#R	Reverse	CCCTGAGGGCAAATTGTGAAAA	22	68.80	Mouse
mBactin#F	Forward	GAGCTACGAGCTGCCTGACG	20	49.0	Mouse
mBactin#R	Reverse	GTAGTTTCGTGGATGCCACAG	21	49.6	Mouse

2.7 Immunoblotting

2.7.1 **ECM-extract Preparation**

Treated tumours were harvested 6 days after the end of the irradiation treatment (unless otherwise specified) whereas untreated tumours were harvested when their tumour reached a volume. Tumours were immediately placed in a p6 well with decellularization buffer containing 0.1% SDS, 0.01% NH4OH in H2O. The well plate was put on rotary shaker for at least 72 hours, until when the tumours became visibly softer. Buffer was changed twice a day. Decellularised tumours were cut in 100 mg pieces (wet weight), aliquoted into 200 μL of ice cold buffer C (Hepes, MgCl2, KCl, EDTA, Sucrose, Glycerol, Sodium OrthoVanadate, Protease Inhibitor Cocktail) of the CNCMS Compartmental Protein Extraction Kit (BioChain Institute, Inc), snap frozen and kept at -20°C until enrichment. The protocol used was estabilished by Dr Arseney Yuzhalin.

2.7.2 **ECM Enrichment**

Frozen ECM samples were homogenized using the Tissue-Tearor tissue homogenizer (BioSpec Products, Inc) for 20 seconds. Samples were then glycosylated with 3000-4000 units of PNGase F (New England BioLabs, Ipswich, MA) and remaining nucleid acids were removed by adding 1 μL of Benzonase® nuclease (Sigma, St Louis, MO) for 1 h at 4°C. The samples were then spun down at 18000 g for 20 min. ECM enrichment was performed accordingly with the CNCMS Compartmental Protein Extraction Kit (Biochain Institute, Inc) protocol. Briefly the supernatant was discarded and the pellet was washed in 400 μL of ice cold buffer W (HEPES (pH7.9), MgCl2, KCl, EDTA, Sucrose, Glycerol, Sodium OrthoVanadate) at 4°C for 5 minutes. Protein extract was spun down at 18000g for 20 minutes and supernatant was discarded. The pellet was resuspended in 400 µl of ice cold buffer W (HEPES (pH7.9), MgCl2, KCl, EDTA, Sucrose, Glycerol, Sodium OrthoVanadate) at 4˚C for 5 min. The washed protein extract was spun down at 18000 g for 20 min. The supernatant was discarded, and the pellet was resuspended in 150 µl of ice cold buffer N (HEPES (pH7.9), MgCl2, NaCl, EDTA, Glycerol, Sodium OrthoVanadate) and incubated at 4°C for 20 minutes to solubilize nuclear proteins. Protein extract was spun at 18000 g for 20 min. The supernatant was discarded, and the pellet was resuspended in 150 µl of ice cold buffer M (HEPES (pH7.9), MgCl2, KCl, EDTA, Sucrose, Glycerol, Sodium deoxycholate, NP-40, Sodium OrthoVanadate) for membrane proteins solubilization. The extracts were then spun down at 18000 g for 20 min, and the supernatant was discarded. The remaining pellet was resuspended in 150 µl of prewarmed buffer CS (Pipes (pH6.8), $MgCl_2$, NaCl, EDTA, Sucrose, SDS, Sodium OrthoVanadate) and incubated at RT for 20 minutes to solubilize

cytoskeleton proteins. Protein extract was spun down at 18000 g for 20 min. Finally, the supernatant was withdrawn, and the pellet was resuspended in 150 µL of buffer C, incubated at 4°C for 5 minutes and then spun for 20 min at 15,000 rpm at 4°C. The remaining insoluble pellet consisting of ECM proteins was then snap-frozen and kept at -20°C.

ECM-enriched pellets were solubilized in a cocktail of reducing agents, namely, 8M urea, 100 mM ammonium bicarbonate, 10 mM dithiothreitol, pH 7.8, and incubated at 37°C for 30-60 min. Iodoacetamide alkylating agent was added to a final concentration of 25 mM and the samples were incubated for 30 min at RT. After this step, 15% of the sample was taken for SDS-PAGE analysis to test the purity of the ECM proteins extraction. Protein samples were then precipitated via methanol/chloroform extraction method. Briefly 600 µL of Methanol and 150 µL of Chloroform were added to 200 µL of sample. After vortexing 450 µL of MilliQ H2O were added and the samples were spun down at 13000 rpm for 1 minute. Supernatant was discarded and 450 µL were added to the pellet. Samples were centrifuged again at 13000 rpm for 2 minutes. After removing the supernatant, the pellet was let to dry and subsequently stored at -80°C. Protein pellets were subsequently reconstituted with 50 µL of 6M urea, 2M thiourea in 25 mM Tris ph8 and vortexed.

2.7.3 **Immunoblotting**

Cells were lysed in RIPA buffer (Sigma) containing cOmplete Mini protease inhibitors cocktail (Roche) and PhosSTOP (Sigma). Cell lysates were cleared by centrifugation at 12000 x g for 20 minutes. Protein concentration of cell lysates was determined using the Pierce™ BCA protein assay (ThermoFisher). Proteins were mixed with LDS loading buffer 4X (Invitrogen)

and/or Guanidine Hydrocloride Solution 8M (Sigma Aldrich), and heated at 60°C for 10 minutes or at 95°C for 5 minutes. Denatured and reduced proteins (10-30 μg per well) were then separated on 4-12% SDS-PAGE gel (Novex) and transferred to a nitrocellulose blotting membrane (Amersham). Membranes were blocked with 5% milk or 3% BSA in PBS for 1 hour and then probed with indicated Abs overnight at 4°C. Following washing, membranes were incubated with HRP-conjugated secondary antibodies and imaged using Li-Cor Odissey Imaging System (Li-Cor).

2.8 Gelatin Zymography Assay

Cells were incubated in free serum media at 37°C in a CO_2 incubator for 24 hours. Media was collected and concentrated 10 times using protein sample ultrafiltration membranes (Merck) and centrifuged (400 x g for 5 min at 4°C) and supernatant retained. Proteins were quantified using the BCA assay and 30 μg of protein lysate per lane were loaded on the gelatin zymography gels, samples were not heated before in order to avoid proteolysis. Precasted 8.5% polyacrylamide co-polymerized with 0.1% w/v gelatin gels (Novex Zymograf Gels, ThermoFisher) were used. The gel was run at 150 V until good separation was achieved. Gels were then washed 2 x 30 min with washing buffer (2.5% Triton X-100 in PBS1X) at RT in agitation. Subsequently gels were incubated O/N at 37°C in a develop buffer (50mM TrisHCl pH 7.5, 5 mM $CaCl_2$, 5 μM $ZnCl_2$, 1% Triton X-100). Gels were then stained with staining solution (0.25% Comassie Brilliant Blue, 45% MetOH, 10% HoAc) for 2 hours at RT on the shaker. After briefly rinsing the gels with H_2O, gels were incubated with destained solution (50mM

TrisHCl pH 7.4, 2% Triton X-100) 3 times for 30 minutes or until bands were clearly seen. Gels were scanned and images taken with hp Scanjet 5590.

2.9 3D Cell Culture

2.9.1 3D Migration Assay

Well plates (Corning 96 well clear round bottom) were coated with 50 μL of 1% agarose. After agarose solidified, $1x10^4$ cells were seeded in a volume of 100 μL per well. Cells were then incubated at 37°C in a CO_2 incubator until they formed spheroids, which requires between 3 and 5 days. Spheroids were then transferred to a p24 well (Corning) coated with 200 μL 1% agarose per well. For 3D invasion 400 μL of the Collagen type 1 solution (1mg/mL Col1a1, 1 M NaOH, 1X HBSS) were added per well. Spheroids were then transferred from a p96 well to p24 well. Images taken 4 hours after the spheroid transfer were tagged as time 0, and then images were taken every 24 hours up to 48 hours using Celigo (Celigo Imaging Cytometer Nexcelom). Using the acquired images, the distance of migrating cells from the 0h perimeter was measured on 8 different positions (radiants) within the same spheroid using ImageJ Software. The mean distance of 3D migration in μm was calculated.

2.9.2 3D Kinetic Assay

Cancer cells were plated in a low attachment round bottom 96 well plate (Spheroid microplate, Corning) in a concentration of $1x10^3$ cells/well. Cells were then centrifuged at 1000xg for 5 minutes in order to favour the cell aggregation. Plates were then incubated at 37°C in 5% CO_2 for few days, until when the

spheroids were formed. Images were taken using Celigo (Imaging Cytometer, Nexcelom) and the area was quantified using Celigo software.

2.10 Cell Proliferation Assay

Cell proliferation was evaluated using the Cell Proliferation (MTT) Kit I (Sigma Aldrich). $1x10_3$ cells were grown in a 96-well plate in a final volume of 100 μL culture medium per well and incubated for 24 hours. After the incubation period, 10 μL of the MTT labelling reagent (final concentration 0.5 mg/mL) was added to each well and plates are incubated for 4 hours. Subsequently 100 μL of the Solubilization solution were added into each well. Plates are allowed to stand overnight in the incubator. The day after plates were checked for the complete solubilization of the purple formazan crystals. Absorbance was measured using a microplate reader (Infinite 200 Pro, Tecan) at the wavelength of 550 nm. Reference wavelength was set at 670 nm.

2.11 Colony Formation Assay

Cancer cells (from 25 to 100) were plated in 6-well plates and incubated at 37°C in 5% CO_2 for 4 hours, to allow the cells to attach. Cells were irradiated with a range of different doses: 0, 2, 4, 6, 8 and 10 Gy. After RT, cells were kept in the incubator for 1 to 2 weeks, until cells in the control plates had formed colonies suitable for counting (>50 cells/colony). All colonies were stained using a mixture of 6 % glutaredehyde and 0.5% crystal violet and dried on the bench at room temperature. Finally, the colony number was counted on the GelCount™ Tumour Colony Counter (Oxford Optronix Ltd, Oxford, UK). The plating efficiency (PE) and survival fraction (SF) were calculated using the following equations: (1)

PE= number of colonies formed in mock irradiated plates/ seeding cell number x 100 %; (2) SF= number of colonies formed/ seeding cells number x PE. The survival fraction data were then plotted in a log10 scale against the RT dose in a linear scale. The survival curves were fitted in GraphPad Prism 5 (GraphPad Software, Inc. San Diego, CA, USA) using the linear quadratic model: $\ln(SF) = -\alpha D - \beta D_2$.

2.12 Animal Model

2.12.1 Mice

Female C57BL/6 and BALB-C/nude mice were purchased from Charles River Laboratories (Wilmington, USA). All mice were used at age between 6-8 weeks and held under specific pathogen-free conditions with humidity and temperature control.

Animal procedures were carried out in accordance with the UK Animal (scientific procedure) Act 1986 and local ethic reviews.

2.12.2 Subcutaneous Tumour Model

Cancer cells (MC38, KPC and PANC-1) were harvested while in their log phase (approximately 70% confluency). A total number of $2.5x10_5$ (resuspended in 100 μL of PBS 1X) were injected subcutaneously into the right flank under inhalation anaesthesia (3% isofluorane). Tumour sizes were measured 3 times per week using a calliper. Tumour volumes were calculated using the formula: Length x $Width_2/2$.

2.12.3 Irradiation Treatment of Subcutaneous Model

Mice were subjected to irradiation treatment when their tumours reach a volume between 80 and 100 mm^3. A fractionated X-Ray radiation dose of 3 Gy per 5 days (equivalent to a single 10Gy dose) was delivered to the tumours using a GulmayRS320 irradiation system (Gulmay Medical Ltd, Surrey, UK). Mice were shielded with only the tumour exposed under anaesthesia. Following IR, mice were culled at different time points accordingly with the experimental design. When the tumour exceed a volume of 500 mm^3 mice were culled. Mice with tumour ulceration were culled and excluded from the analysis.

To determine the overall survival of the treated or untreated mice, Kaplan-Meier analyses was used and the log-rank Mantel-Cox test was employed to determine any statistical difference between the survival curves of the cohorts.

2.13 Immunohistochemistry

2.13.1 Section Preparation

After removal of the tumour from the mouse body, samples were briefly rinsed in PBS and divided in two. Half of the tumour was fixed in 4% parafolmaldeide at 4°C for 48 hours. After 24 hours samples were placed in a solution of 30% sucrose and stored at 4°C until the samples drop to the bottom of the falcon tube (changing solution every day). Subsequently samples were embedded in OCT and freeze placing them on a support with liquid nitrogen. Samples were stored at -20°C. The frozen tissue was cut using a cryostat (Leica CM3050 S Research Cryostat) at 10 μm and the sections were stored at -80°C. Before staining sections were left air drying 30 minutes at room temperature.

2.13.2 Immunofluorescence

Sections were fixed in 4% PFA or 10% acetone. After fixation sections were blocked in a solution with 5% BSA, 5% serum and 0.5% triton X-100 in PBS for 1 hour in a humified chamber. Tissues were incubated in the appropriate concentration of primary antibody or is IgG control. Incubation of all primary antibodies was performed overnight at 4°C.

After the removal of the primary antibody by washing with PBS, Alexa-flour conjugated secondary antibodies at a final concentration of 8 μg/mL were added and slides were incubated for 1 hour at room temperature. After a final washing step, sections were counterstained with Hoechst at a final concentration of 1μg/mL (Sigma Aldrich) before being mounted with glass coverslips and visualised using a laser scanning confocal (Andor Dragonfly or Zeiss LSM780).

2.13.3 Picrosirius Red Staining

The staining was performed using the Picrosirius Red Stain Kit (abcam). Sections were left 30 minutes at room temperature to melt OCT, then they are briefly rinsed in PBS 1X. Sections are covered in picrosirius red solution and incubate for 60 minutes. After washing with acetic acid solution and with absolute alcohol, slides were dehydrated, cleared and mounted. Images were taken with the Aperio CS2 Slide Scanner (Leica Biosystems).

2.14 Second Harmonic Generation (SHG)

2.14.1 Imaging

Second-harmonic generation microscopy is a label-free optical imaging technology which can detect and quantitate collagen in tissue sections without

immunostaining. Slides were air dried for 20 minutes at RT, rinsed in PBS 1X and then mounted with a coverslip.

The SHG images were captured with an excitation wavelength of 890 nm (MaiTai laser emission range is 690-1040 nm), a pulse length of approximately 100 fs (check) and an emission filter centered at 445 nm. The microscope used is a two photon confocal microscope (Zeiss LSM 880). Tile scan and Z-slides were captured for each sample, for a total of 3 images for the same treatment.

2.14.2 **SHG Analysis and quantification**

Analysis and quantification of the SHG images was performed applying a MatLab algorithm called CT-FIRE[105]. Prior to quantification of the collagen fibres, all SHG images were transformed into 8-bit images. CT-FIRE combines the advantage of the Discrete Curvelet Transform for denoising the image and enhancing the fibre ridge features with the advantage of a fibre tracing algorithm for automatic fibre extraction, being capable of extracting fibre geometric information such as length, angel, width, and curvature of each fibre. Four quantitative parameters were analysed using CT-Fire: straightness, angle, length and width (http://loci.wisc.edu/software/ctfire). Of these parameters, alignment reflects the overall orientation of all collagen fibres, and its value ranges from 0 to 1, where 1 indicates that all fibres are aligned at the same angle. Straightness also ranges from 0 to 1, and to calculate this parameter, the linear length of the fibre was divided by the distance along the fibre. Angle shows the distribution of the absolute angle in a range from 0 to 180 degrees.

2.15 Oncomine Analysis

DNA microarrays have been widely used for cancer transcriptome analysis, however, the majority of these data were not easily accessible or comparable. Oncomine is a bioinformatics database which provide biomedical researchers with a collection of standardised analysis and cancer transcriptomes. *Rhodes et al*[106,107] analysis of cancer transcriptome data has identified the genes, pathways, and networks deregulated across 18,000 cancer gene expression microarrays among 35 cancer types.

ONCOMINE gene expression array datasets (https://www.oncomine.org/), an online cancer microarray database, was used to analyze the transcription levels of the COL5a1 in different cancers. The mRNA expressions of COL5a1 in clinical cancer specimens were compared with that in normal controls, using a Student's t test to generate a p value. The cut-off of p value and fold change were defined as 0.01 and 2, respectively.

2.16 Statistical Analysis

Statistical analyses were performed using GraphPad Prism. To assess if the data were sampled from populations that followed a Guassian distribution we used the Prism D'Agostino and Pearson test.

When data were normally distributed we performed t-Test analysis. When data sets were not assuming a normal distribution or the data set was too small to assume a gaussian distribution we used the non parametric Mann-Whitney U test. Statistical analysis were conducted in this way unless differently indicated

3 Chapter 3 – Irradiation affects Col5a1 expression

3.1 Introduction

3.1.1 **COL5A1 as an important mediator in cancer research**

We identified COL5A1 as our target of interest for different reasons. First of all this protein is overexpressed in the majority of cancer types and in fibrosis. Its overexpression is often correlated with a worse prognosis of survival[64].

COL5A1 is present in the majority of connective tissue matrices where it plays a functional role in maintaining tissue integrity. During malignant transformation COL5A1 is overexpressed and a study in pancreatic ductal adenocarcinoma showed that, via activation of FAK signalling, COL5A1 affects cancer cell viability, proliferation, migration and the formation of metastases[72]. Various bioinformatic analyses confirmed the overexpression of COL5A1 as well as its correlation with tumour progression in different cancer types such as breast cancer[108], oral squamous cell carcinoma[109], thyroid carcinoma[110], ovarian cancer[111], gastric cancer[112], papillary thyroid carcinoma[75] and lung cancer[113]. Early in 2019, *Mo et al.* published a study based on the analysis of data from the Cancer Genome Atlas (TCGA) and the Gene Expression Omnibus (GEO) to assess *COL5A1* relevance in breast cancer[114]. They found that COL5A1 was highly expressed in 90.4% of the invasive breast cancer samples analysed, in addition BC patients with a *COL5A1* mutation had a poor prognosis. The crucial function of COL5A1 in the oncogenesis of breast cancer was also recently confirmed by *Ren et al*[115]. These two studies suggest a potential role for COL5A1 as a detection factor in BC diagnosis.

Despite being a minor collagen, COL5A1 is fundamental in assembling the ECM and in fibrillogenesis[116,117]. COL1A1, the most abundant protein in the human body and fundamental ECM component, is capable of self-assembling in fibrils *in vitro*. *In vivo*, however, collagen I molecules face many potential-binding

partners that could sequester collagen molecules into dead-end molecular interactions, lowering the effective concentration of collagen monomers available to form fibrils. Therefore COL5A1 is used *in vivo* by cells to nucleate collagen fibrils[117], whereas fibronectins and integrins specify their site of assembly. The role of COL5A1 in shaping the ECM organization, given the relation between ECM and cancer progression[118], makes COL5A1 an intriguing target to investigate.

Despite the growing interest in COL5A1 role in cancer progression its role in the radiation response is still not well investigated.

3.1.2 **Second-Harmonic generation collagen detection as a potential cancer diagnostic marker**

Second-Harmonic generation microscopy emerged as a powerful tool to evaluate extracellular matrix structure, and in particular to image fibrillar collagen in a diverse range of tissues[119].

Second Harmonic Generation microscopy is based on an optically nonlinear coherent process in which the emitted light has exactly half of the wavelength of the two incident photons[120]. Biological materials can be highly polarizable and often assemble into large, ordered non-centrosymmetric structures[121]. This technique may represent a more objective and quantitative method for cancer prognostication. Differently from fluorescence which is emitted from all the angles, SHG has a well defined emission direction that carries details information about the packing of fibres and fibrils[122–124].

SHG feasibility in quantitatively assessing collagen signals has been shown to have potential applications for cancer diagnosis by revealing changes

in the ECM in tumours compared with healthy tissues. For example, the *Dong lab* use SHG to identify tumour borders in basal cell carcinoma lesions by assembling collagen imaging[125], or in small biopsies[60]. Collagen density, as well as fibre width, length and straightness were inversely correlated with patient overall survival time in different cancer types such as breast cancer[126], gastric cancer[127], pancreatic[128], oesophageal[129] and ovarian cancer[130]. Among those width was the parameter which show major clinical relevance[127]. In breast cancer it has been shown that the detection of a tumour associated collagen signature (TACS) in routine histopathological evaluation can serve as a predictive biomarker of disease recurrence and potential survival[61].

Similarly, *in vivo* data revealed that specific TACS can predict recurrence in murine models[131,132,133]. For example, using a breast cancer *in vivo* model, *Provenzano et al*, identified distinct stages of invasion by measuring changes of the angle of collagen fibres with respect to tumour boundaries[132].

Given the critical role of collagen organization in determining different cancer development and progression, it is not surprising that targeting the stroma is a potential therapeutic strategy for tumour control[134,135].

In this thesis, SHG signatures of width, length, alignment and orientation have been used to show differences in the structure of the ECM in unirradiated and irradiated tumour samples.

3.2 Results

3.2.1 **Irradiation affects tumour growth *in vivo***

Radiation reduces tumour growth *in vivo*. To investigate the effect of a fractionated radiation dose on tumour growth in a C57BL/6 mice model we used a fractionated dose of 5 times 3 Gy, corresponding to a 10 Gy single dose. Previous unpublished studies in our lab showed that a fractionated dose in the subcutaneous model decreased side effects and kept tumour growth consistent within the same groups compared with the same dose given in a single shot. Samples were collected 6 days after the end of the radiation treatment, equivalent to 11 days after tumours reached a volume of 80-100 mm^3. The first experiment was set up with the cell line MC38, a colorectal murine cell line. We defined 3 different time points to look at the effects of irradiation on the ECM proteins: 6, 10 and 20 days after the end of the radiation treatment (**Figure 4A**). Mice injected with MC38 cell line, and then irradiated, reached a tumour size of 500mm^3 with 13 days of delay compared with the unirradiated mice (**Figure 4Bi-Biii**). The Kaplan Meier survival curve confirmed a delay after irradiation of 13 days (**Figure 4Biii**). Compared with the untreated group, the irradiated MC38 tumours volume was significantly reduced. Untreated tumours reached the ethical end point of 500 mm^3 7 days after injection, on the same day irradiated tumours volume was around 300 mm^3 (**Figure 4Bii**).

Radiation proved effective also on the PANC-1 xenograft subcutaneous model. Irradiated tumours were 3 times smaller than the controls 6 days after the end of the treatment cycle (**Figure 4Di**). Tumour volume size at day 11 was approximately 500 mm^3 for unirradiated PANC-1 tumour samples, and 45% less for irradiated tumours (**Figure 4Dii**).

The irradiation treatment did not affect the tumour growth of KPC subcutaneous tumours (**Figure 4Ci**). On the day when KPC control tumours reached the ethical end point of 500 mm^3 11 days after injection, the average tumour volume of irradiates samples was not statistically different (**Figure 4Cii**). This cell line is known to be radioresistant.

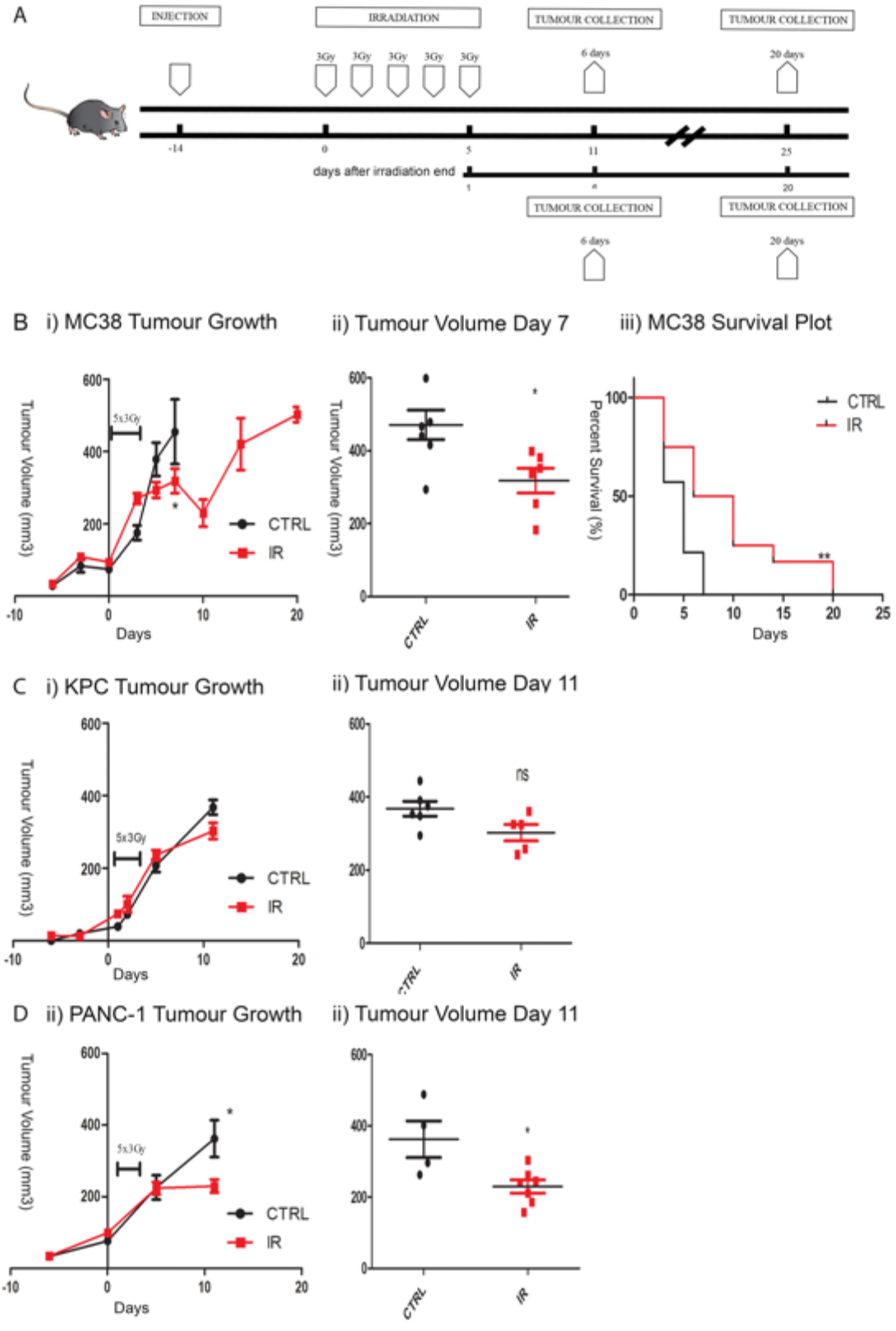
A
INJECTION
IRRADIATION
TUMOUR COLLECTION
TUMOUR COLLECTION
3Gy 3Gy 3Gy 3Gy 3Gy
6 days
20 days
-14
0
5
11
25
days after irradiation end
1
n
20
TUMOUR COLLECTION
TUMOUR COLLECTION
6 days
20 days
B i) MC38 Tumour Growth
ii) Tumour Volume Day 7
iii) MC38 Survival Plot
Tumour Volume (mm3)
5x3Gy
CTRL
IR
Days
Percent Survival (%)
C i) KPC Tumour Growth
ii) Tumour Volume Day 11
NS
D ii) PANC-1 Tumour Growth
ii) Tumour Volume Day 11

Figure 4: Irradiation affects tumour growth A) *In vivo* experiment time line. **B)** Bi) MC38 WT tumour growth in untreated and irradiated samples. Bii) Tumour size volumes measured at day 7. Biii) Kaplan-Meier curve. **C)** Ci) KPC WT tumour growth in untreated and irradiated samples. Cii) Tumour size volumes measured at day 11. **D)** Di) PANC-1 WT tumour growth in untreated and irradiated samples. Dii) Tumour size volumes measured at day 11. Statistical analysis have been performed as described in materials and methods (*$p<0.05$, **$p<0.01$, ***$p<0.005$).

3.2.2 **Col5a1 expression decreases in tumours after exposure to irradiation**

We first sought to determine whether IR affected Col5a1 expression in cancer cell *in vivo* tumours. MC38 subcutaneous tumours grown in C57BL/6 mice were subjected to fractionated (3Gy x 5F, 1 F x day) IR dose. At 3, 6, 10 and 20 days after the end of the radiation treatment, tumours were collected. Control tumours were collected when their volume was comparable to irradiated tumours. Immunohistochemistry showed a decrease in Col5a1 amounts **(Figure 5A)**. The expression level decreased by roughly 50% after irradiation **(Figure 5B)**. Strikingly the decrease in Col5a1 expression was evident as soon as 3 days after the irradiation treatment. A similar finding has been confirmed by Western Blot **(Figure 5C)**. Similar results were seen in tumours derived from two additional cell lines: KPC, a murine pancreatic cancer cell line, and PANC-1, a human adenocarcinoma pancreatic cell line **(Figure 5D and 5F)**. KPC subcutaneous tumours grown in C57BL/6 mice, and PANC-1 tumours in BALB-C mice were subjected to the fractionated (3Gy x 5F, 1 F x day) IR dose. Tumours were collected 6 days after the end of the IR treatment. Control tumours were collected as explained above. COL5A1 expression decreased to a greater extent in KPC and PANC-1 tumours after IR as shown in **Figure 5E** and **5G**.

We next sought to determine if IR also affects Collagen 1 expression. However Collagen 1 levels in MC38 tumours as evaluated by immunohistochemistry did not change at any of the time points **(Figure 6A-B)**. Nor did Collagen I levels change after IR in KPC tumours **(Figure 6C-D)**.

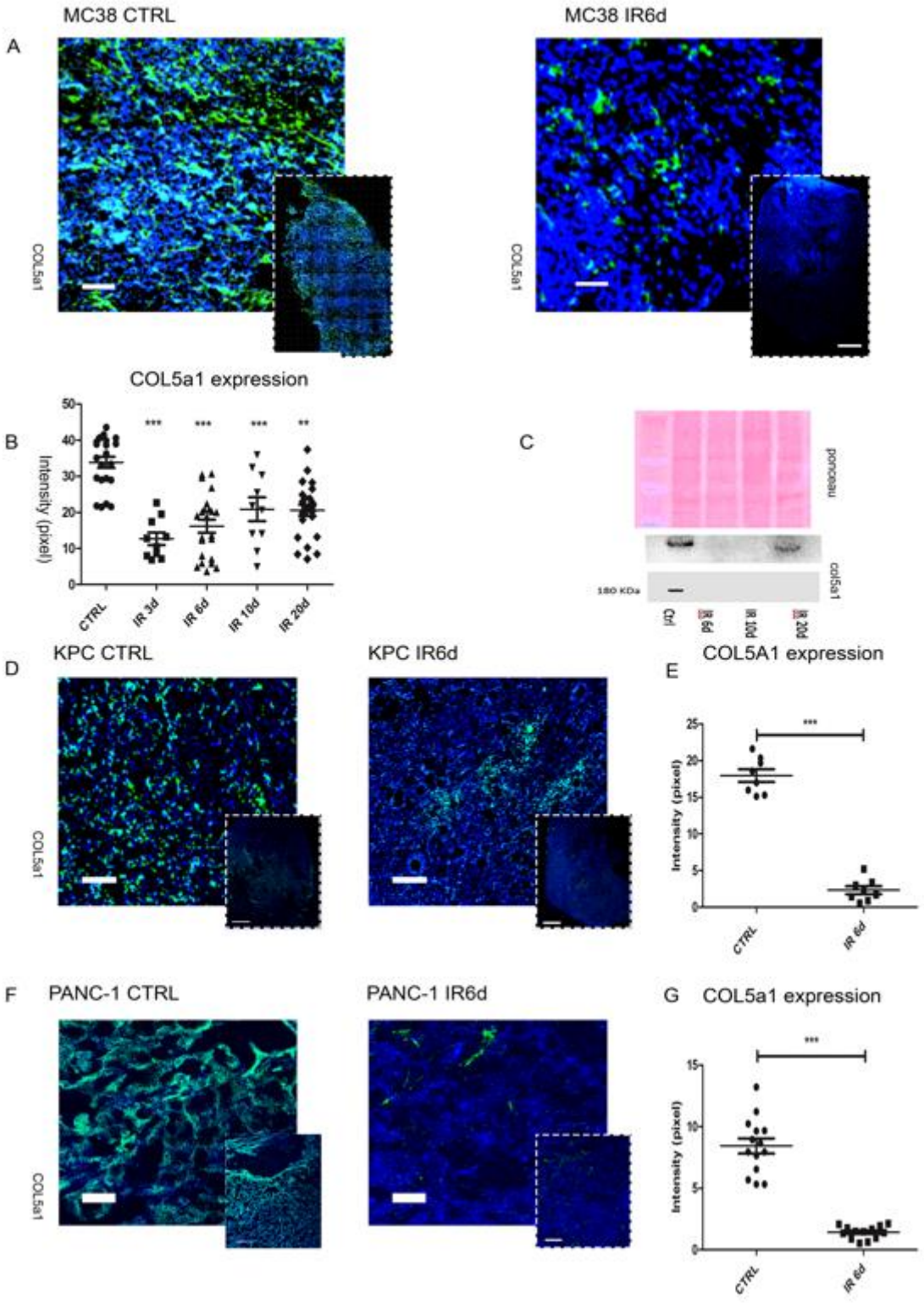
A
MC38 CTRL
MC38 IR6d
COL5a1
COL5a1
B
COL5a1 expression
Intensity (pixel)
CTRL
IR 3d
IR 6d
IR 10d
IR 20d
C
ponceau
col5a1
180 KDa
Ctrl
IR 6d
IR 10d
IR 20d
D
KPC CTRL
KPC IR6d
COL5a1
E
COL5A1 expression
Intensity (pixel)
CTRL
IR 6d
F
PANC-1 CTRL
PANC-1 IR6d
COL5a1
G
COL5a1 expression
Intensity (pixel)
CTRL
IR 6d

Figure 5: Radiation affects Col5a1 Expression. A) Representative images of immunofluorescence staining of MC38 subcutaneous tumour samples. Col5a1 is shown in green. (Scale bar=2mm). **B)** Images from MC38 tumour samples were quantified using ImageJ. Statistical significance was assessed by the Mann-Whitney *t*-test: $^{**}p < 0.005$ was considered significant; $^{***}p < 0.001$ very highly significant. **C)** Western Blot analysis of col5a1 at different time points after irradiation. (The two blot shown are representative of 3 independent repeats from two independent protein extracts from in vivo tumour samples). A Ponceau staining has been used as a loading control. **D)** Representative images of immunofluorescence staining in KPC subcutaneous tumour samples. Col5a1 is shown in green. (Scale bar=2mm). **E)** Quantification of Col5a1 expression in KPC tumour samples. Images were quantified using ImageJ. Statistical significance was assessed by the Mann-Whitney *t*-test: $^{***}p < 0.001$ very highly significant. **F)** Representative images of immunofluorescence staining in PANC-1 subcutaneous tumour samples. COL5A1 is shown in green. (Scale bar=2mm). **G)** Quantification of COL5A1 expression in PANC-1 tumour samples. Images were quantified using ImageJ. Statistical significance was assessed by the Student's *t*-test: $^{***}p < 0.001$.

3.2.3 **Col5a1 RNA decreased after irradiation**

We looked for explanations to account for the decrease in Col5a1 expression in tumours after irradiation. We investigated three of many possible reasons including alteration in fibroblasts, gene downregulation and increase in proteolytic enzymes such as MMP-2 and MMP-9 known to cleave collagens, both *in vivo* and *in vitro*.

Fibrosis is a late effect of radiation. Fibroblasts in tumours following radiation, are more activated and produce increased amounts of ECM proteins, including collagens, leading to fibrosis. Interestingly enough we saw that in MC38 tumour fibroblast activation as judged by α-sma expression did not change 6 days after irradiation **(Figure 6E-F)**, whereas in KPC there is a strong activation **(Figure 6G)**. In KPC tumours α-sma expression increased by roughly 3 times **(Figure 6H)**. This results suggest that fibroblast activation, as assessed by α-sma staining, was not related with Col5a1 synthesis, suggesting that collagen-5a1 was produced by tumour cells and not by fibroblasts.

We performed RT-PCR to detect *Col5a1* expression both *in vivo* and *in vitro*. RNA was extracted from MC38 tumours, control tumours and tumours harvested 6 days after irradiation. After 35 cycles no signal was detected for *Col5a1* expression in the irradiated samples **(Figure 7A)**. MC38 cells in tissue culture were irradiated with a single dose of 10Gy, and collected at two different time points: 72 and 120 hours after irradiation. In both irradiated samples *Col5a1* gene expression is about 40% compared to untreated cells **(Figure 7B)**. This suggest that irradiation mediated downregulation of *Col5a1* expression was gene regulated. KPC and MC38 cell lines do not show any mutation in COL5a1 or any

other Col gene, as reported in the Cancer Cell Line Encyclopedia (Novartis/Broad)[136].

We looked for matrix metalloproteinases. MMP-9 has been shown to cleave type I, II, and V collagens[137]. MMP-2 and MMP-9 in particular are thought to play important roles in the final degradation of fibrillar collagens, such as Col5A1. We investigated MMP-9 expression in tumour samples by western blot **(Figure 7C)**. MMP-2 activity in the conditioned media was analysed by using a gelatin zymography assay **(Figure 7D)**. The assay is based on gelatin cleavage by gelatinases including active form of MMP-2 and less efficiently by other MMPs[138139]. Activation of MMP-2 includes its binding to the cell surface MT1-MMP/TIMP-1 complex with subsequent cleavage of the pro-MMP2 inactive form by TIMP-2. The cleaved form matures to a intermediate activated form that is subsequently released from cell surfaces into the extracellular milieu. Only this active form is present in the extracellular medium and is able to digest gelatin.

In both cases we failed to see any difference between untreated controls and irradiated samples.

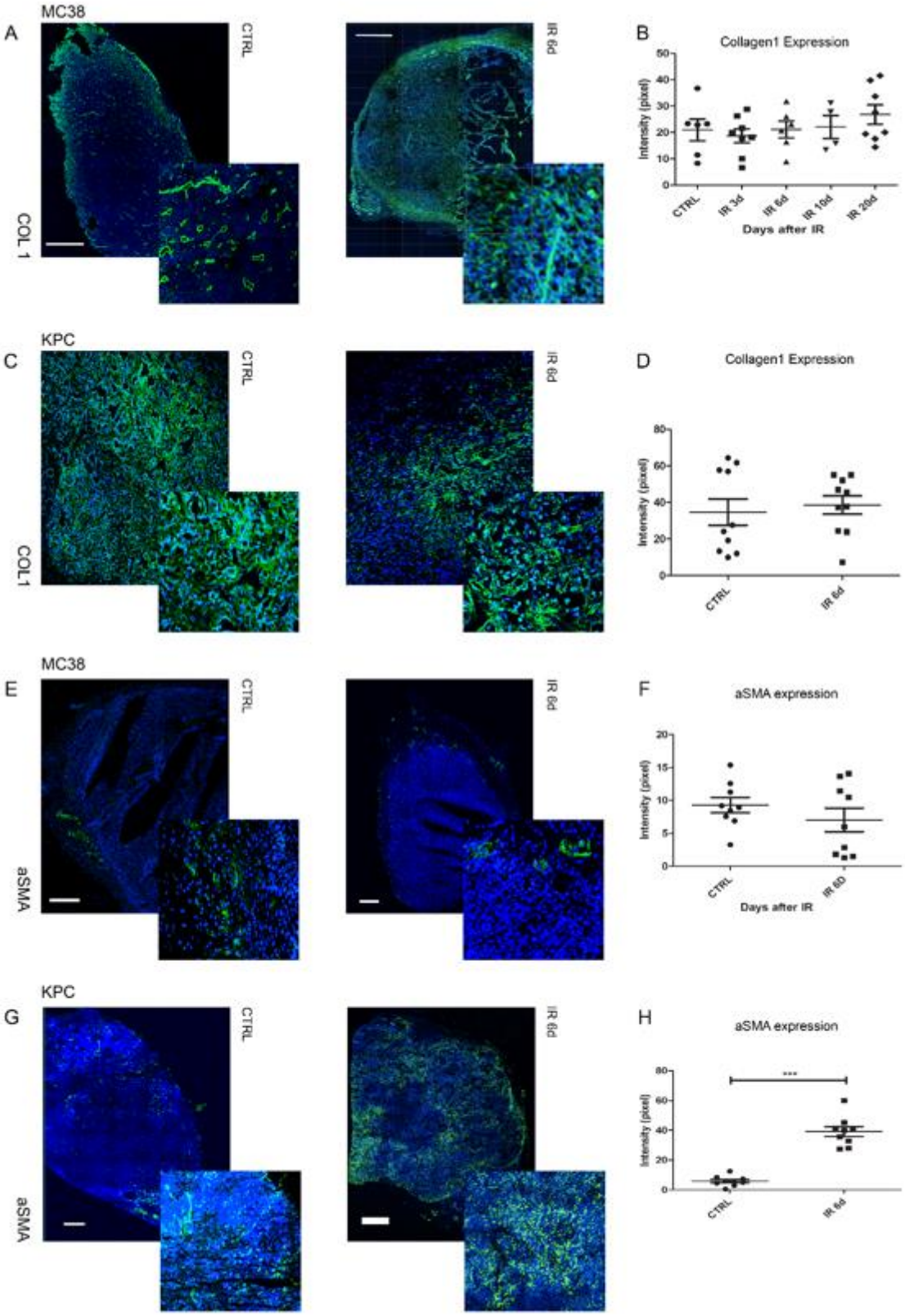
A
MC38
CTRL
IR 6d
COL 1
B
Collagen1 Expression
Intensity (pixel)
CTRL
IR 3d
IR 6d
IR 10d
IR 20d
Days after IR
C
KPC
CTRL
IR 6d
COL1
D
Collagen1 Expression
Intensity (pixel)
CTRL
IR 6d
E
MC38
CTRL
IR 6d
aSMA
F
aSMA expression
Intensity (pixel)
CTRL
IR 6D
Days after IR
G
KPC
CTRL
IR 6d
aSMA
H
aSMA expression
***
Intensity (pixel)
CTRL
IR 6d

Figure 6: Collagen1 and α-SMA expression are not affected by Radiation. A) Representative images of immunofluorescence staining in MC38 subcutaneous tumour samples. Collagen1 is shown in green. (scale bar=2mm). **B)** Quantification of Collagen1 expression in MC38 tumour samples. Images were quantified using ImageJ. Statistical significance was assessed by the Mann-Whitney's *non parametric* test: differences were not significant. **C)** Representative images of immunofluorescence staining in KPC subcutaneous tumour samples. Collagen1 is shown in green. (scale bar=2mm). **D)** Quantification of Col1a1 expression in KPC tumour samples. Images were quantified using ImageJ. Statistical significance was assessed by the Student's *t*-test: differences were not significant. **E)** Representative images of immunofluorescence staining in MC38 subcutaneous tumour samples. α-Sma is shown in green. (scale bar=2mm). **F)** Quantification of α-Sma expression in MC38 tumour samples. Images were quantified using ImageJ. Statistical significance was assessed by the Student's *t*-test: differences were not significant. **G)** Representative images of immunofluorescence staining in KPC subcutaneous tumour samples. α-sma is shown in green. (scale bar=2mm). **H)** Quantification of α-Sma expression in KPC tumour samples. Images were quantified using ImageJ. Statistical significance was assessed by the Student's *t*-test: differences were not significant.

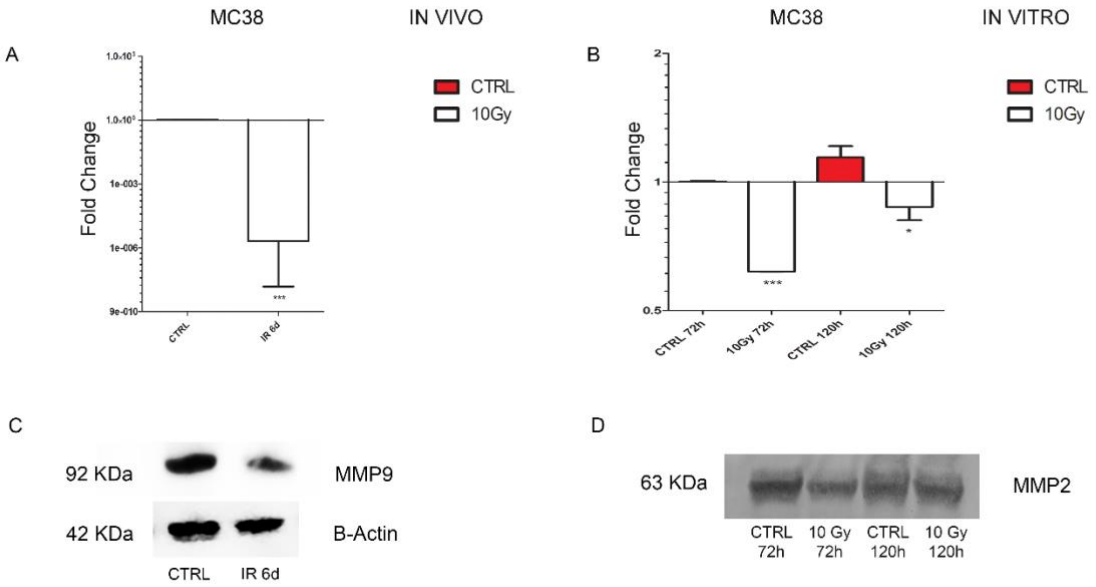

Figure 7: *Col5a1* expression is regulated through transcription. A) Relative levels of *Col5a1* normalised to β-actin as a housekeeping gene. Gene expression in control in MC38 subcutaneous tumour samples (n=3). (***p<0.001). **B)** Relative levels of Col5a1 gene expression normalised to β-actin gene expression in controls in MC38 cells. (*p<0.05, ***p<0.001) **C)** Western Blot analysis of MMP9 in controls and after irradiation in *in vivo* MC38 subcutaneous tumour samples. (the blot is representative of 3 different repeats). Western Blot of β-actin has been used as a loading control. **D)** Gelatin-Zymography assay for cleaved active-MMP2 in irradiated and not irradiated cells at two different time points.

3.2.4 **COL5a1 as a cancer-associated gene**

In order to identify COL5A1 as a cancer-associated gene we queried the Oncomine database to systematically assess gene expression levels of COL5A1 in a variety of carcinomas. We used stringent criteria of a 2 fold change for COL5A1 expression and a p-value of 1^{-4} for COL5A1 analysis. We found that COL5A1 is highly overexpressed in the following cancer versus normal datasets: brain and CNS, colorectal, oesophageal, breast, gastric, head and neck, liver, lung, pancreatic cancers, leukemia, melanoma and sarcoma. In the cancer vs cancer, multi-cancer datasets, *COL5A1* was overexpressed in brain and CNS cancer, lymphomas and other cancers (**Figure 8**). The overexpression and the underexpression were determined based on the gene rank percentile.

The outlier analysis, which is used to determine significant *COL5A1* expression in a subset of the patient samples, showed that *COL5A1* is both over- and under-expressed across the analysed cancers (Oncomine database). It showed that there were 129 analysis which showed a significant increase in *COL5A1* expression and 83 which displayed a significative decrease in *COL5A1* expression.

We further queried the analyses which had a significant increase in *COL5A1* expression in two different cancers: colorectal and pancreatic cancer. As demonstrated in **Figure 9A**, the Skrzypczak colorectal cancer dataset[140], comprised of 15 patient samples, showed a statistically significant overexpression of *COL5A1* mRNA (p-value = $1.81^{-9)}$ in colon carcinoma compared to normal tissue. **Figure 9B** confirmed the statistically significant overexpression of *COL5A1* mRNA (p-value 1.64^{-7}). Gene lists were rank-ordered by p-value. **Figure 9C** shows a statistically significant overexpression

of *COL5A1* mRNA, (p-value=4.32^{-8}) in pancreatic adenocarcinoma compared with normal pancreatic tissue in the Segara Pancreatic cancer dataset[141], comprised of 17 patient samples. This data analysis suggest that *COL5A1* overexpression correlated with clinical outcome.

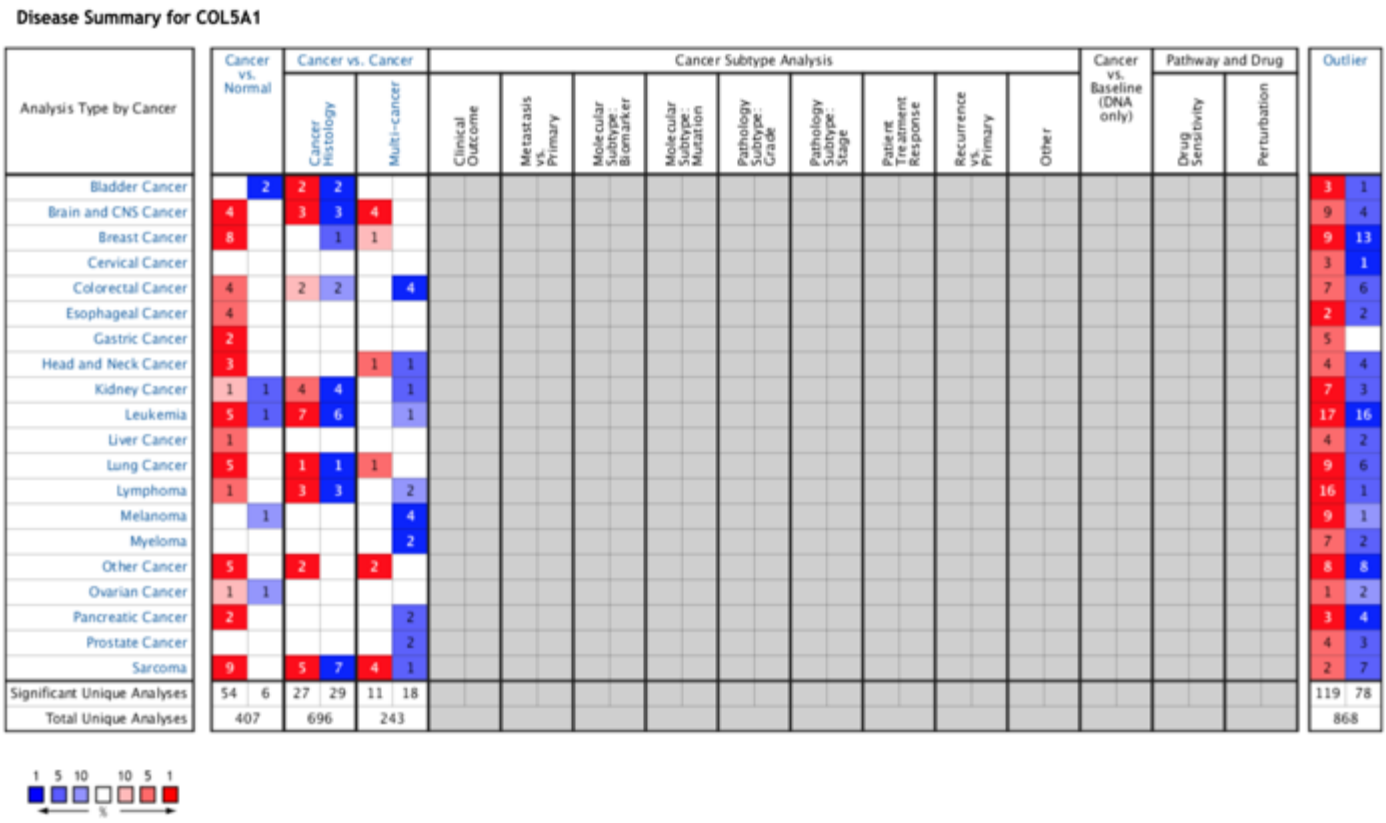

Figure 8: Oncomine analysis. Disease summary for *COL5A1*. The Oncomine database was queried for *COL5A1* based on the following: cancer type, cancer versus normal, cancer versus cancer, cancer subtype, cancer versus baseline, pathway and drug and outlier analyses. Cells in red represents *COL5A1* overexpression and cells in blue represents *COL5A1* underexpression. This disease summary was performed using a criterion of a 2 fold change for *COL5A1* expression and a p-value of 0.0001.

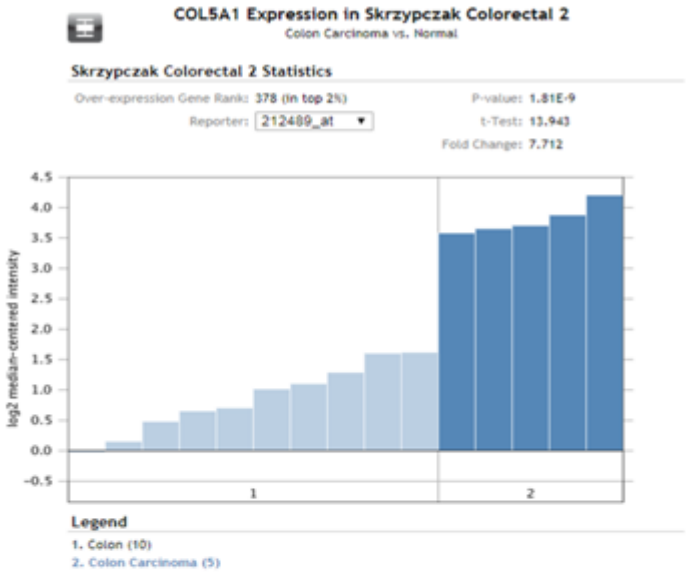
COL5A1 Expression in Skrzypczak Colorectal 2
Colon Carcinoma vs. Normal
Skrzypczak Colorectal 2 Statistics
Over-expression Gene Rank: 378 (in top 2%)
Reporter: 212489_at
P-value: 1.81E-9
t-Test: 13.943
Fold Change: 7.712
log2 median-centered intensity
Legend
1. Colon (10)
2. Colon Carcinoma (5)

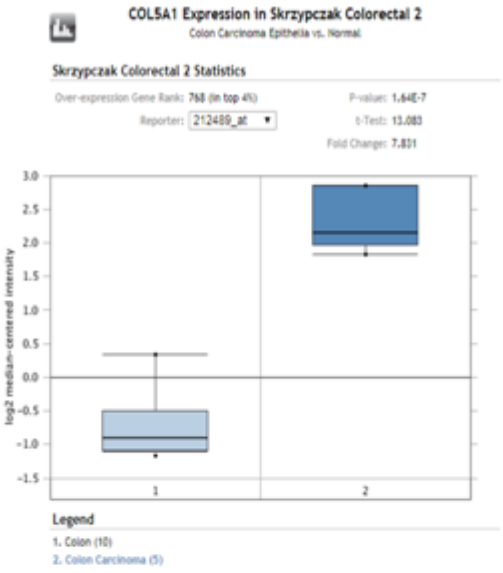
COL5A1 Expression in Skrzypczak Colorectal 2
Colon Carcinoma Epithelia vs. Normal
Skrzypczak Colorectal 2 Statistics
Over-expression Gene Rank: 768 (in top 4%)
Reporter: 212489_at
P-value: 1.64E-7
t-Test: 13.083
Fold Change: 7.831
log2 median-centered intensity
Legend
1. Colon (10)
2. Colon Carcinoma (5)

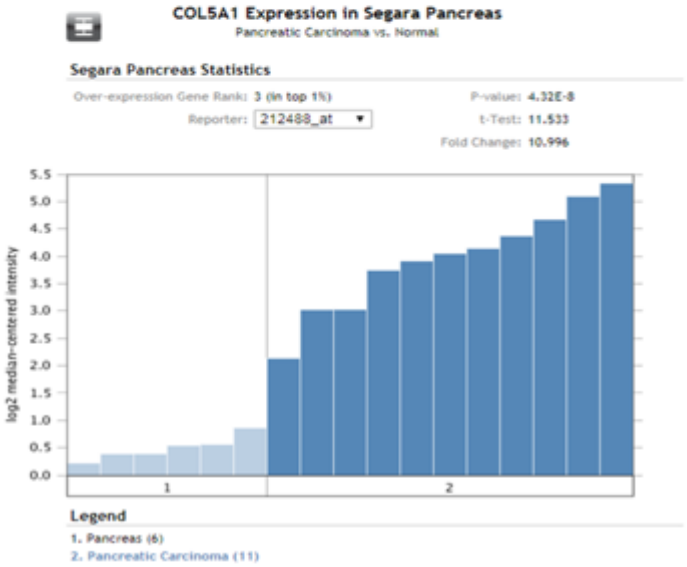
COL5A1 Expression in Segara Pancreas
Pancreatic Carcinoma vs. Normal
Segara Pancreas Statistics
Over-expression Gene Rank: 3 (in top 1%)
Reporter: 212488_at
P-value: 4.32E-8
t-Test: 11.533
Fold Change: 10.996
log2 median-centered intensity
Legend
1. Pancreas (6)
2. Pancreatic Carcinoma (11)

Figure 9: *COL5A1* overexpression in colorectal and pancreatic carcinoma (Oncomine). (A) *COL5A1* overexpression in colorectal adenocarcinoma versus colon normal tissue in the Skrzypczak dataset, with an overexpression generank of 2%. (B) *COL5A1* expression in colorectal adenocarcinoma versus colon normal tissue in the Skrzypczak dataset, with an overexpression generank of 4%. (C) *COL5A1* expression in pancreatic adenocarcinoma versus normal tissue in the Segara dataset, with an overexpression generank of 1%.

3.2.5 **Irradiation affects Collagen organization**

Col5a1 has been demonstrated to be a central regulator in matrix assembly and tissue function in the corneal stroma[66] and skin. In the absence of Col5a1 fibril organization and tissue architecture were disrupted[66]. After showing that irradiation decreased Col5a1 expression **(Figure 5)**, we sought to determine the effect of irradiation and Col5a1 decrease on collagen organisation. Collagen fibres were hierarchically ordered in parallel orientation[142]. We used two different methods to visualize collagen: Picrosirius Sirius Red staining and Second Harmonic Generation imaging. Sirius Red is an elongated dye molecule with sulphonic acid groups that reacts with basico-amino groups such as lysine and hydroxylysine and the guanidine group of arginine that are abundant in the collagen molecule[143]. Therefore, Sirius Red reacts with and becomes bound to all the varying isoforms of collagen. In bright field microscopy, collagen appears as bundles of pink to red fibres after staining. Picrosirius Red was used to stain MC38, PANC-1 and KPC tumours **(Figure 10A)**. MC38 tumours were intensely stained but the dye did not outline any fibrous- shaped structure.

Picrosirius red staining in PANC-1 samples **(Figure 10D)** showed an increase in positive area percentage after irradiation **(Figure 10E)** while there was no significant change in the KPC tumour staining. Overall these studies indicated the difficulties in the generation of and interpretation of Picrosirius Red staining. **(Figure 10Bi-ii-iv-v) (Figure 10Biii-vi) (Figure 10C)**.

To overcome the limitations of Picrosirius Red staining, we turned to Second Harmonic Generation imaging. SHG is of high specificity for the detection of collagen fibres. These collagen parameters include alignment, density, length, width, and straightness, parameters which are frequently applied for

characterization of collagen fibres. The open-source software CT-FIRE[105] allowed me to automatically extract and analyse these parameters from the collagen fibres in SHG images **(Figure 11C)**.

Collagen bundle patterns displayed marked differences within a single tumour with or without irradiation. In MC38 tumour samples, the intensity of signal from collagen bundles and their size, the width of the fibres and their length decreased significantly after irradiation **(Figure 11A)**. At the same time the angle and straightness of the collagen fibres did not show significant differences after radiation **(Figure 11B)**. The mean width calculated in pixels was reduced from 4.5px to 3.6px **(Figure 11Bii)**. The impact of radiation on collagen structure was even more dramatic in KPC samples. KPC control tumours were characterised by a bigger deposition of fibrous stroma than MC38 samples, nonetheless, irradiation led to a very similar collagen disorganization **(Figure 11D)**. The straightness and angle of collagen fibres did not significantly change in KPC samples either, suggesting that irradiation did not have any effect on collagen orientation **(Figure 11Di-iv)**. Fibre width instead decreased by roughly 20% **(Figure 11Dii)**. Irradiation also significantly shortened the fibre length from 62 to 54 pixels **(Figure 11Diii)**.

Interestingly collagen fibres length and width have been reported as a valuable prognostic marker in a study comparing collagen parameters with 5-year overall survival patients' data[127]. Width was the strongest prognostic signal. Its prognostic value has been evaluated as stronger than traditional parameters such as tumour invasion depth or node metastasis. In the same study collagen fibres alignment and straightness did not show any significant correlation with 5 year OS[127].

This observation together with our findings suggest that the effects of radiation on tumour growth could also be mediated by selectively reorganising collagen deposition. In particular shortening and shrinking collagen fibres.

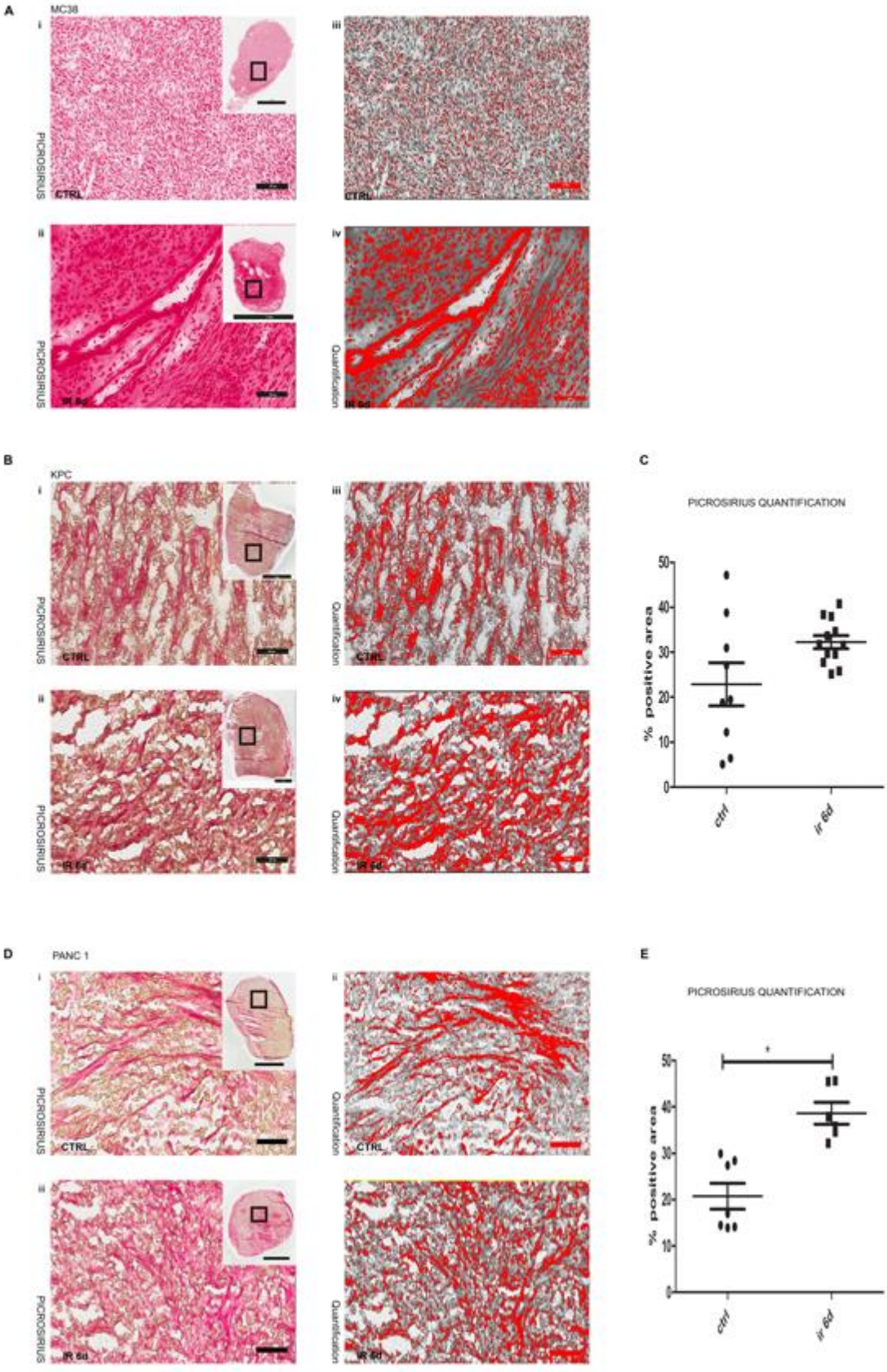
A
MC38
i
PICROSIRIUS
CTRL
iii
CTRL
ii
PICROSIRIUS
IR 6d
iv
Quantification
IR 6d
B
KPC
i
PICROSIRIUS
CTRL
iii
Quantification
CTRL
ii
PICROSIRIUS
IR 6d
iv
Quantification
IR 6d
C
PICROSIRIUS QUANTIFICATION
% positive area
0
10
20
30
40
50
ctrl
ir 6d
D
PANC 1
i
PICROSIRIUS
CTRL
ii
Quantification
CTRL
iii
PICROSIRIUS
IR 6d
Quantification
IR 6d
E
PICROSIRIUS QUANTIFICATION
*
% positive area
0
10
20
30
40
50
ctrl
ir 6d

Figure 10: Picrosirius Red staining of tumour samples A) Representative images of MC38 tumour samples stained with Picrosirius Red Staining : 100x magnification detail (Scale bar=100um) with an entire tile scan detail on top right (Scale bar=2mm) control (i) and irradiated sample (iii). An example of collagen segmentation control (ii) and irradiated sample (iv). **B)** Representative images of KPC tumour samples stained with Picrosirius Red. From the left: 100x magnification detail (Scale bar=100um) with an entire tile scan detail on top right (Scale bar=2mm) control (i) and irradiated sample (iii). An example of collagen segmentation control (ii) and irradiated sample (iv). **C)** Collagen quantification. Paired t-test has been performed, differences are not significative. **D)** Representative images of PANC-1 tumour samples stained with PIcrosirius. From the left: 100x magnification detail (Scale bar=100um) with an entire tile scan detail on top right (Scale bar=2mm) control (i) and irradiated sample (iii). An example of collagen segmentation control (ii) and irradiated sample (iv). **B)** Representative images of KPC tumour samples stained with Picrosirius Red. From the left: 100x magnification detail (Scale bar=100um) with an entire tile scan detail on top right (Scale bar=2mm) control (i) and irradiated sample (iii). An example of collagen segmentation control (ii) and irradiated sample (iv). Paired t-test has been performed (*$p<0.05$)

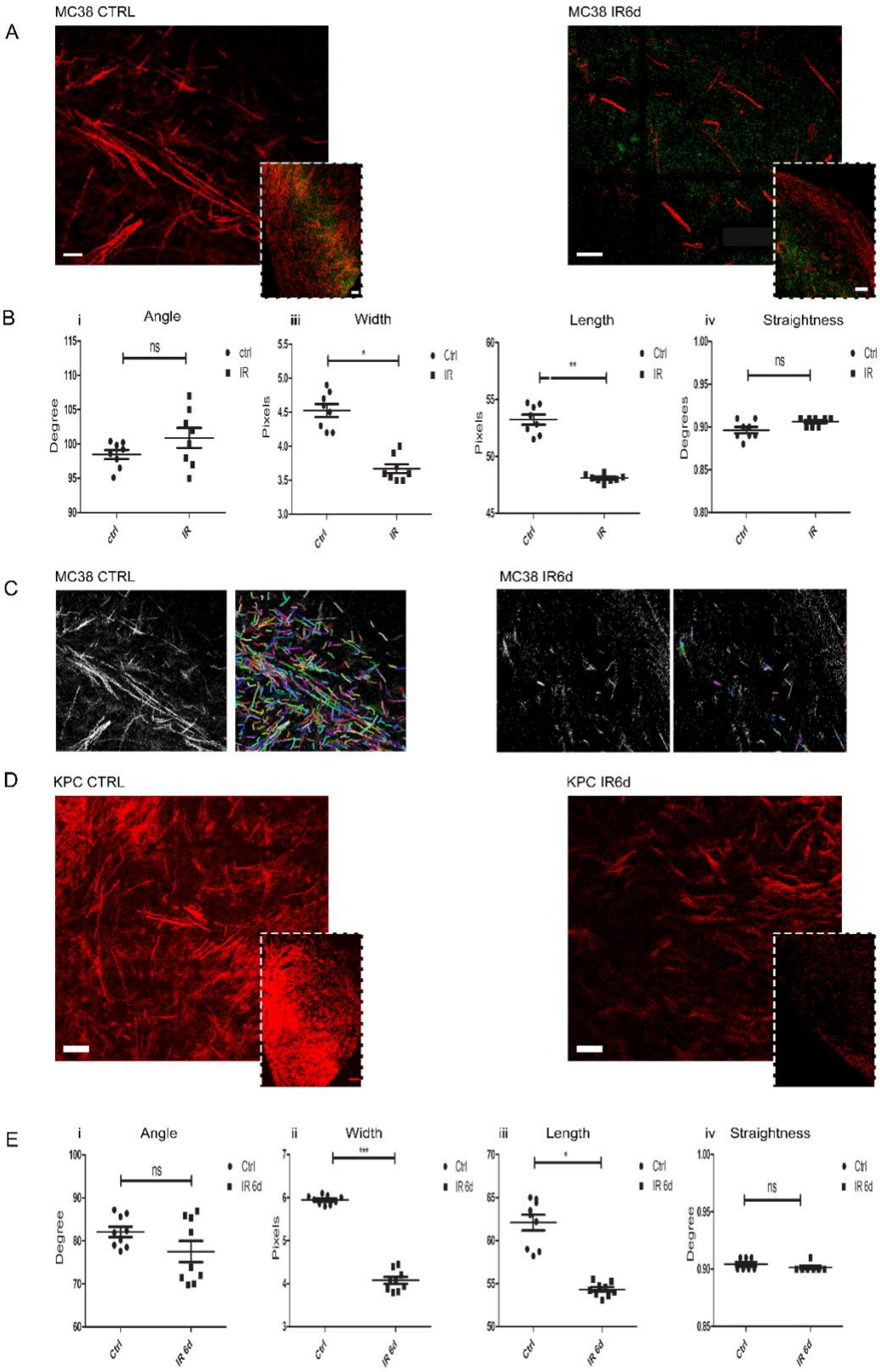
A
MC38 CTRL
MC38 IR6d
B
i
Angle
ns
ctrl
IR
Degree
iii
Width
*
Ctrl
IR
Pixels
Length
**
Ctrl
IR
Pixels
iv
Straightness
ns
Ctrl
IR
Degrees
C
MC38 CTRL
MC38 IR6d
D
KPC CTRL
KPC IR6d
E
i
Angle
ns
Ctrl
IR 6d
Degree
ii
Width
***
Ctrl
IR 6d
Pixels
iii
Length
*
Ctrl
IR 6d
iv
Straightness
ns
Ctrl
IR 6d
Degree

Figure 11: Second Harmonic Generation (SHG) Imaging and quantitative analysis of collagen fibres. A-C) Second harmonic generation microscopy of subcutaneous MC38 and KPC tumours. Collagen fibres are shown in red. **B)** Collagen fibres were automatically extracted for analysis using the open-source software CT-FIRE. **C-E)** Quantitative parameters including angle (i), width (ii), length (iii) and straightness (iv) calculation was based on the segmented SHG images (n=3, *p<0.05, **p<0.01)

3.2.6 **Collagen parameters in relation to clinical outcome**

It is known that the fibrillar collagen network in tumour and normal tissues is different due to remodelling and increased amounts of some components of the extracellular matrix resulting from the malignant process[144,145]. While collagen characteristics in colorectal cancer are not well described, collagen patterning has been linked to tumour behaviour and clinical factors in other malignancies. SHG microscopy has shown promise in studying other cancers including those arising in the breast[145,126], ovaries[144], kidneys[146] and pancreas[128].

The aim of this experiment was to compare *in vivo* results from SHG imaging with those from some clinical samples, and not to assess if SHG can be used as a prognostic clinical marker for colorectal cancer. To assess collagen organization from colorectal cancer patients, we made use of a tissue array, created from archived samples from patients, which had substantial follow-up data. We compared cancer related collagen parameters values to the normal tissue **(Figure 12A)**. Interestingly in the TMA the only two parameters changing with the stage were fibre width and length, with no significative changes in fibre straightness or angle **(Figure 12Bi-iii)**. Collagen fibres were elongated in tumour stages compared to normal colon. There were no significative differences in the fibre length between the different stages of cancer **(Figure 12Bii)**, suggesting that collagen fibre elongation is important in the early malignant process. Fibre width decreased along with tumour progression. Based on our TMA collagen, fibre width increased significantly in the tumour stage I, and gradually decreased in the next stages reaching the same width as normal samples in stage IV **(Figure 12Biv)**.

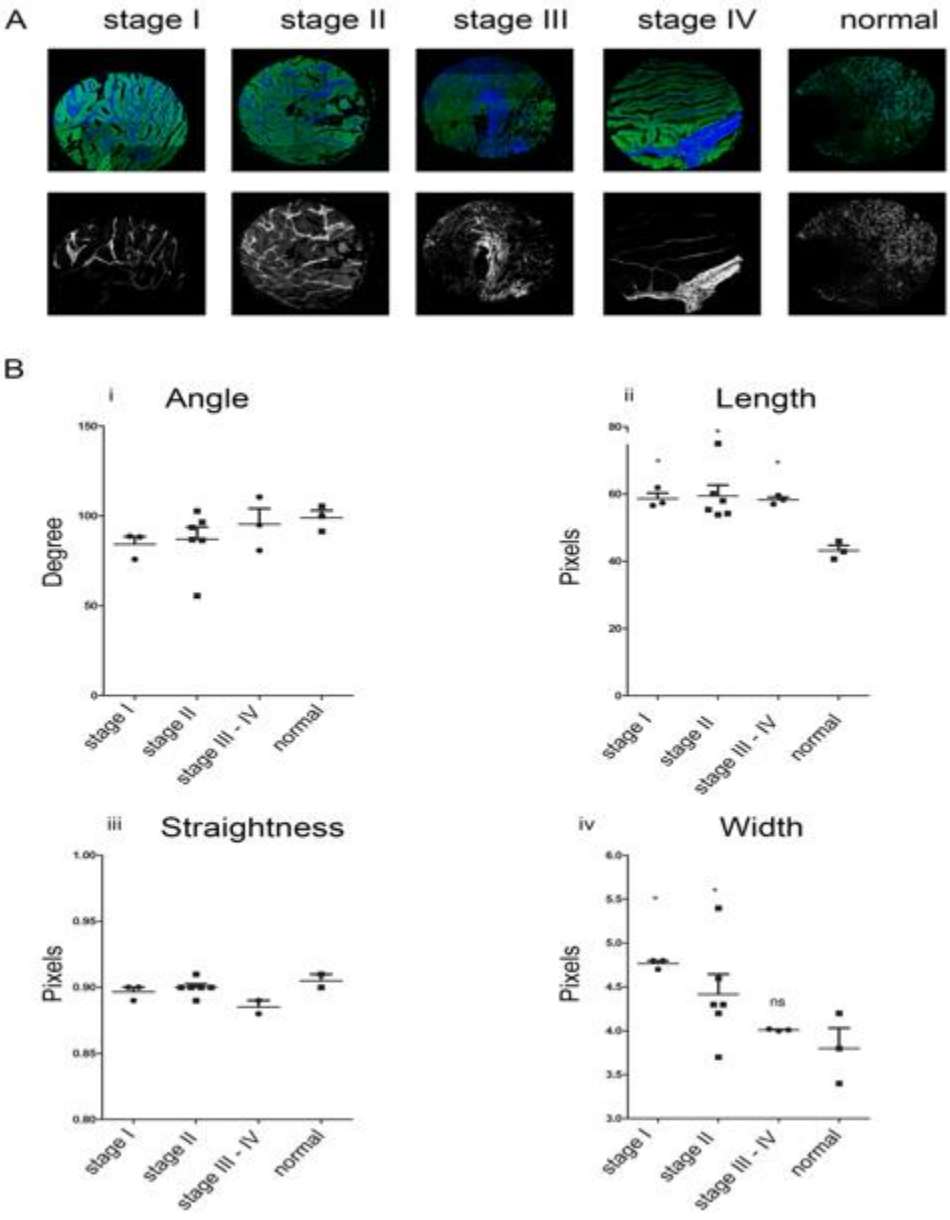
A
stage I
stage II
stage III
stage IV
normal
B
i
Angle
Degree
ii
Length
Pixels
iii
Straightness
Pixels
iv
Width
Pixels
ns
stage I
stage II
stage III - IV
normal

Figure 12: SHG images from a colon carcinoma TMA A) Representative SHG images of colorectal cancer tissue microarray (Co702a BioMax). In the first row collagen fibres are shown in blue, autofluorescent signal is shown in green. In the second row collagen fibres are shown in white on a black background. **B)** The quantitative parameters angle (i), length (ii), straightness (iii) and width (iv) were calculated basing on SHG images (n=3). A Statistical Mann-Whitney's unpaired test was performed (*$p<0.05$, **$p<0.01$)

3.3 Discussion:

3.3.1 Summary of findings in current study

In this study we showed that irradiation downregulated gene expression of *Col5a1* and subsequently its protein level. We also showed that irradiation affected collagen organisation using SHG to quantify changes in four different collagen markers: length, angle, width and straightness. The two parameters with a proven clinical relevance, width and length, were the only ones to change.

3.3.2 Irradiation decreases Col5a1 expression

Radiotherapy plays a central role in cancer therapy, its role in DNA damage and cell death is well established but less is known about the effects of radiation on the ECM. In our first experiment we used a fractionated dose of 5x3Gy to assess the changes in the irradiated ECM compared with the untreated matrix.

We assessed the effect of a fractionated dose of 5x3 Gy on tumour growth in three different animal models, using two pancreatic cancer cell lines, KPC and PANC1, and one murine colorectal cancer cell line, MC38.

We saw that irradiation decreased Col5a1 protein expression, but not Col1a1 protein levels. Irradiation decreased Col5a1 protein expression in three different cell lines, as tested with immunostaining. Col5a1 is normally present in the ECM of tissues that also express Col1. However, some studies showed that in some cancer types Col5a1 expression increased concomitantly with no changes in Col1a1 expression. For example, *Marian and Danner* showed that in a skin cancer model, tumour development was associated with an increase in Col5a1 expression in the dermis, and a lack of changes in the levels of Col1a1. These data suggest that Col5a1 may contribute to tumour progression, disturbing the interactions between the dermis and the epidermis[147]. Studies in the corneal stroma showed that Col5a1 regulates fibril architecture through its interactions with Col1a1. The interaction between the two collagen proteins is a mechanism capable of modulating fibril diameter and concurs in the regulation of collagen fibril diameters[116].

In addition, previous studies showed that Col5a1 had been found to be overexpressed in cancer and fibrosis[64,72,148]. However, there are not studies

investigating the radiation modulation of Col5a1 expression in the short and medium term after the treatment, before fibrosis.

Alpha-sma (α-sma) is a target for activated fibrogenic cells, myofibroblasts. However different studies suggests combining the expression of α-sma with Col1a1 to investigate fibrosis, considering that judging α-sma expression evaluation is not sufficient to define a fibrotic state[149,150]. In our study we looked at α-sma expression to understand if Col5a1 changes in protein expression could have been related to a change in the fibroblast population. Given that α-sma expression either increased in KPC or did not change in MC38, we concluded that the Col5a1 expression decrease after radiation was not related to fibroblast activation.

It is well established that fibrosis is a pathological condition due to fibroblast alteration, specifically an abnormal collagen deposition by myofibroblasts, after irradiation. Changes described in the pathology literature include patchy replacement of parenchyma by irregular and dense collagen fibres[151] which involved tissue stiffening, meaning that tissue become hardened, rigid and less compliant then normal, impairing normal tissue functionality. Therefore, our hypothesis is that in the short to mid term, from 3 days to 20 days in MC38, or just 6 days after radiation in PANC-1 and KPC, IR effects led to a downregulation of Col5a1, whose role was assembling Col1 fibres in a precise order. We could address the difference in α-sma production between KPC and MC38 considering that the subcutaneous tumour originated were histologically different. KPC cells gave rise to a fibrous subcutaneous tumour similar to the human pancreatic tumour microenvironment which KPC tumours histologically

resemble, whereas MC38 cells generated a less fibrous tumour mainly composed of tumour cells.

Our data showed the decrease of COL5a1 to be gene regulated. The transcriptional regulation of COL5a1 had been studied by *Yoshioka et al*[152]. They showed that in order to be transcribed, COL5a1 needs the ubiquitous expression of the transcription factor Sp1 and CBF/NF-Y[152]. In addition, Sp7/Osterix binds to the Sp1 site of COL5a1 and increase specifically the transcriptional activity in osteoblastic cells[153]. Gene expression was then controlled by a series of complex interaction of many factors. Previous studies also showed that miR-29 mediates TGF-β1-induced ECM synthesis through PI3K-AKT pathway in human lung fibrosis[154] whereas the TGF-β/Smad signalling pathway is involved in miR-29 regulation in renal fibrosis[155]. miR-29 also downregulates the expression of *COL5A1* in MC3T3-E1 cells and NIH3T3 cells post-transcriptionally[156]. In addition, TGF-β directly activates *COL5A1* gene in the osteoblast cell line MC3T3-E1 during osteogenesis[157] and in mouse hepatic stellate cells. *COL5A1* gene activation is followed by the deposition of COL5A1, COL1A1 and COL3 proteins and their fibrillar assembly[64]. TGF-β also plays a role in the radiation response and in the fibrotic process[158]. Therefore, in the future, it would be useful to investigate the role of TGF-β in relation to Col5a1 expression in our animal models.However, even if our data are consistent with the idea that Col5a1 dowregulation led to a decrese in protein expression other reasons can not be excluded.

MMP-2 and MMP-9 had been reported as metalloproteinases degrading denatured Col5a1[64] and native Col5a1 respectively. We did not see any change in the level of MMP-9 or in MMP-2 activity and we concluded they had no role in

degrading Col5a1 protein in our model. However, other enzymes activity, such as TIMP-1, needs to be investigated.

All the cited studies have been conducted on *COL5A1* gene regulation in fibroblasts, therefore further studies need to be done to better understand which pathway regulates *COL5A1* expression in cancer cells.

In our study we did not reach the fibrotic stage, and the changes we assessed in the ECM composition were opposite to the abnormal overproduction of ECM molecules that characterise fibrosis.

3.3.3 **Irradiation affects collagen organization**

The second part of this chapter focuses on the processes of degradation of collagen under the influence of ionizing radiation, using an *in vivo* subcutaneous model and two different cell lines, MC38 and KPC, and employing a fractionated dose of 5x3Gy.

We evaluated changes in the collagen organization qualitatively with Red Picrosirius staining and quantitively with SHG. We showed that, after radiation, *in vivo* cancer samples showed a disorganised bundle of collagen fibres.

Previous studies showed that, in cancer, collagen fibre density increases and there is a change in fibre reorganization. For example, in 2017 *Zhou et al*[127] showed that, compared with their non plastic counterparts, collagen fibre alignment, width, length and straightness in gastric cancer were intensively elevated, showing that the structure and organization of collagen fibres in the tumour microenvironment were deeply reorganised. Subsequently, they screened those five parameters (straightness, density, length, width and alignment) to understand if any of those could have been used as a prognostic marker. As an end point they used 5-year overall survival. They found out that three of these collagen parameters were able to predict survival (density, length and width), whereas collagen alignment and straightness were not good predictors. The strongest prognostic marker identified was width[127]. In line with *Zhou et al* findings, our data showed that radiation had an effect in reducing only collagen width and length. This mean that the effect of radiotherapy on the collagen organization led to a reduction of width and length back to healthy levels, suggesting that a possible mechanism by which radiation kill cancer cells is through the reshaping of the collagen fibres.

The effect of radiation on collagen organization in the period before fibrosis evolves are less investigated. However, *Maslenikova et al* published a comprehensive study with the evaluation of the dose-time dependences of structural changes occurring in collagen within 24 hours to three months after gamma-irradiation at doses from 2–40 Gy *in vivo*[159]. They found that the radiation-induced modifications of collagen could be observed as early as 24 hours after irradiation to a dose of 2 Gy. This, together with our findings, suggest that radiation affects the ECM organization, and in particular collagen fibres, early after the irradiation treatment.

To conclude, taking into consideration the involvement of Col5a1 in the assembly of Col1a1 fibres and in fibrillogenesis together with its downregulation after radiation, we suggest that the absence of Col5a1 was connected with the downregulation of collagen fibres.

4 Chapter 4 – *Col5a1* downregulation affects tumour growth

4.1 Introduction

4.1.1 The importance of 3D Culture in tumour microenvironmental studies

Cell culture is an invaluable tool in studying cell biology, tissue morphology, mechanisms of diseases, drug action, protein production and the development of tissue engineering[160]. It is also a fundamental step in the preclinical validation process in cancer drug discovery. Standard two-dimensional cell cultures are simple and convenient, but present significant limitations in reproducing the complexity and pathophysiology of *in vivo* tumour tissue[161].

Three-dimensional culture systems are of great interest in cancer research since tissue architecture and the extracellular matrix (ECM) influence the tumour development and the response to microenvironmental signals may be more closely replicated than in 2D[33]. Solid tumours grow in a three-dimensional (3D) spatial conformation, as a result they are heterogeneously exposed to oxygen and nutrients, as well as to other physical and chemical stresses. A 2D monolayer culture is not able to mimic this diffusion-limited distribution of oxygen and nutrients to cancer cells[161]. In addition, comparative studies of WT and tumour cells in monolayer cultures have shown that cancer cells lose their ability to retain some of the ECM components, such as fibronectin or laminin when cultured in a monolayer [162]. In contrast, tumour cell spheroids synthesised and retained some of the components commonly present in tumours and healthy ECM, such as proteoglycans, fibronectin, laminin [162].

Three dimensional (3D) ECM-based models were developed in order to better mimic physiological conditions and recreate cell-ECM interactions, making cells grew embedded in ECM proteins matrix. Crucial factors of the tumour response like hypoxia, pH or tumour resistance mechanisms can be easily

investigated *in vitro* using a 3D approach. In addition, morphology may play an important role in cell behaviour. Whereas 3D ECM grown tumour cells have a round cell shape similar to tumour cells from cancer biopsies, 2D grown cells grow on a monolayer are flat and spread. As showed by *Cordes et al*, these morphological differences are highly likely to contribute to the different responses in regard to radiosensitivity in 3D and 2D cultures[163].

In order to address the hypothesis that Col5a1 has a role in tumour behaviour or in response to radiation we used a 3D *in vitro* model to better mimic physiological conditions.

4.2 Results

4.2.1 **The downregulation of Col5a1 affects *in vitro* migration and tumour growth**

To address the role of Col5a1 in colorectal and pancreatic cancer we knocked-down *Col5a1* expression in murine MC38 and KPC cancer cells using lentiviral-based siRNA. After selection using puromycin, cells were examined for *Col5a1* expression by quantitative RT-PCR at three different time points. *Col5a1* siRNA introduction led to gene downregulation. In particular, there was a 3.4 fold decrease after 24 hours, of 6.5 after 48 hours and of 2.3 after 72 hours. In the cells transfected with a non-targetting siRNA (nt_siRNA) *Col5a1* gene expression increased at 48 hours, but then returned to baseline **(Figure 13A)**. Based on these results we decided to use the siRNA transfected cells 48 hours after transfection.

Cells with downregulation of *Col5a1* were then compared to the controls cells for proliferation, radiosensitivity, migration and growth *in vitro*.

MTT was used to detect the effects of *Col5a1* downregulation on cell proliferation in KPC. When the expression of *Col5a1* was downregulated, cell proliferation was approximately two times lower compared with the control group **(Figure 13B)**.

To further investigate the role of *Col5a1* in radio-responsiveness colony formation was assayed after IR exposure. Plating efficiency, as the percentage of cells that give rise to colonies, was calculated for both MC38 and KPC. In WT MC38 PE was 65.3%, decreasing to 52.3% in the *Col5a1* KD cell line **(Figure 13C)**. Plating efficiency for both control and *Col5a1* KD KPC cells was close to 100%. In KPC the number of colonies formed by *Col5a1*-siRNA cells were not significantly different from that of control cells **(Figure 13F)**. We also performed

clonogenic survival assays with these cells. Here survival after radiation was not significantly changed by *Col5a1* KD in both cell types. **(Figure 13E)**. Thus in both cell lines tissue culture radiosensitivity was not increased by *Col5a1* knock-down.

We next conducted studies using 3D MC38 and KPC multicellular spheroids embedded in a collagen I based matrix **(Figure 14A-C)**. The invasiveness of each carcinoma spheroid was assessed calculating the diameter of the invaded area as described in Materials and methods, normalized to the initial diameter of the spheroid. Compared to the controls, MC38 *Col5a1* knock-down spheroids showed that a decrease of *Col5a1* expression significantly reduced invasion of the cells into the surrounding matrix **(Figure 14B)**. 48 hours after being embedded in collagen matrix, KPC WT spheroids migrate 60% more than *Col5a1* KD spheroids, suggesting that reduced expression of *Col5a1* reduced cancer migration. However, 24 hours after embedding, both spheroids showed a similar rate of migration, suggesting that *Col5a1* downregulation did not inhibit the migration process in the early stages perhaps before deposition of this collagen **(Figure 14D)**.

To further determine the importance of Col5a1 in 3D tumour growth, *Col5a1* KD and WT MC38 spheroids were grown for 6 days and their diameter was measured at day 1, 3 and 6 **(Figure 14E)**. Reduction of *Col5a1* expression had a significant correlation with 3D tumour growth, suggesting a role for Col5a1 in tumour growth **(Figure 14F)**.

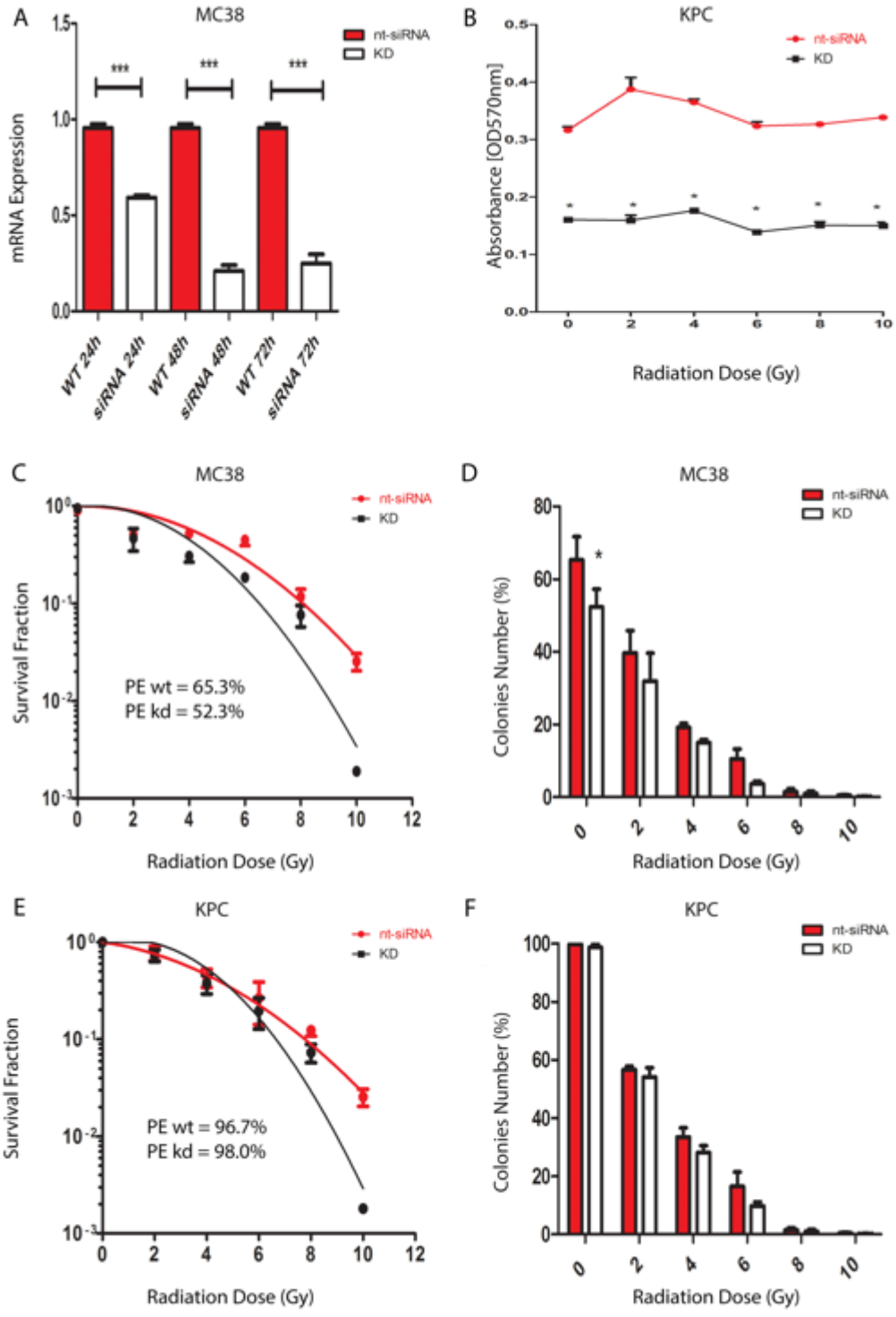
A
MC38
nt-siRNA
KD
mRNA Expression
1.5
1.0
0.5
0.0
***
***
***
WT 24h
siRNA 24h
WT 48h
siRNA 48h
WT 72h
siRNA 72h
B
KPC
nt-siRNA
KD
Absorbance [OD570nm]
0.5
0.4
0.3
0.2
0.1
0.0
0
2
4
6
8
10
Radiation Dose (Gy)
C
MC38
nt-siRNA
KD
Survival Fraction
PE wt = 65.3%
PE kd = 52.3%
Radiation Dose (Gy)
D
MC38
nt-siRNA
KD
Colonies Number (%)
80
60
40
20
0
*
Radiation Dose (Gy)
E
KPC
nt-siRNA
KD
Survival Fraction
PE wt = 96.7%
PE kd = 98.0%
Radiation Dose (Gy)
F
KPC
nt-siRNA
KD
Colonies Number (%)
100
80
60
40
20
0
Radiation Dose (Gy)

Figure 13: Col5a1 KD affects MC38 and KPC *in vitro* phenotype. A) Demonstration of *Col5a1* KD (KD). KPC and MC38 cells were transfected with siRNA and nt-siRNA and collected after 24h, 48h and 72h. The graph shows the fold change of *Col5a1* fold normalised to beta-actin. Data were plotted in log2 scale and presented as mean + SD (*p <0.05). **B)** Radiation dose-response curves via MTT proliferation assays in pancreatic cancer cell line KPC. Experiments were done in triplicate and were independently repeated three times (*p <0.05). **C-E)** Clonogenic survival after Col5a1 KD. 3 independent replicates were performed per cell line. **D-F)** Statistical results of colony-forming assays presented as percentage of colonies numbers in the respect of the number of seeded cells. Statistical significance was assessed by the Whitney-Mann unpaired test (differences were statistically not significant). The data in the graphs were expressed as mean number ± SD of three different experiments.

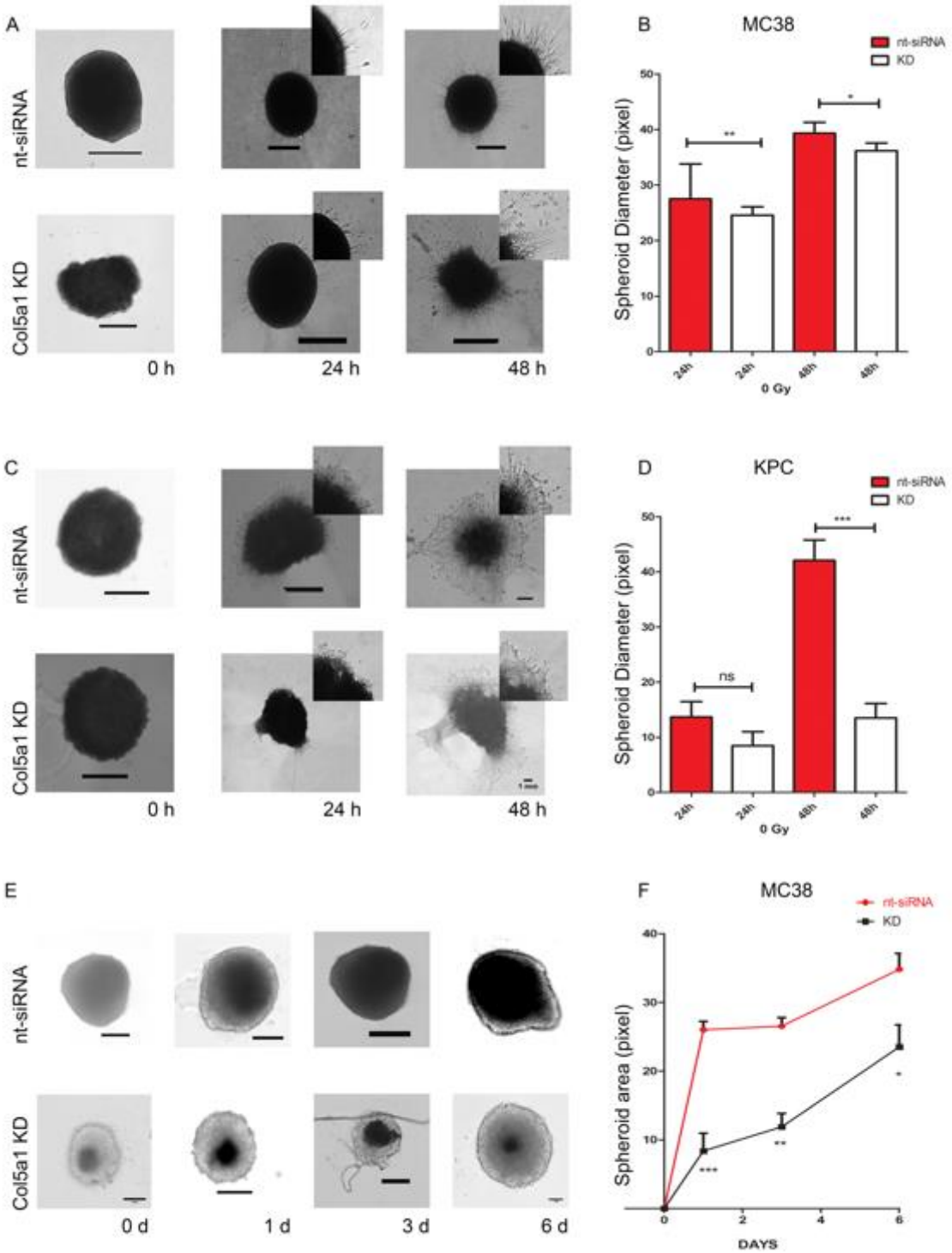
A
nt-siRNA
Col5a1 KD
0 h
24 h
48 h
B
MC38
nt-siRNA
KD
Spheroid Diameter (pixel)
0 Gy
C
D
KPC
ns
E
0 d
1 d
3 d
6 d
F
Spheroid area (pixel)
DAYS

Figure 14: Col5a1 KO affects MC38 and KPC 3D migration and growth

A-C) Spheroid Migration Assay. Cells were transfected with siRNA *Col5a1* or NT-siRNA and cultured in agarose for 24 hours. Spheroids were allowed to grow for 72h at 37C. Pictures were taken with Celigo at 0h, 24h and 48h after the embedding in collagen (Scale bar=1mm). **B-D)** Invasion assay quantification. Images were quantified using ImageJ (n=10 spheroids per condition in three independent experiments). **E)** Spheroid Kinetic Assay. MC38 wt and transfected cells were allowed to form spheroids for 5 days. Spheroids were imaged using Celigo at day 0,1, 3, and 6 after spheroid formation (scale bar=1 mm). **F)** Spheroid size has been quantified calculating the area using ImageJ (n=8 spheroids/treatment in three independent replicates). (*p<0.05, **p<0.01, ***p<0.001).

4.2.2 *Col5a1* deletion in KPC enhances radio sensitivity

To further explore the functional significance of *Col5a1*, we established a *Col5a1* knockout KPC cell line using the CRISPR-Cas9 gene editing system. We selected the cells with puromycin and seeded 0.5 cell/well in a p96 well. Next we isolated 8 single colonies from the transfected cells and confirmed the knockout efficiency through RT-PCR. The *Col5a1* RNA could not be detected in any of them **(Figure 15A)**. To assess the role of *Col5a1* in cell proliferation we then assessed the cell growth rate and we performed a MTT assay to examine cell proliferation. The absence of Col5a1 caused a delay in cell growth from the second day after plating, reaching a decrease in growth of around 80% on day 4 after the cell seeding **(Figure 15B)**. The MTT proliferation assay also showed that the KD of Col5a1 slowed cell proliferation. **(Figure 15C)**. These experiments suggest that complete absence of *Col5a1* has a more severe phenotype than KD with some Col5a1 still present.

The clonogenic colony formation assay was employed to determine the radiosensitivity of *Col5a1* KO KPC compared to WT KPC cell line. Our results showed that *Col5a1* KO cells were more sensitive to the killing effects of radiation than WT cells **(Figure 15D-E-F)**. Representative images of the size and number of colonies per well are shown in **Figure 15D**. With no radiation there were significant differences in plating efficiencies between the different clones. **(Figure 15E)**. Radiation decreased the number and survival of colonies in all three groups in a dose-dependent manner, and *Col5a1* KO cells were more sensitive than the WT group. Specifically, the difference was statistically significant for radiation doses of 2 and 4 Gy (***$p<0.001$) **(Figure 15E-F)**.

These results indicated that *Col5a1* knockout can enhance the radiosensitivity of KPC cells. When we compared *Col5a1* KO KPC cells to *Col5a1* KD KPC cells we noticed that the complete silencing of the protein correlated with a stronger effect on radiosensitivity in KPC.

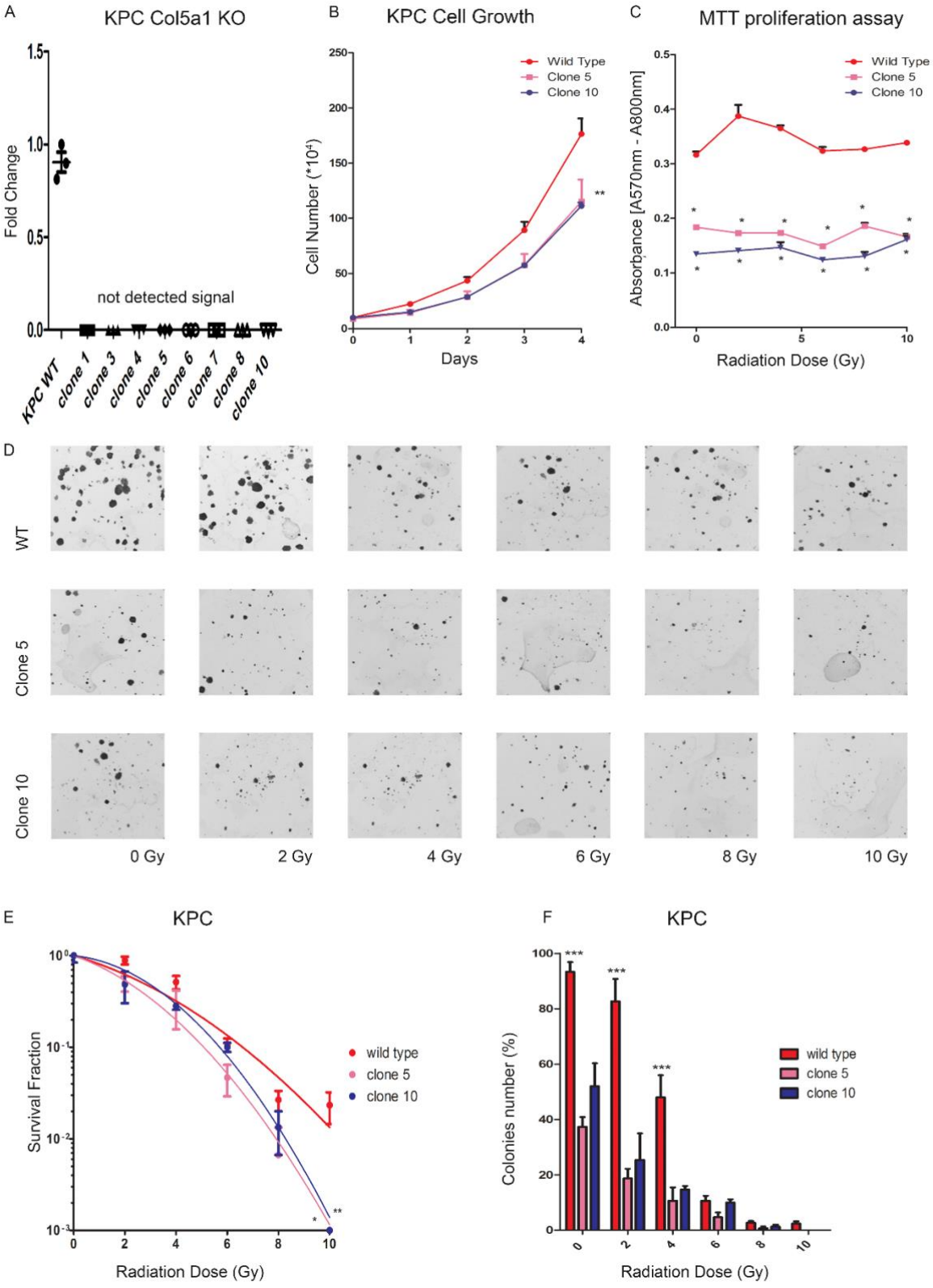
A
KPC Col5a1 KO
Fold Change
not detected signal
KPC WT
clone 1
clone 3
clone 4
clone 5
clone 6
clone 7
clone 8
clone 10
B
KPC Cell Growth
Wild Type
Clone 5
Clone 10
Cell Number (*10⁴)
Days
C
MTT proliferation assay
Absorbance [A570nm - A800nm]
Radiation Dose (Gy)
D
WT
Clone 5
Clone 10
0 Gy
2 Gy
4 Gy
6 Gy
8 Gy
10 Gy
E
KPC
Survival Fraction
wild type
clone 5
clone 10
Radiation Dose (Gy)
F
KPC
Colonies number (%)
wild type
clone 5
clone 10
Radiation Dose (Gy)

Figure 15: Effect of Col5a1 KO on MC38 and KPC *in vitro*

A) Confirmation of *Col5a1* KO. Graphs shows *Col5a*1 fold change to Col5a1 by qRT-PCR. Data were presented as mean ± SEM. **B)** Growth curve was performed counting cells daily for 4 days. Error bars represent mean ± SEM of 3 experiments. **C)** Radiation dose-response curves via MTT proliferation assays in pancreatic cancer cell line KPC WT and KO cells clones 5 and 10. Experiments were done in triplicate and were independently repeated three times. **D)** Culture dishes with stained colonies of a representative experiment. **E)** Statistical results of colony-forming assays presented as percentage of colonies numbers in the respect of seeded cells. Statistical significance was assessed by the Witney Mann's unpaired test: $^{*}p < 0.05$ was considered significant; $^{***}p < 0.001$ very highly significant. The data in the graphs are expressed as mean number ± SD of three different experiments. **F)** Survival fraction after *Col5a1* KO. 3 independent replicates were performed per cell line. (*p<0.05, **p<0.01, ***p<0.001).

4.2.3 *Col5a1* KO affects 3D migration by KPC

We next investigated whether the *Col5a1* influence on cell migration was confirmed in our KO model. We previously showed that *Col5a1* KD reduced migration by 60% over 48 hours in KPC. We repeated this assay with the seven different KPC *Col5a1* KO clones generated by Crispr/Cas9 to confirm the role of *Col5a1* in tumour migration. With no radiation, WT spheroids showed a migration increase of almost 100% in 48 hours. All the KO clones except for clone 5 showed a much slower migration rate, suggesting that the lack of *Col5a1* affects their ability to migrate **(Figure 16A-Bi-ii)**.

Following radiation, migration of cells in WT KPC spheroids was reduced **(Figure 16C-E)**. Cells from *Col5a1* knock-out KPC spheroids had a high degree of variability from clone to clone and radiation dose. After 2 Gy radiation, Clone 1 migration was inhibited similarly to WT. Clone 2 and clone 4 significantly shrunk 48 hours after radiation, and in contrast Clone 5, 6, 8 and 10 increased migration **(Figure 16Dii)**. A 10 Gy dose led to an increase in migration in the majority of the clones. Clone 4, 5, 6, 8 and 10 showed a significant increase in migration, that is in contrast to clone 4 for which a 2 Gy dose led to a decrease in migration. The 10Gy dose inhibited migration for clone 2 spheroids **(Figure 16Fii)**. Whereas outgrowing WT KPC cells appeared as scattered, ameboid-like migrating cells after irradiation, the highly migrating spheroids, such as WT 0Gy, Clone 10 after irradiation and Clone 5, remained interconnected, suggesting collective migration. Overall there was no pattern apparent for these results.

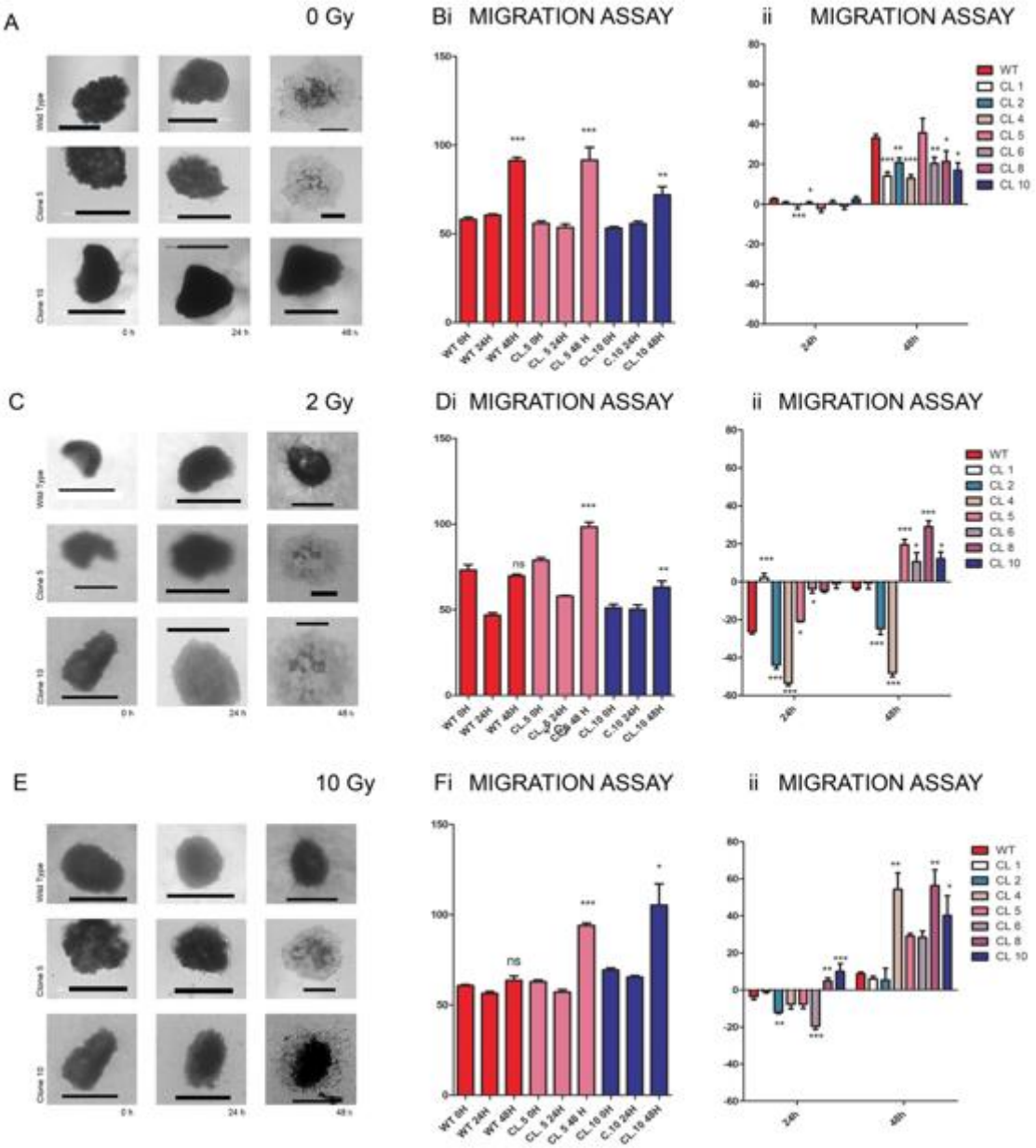
A
0 Gy
Bi MIGRATION ASSAY
ii MIGRATION ASSAY
C
2 Gy
Di MIGRATION ASSAY
ii MIGRATION ASSAY
E
10 Gy
Fi MIGRATION ASSAY
ii MIGRATION ASSAY
WT
CL 1
CL 2
CL 4
CL 5
CL 6
CL 8
CL 10
24h
48h
ns

Figure 16: 3D Migration Assay. A-C-E) 3D Spheroids Migration Assay. WT and KO cells were cultured in agarose for 24 hours. Spheroids were allowed to grow for 72h at 37C. Pictures were taken with Celigo at 0h, 24h and 48h after the embedding in collagen (Scale bar=500um). Representative images of WT, clone 5 and clone 10 spheroids. Spheroids were treated with different radiation doses: 0 Gy (A), 2 Gy (C) and 10 Gy (E). **B-D-F)** Invasion assay quantification. Images were quatified using ImageJ (n=10 spheroids per condition in three independent experiments). Spheroids were treated with different radiation doses: 0 Gy (B), 2 Gy **(D)** and 10 Gy **(F)**. **Bi-Di-Fi)** Clone 5 and clone 10 spheroid migration 0, 24 and 48 hours after the embedding in collagen. **Bii-Dii-Fii)** Migration assay graph normalised to spheroid length at 0h. (*p<0.05, **p<0.01, ***p<0.005).

4.2.4 **Col5a1 KO affects tumour growth *in vivo***

To further evaluate the impact of *Col5a1* on tumour growth, we examined tumorigenesis *in vivo*. After subcutaneous injection of the WT and KO cells ($2.5x10_5$) into the right flank of C57/Bl6 mice to allow tumour formation, we monitored tumour growth for a maximum of 32 days. Compared with the WT group, the subcutaneous tumours from 3 different KO cells were significantly reduced in volume **(Figure 17Ai)**. WT tumours reached the ethical end point 22 days after injection, on the same day KO tumours volumes were reduced by a percentage range between 55 and 80% (tumour volumes range: 200 mm_3 - 450 mm_3) **(Figure 17Aiii)**. The Kaplan Meier survival analysis demonstrated that the absence of Col5a1 in tumour cells prolonged the time until the ethical endpoint was reached. The average times were 22 days for the WT group, 26 days for Clone 5 and 30 days for Clone 8 and 10 **(Figure 17Aii)**. Thus, ablation of *Col5a1* resulted in slower growing tumours.

After radiation, however, the tumour growth of *Col5a1* KO groups was not different from the WT **(Figure 17Bi)**. This result was confirmed by the Kaplan Meier analysis, showing that the average survival time was 32 days for all the groups **(Figure 17Bii)**. Another way to describe this result is that irradiation had a stronger effect on retardation of WT tumour growth than on the KO tumours **(Figure 17Ci)**. On day 22, the tumour volume of control samples was up to 1000 mm_3, whereas the irradiated samples showed an average volume of 400 mm_3 **(Figure 17Ciii)**. The Kaplan Meier survival curve of WT tumours showed a delay of 10 days after irradiation until endpoint **(Figure 17Cii)**. Clone 5 seemed to be affected more from radiation than to Clone 10. The tumour growth rate was significantly slowed down after irradiation in Clone 5 group but not for Clone 10

(Figure 17Di-Ei). Tumour volume size at day 26 was approximately 1000 mm^3 for unirradiated clone 5 samples, and 45% less for irradiated tumours **(Figure 17Diii)**. Clone 10 tumours volumes did not show any statistical difference with or without irradiation **(Figure 17Eiii)**. The Clone 5 Kaplan Meier survival curve delay after irradiation consisted in 6 days **(Figure 17Dii)**, and 2 days for clone 10 **(Figure 17Eii)**. Just as absence of *Col5a1* led to decreased cellular growth in tissue culture, it also led to decreased tumour growth. After radiation the clones without *Col5a1* had a much reduced growth delay.

We might also speculate that the reduction in the tumoural Col5a1 resulting from radiation rendered the microenvironment from the WT more similar to the *Col5a1*KO leading to comparable growth rates. This hypothesis remains to be tested.

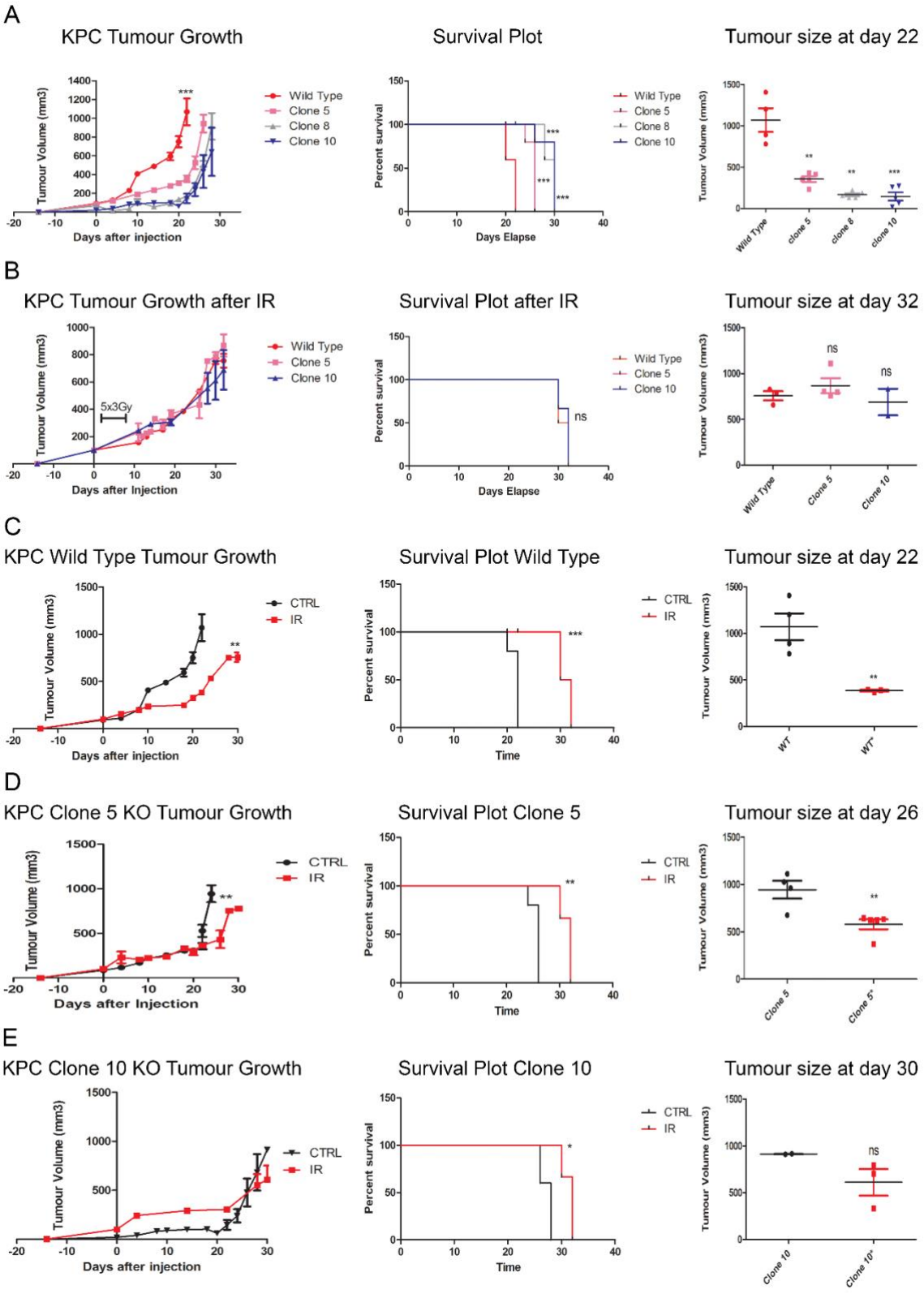
A
KPC Tumour Growth
Tumour Volume (mm3)
Days after injection
Wild Type
Clone 5
Clone 8
Clone 10
Survival Plot
Percent survival
Days Elapse
Tumour size at day 22
B
KPC Tumour Growth after IR
5x3Gy
Survival Plot after IR
ns
Tumour size at day 32
C
KPC Wild Type Tumour Growth
CTRL
IR
Survival Plot Wild Type
Time
Tumour size at day 22
WT
WT*
D
KPC Clone 5 KO Tumour Growth
Survival Plot Clone 5
Tumour size at day 26
Clone 5
Clone 5*
E
KPC Clone 10 KO Tumour Growth
Survival Plot Clone 10
Tumour size at day 30
Clone 10
Clone 10*

Figure 17: WT and *Col5a1*KO tumour growth. A) On the left, WT and *Col5a1* KO KPC tumour growth in untreated samples. In the middle, Kaplan-Meier curve. On the right tumour size volume measured at day 22. **B)** On the left, WT and *Col5a1* KO KPC tumour growth in irradiated samples. In the middle, Kaplan-Meier curve. On the right tumour size volume measured at day 32. **C)** On the left, WT KPC tumour growth in both irradiated and unirradiated samples. In the middle, Kaplan-Meier curve. On the right tumour size volume measured at day 22. **D)** On the left, Clone 5 *Col5a1* KO KPC tumour growth in both irradiated and unirradiated samples. In the middle, Kaplan-Meier curve. On the right tumour size volume measured at day 26. **E)** On the left, Clone 10 *Col5a1* KO KPC tumour growth in both irradiated and unirradiated samples. In the middle, Kaplan-Meier curve. On the right tumour size volume measured at day 30. Statistical analysis have been performed (*p<0.05, **p<0.01, ***p<0.005).

4.2.5 **Col5a1 levels in Irradiated tumours**

To examine the extent of Col5a1 expression in the subcutaneous tumours generated, we assessed the protein expression through immunofluorescence. Due to the elimination of *Col5a1* in the clones the tumour cells cannot supply Col5a1 to the tumour microenvironment, but other cells incorporated into the tumour stroma may do so. As expected, Col5a1 was highly expressed in unirradiated WT tumours. Clone 5 and clone 10 showed very low Col5a1 expression, suggesting that tumour cells were the main source of Col5a1 in this model **(Figure 18A)**. Consistent with previous results, irradiation led to decreased Col5a1 expression in the WT tumours. Irradiation led to an increase in Col5a1 expression in the KO clones **(Figure 18A-B)**. Col5a1 expression in KO samples was almost three times more abundant than in the unirradiated WT. Col5a1 expression intensity in clone 5 irradiated samples was around 38 pixels and around 50 pixels for irradiated clone 10, whereas it was around 18 pixels in untreated WT samples **(Figure 18B)**. Thus there seems to be a compensatory mechanism for Col5a1 expression after radiation.

We then stained for α-sma expression in subcutaneous Col5a1 KO tumour samples (**Figure 19**). We failed in registering any change in α-sma expression. This suggests that, in our model, Col5a1 was not produced from fibroblasts. However, the result we show here came from a single α-sma staining experiment on a limited number of samples. Therefore further experiments are needed.

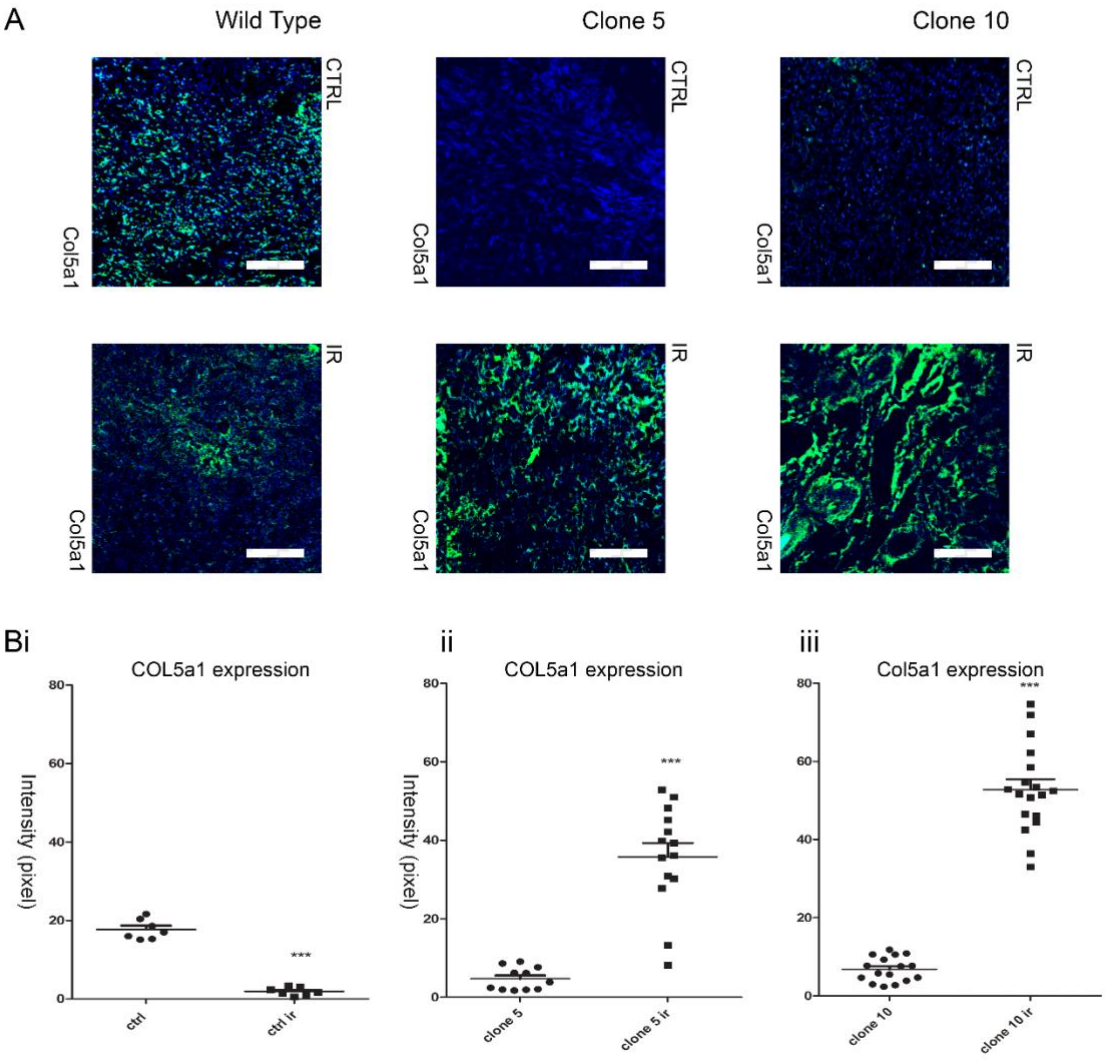

Figure 18: Col5a1 expression increase in KO clones after irradiation

A) Representative images of immunofluorescence staining in *Col5a1* KO KPC subcutaneous tumour samples. Col5a1 is shown in green. (scale bar=2mm). **B)** Quantification of Col5a1 expression in *COL5a1* KO KPC tumour samples. Images were quantified using ImageJ. Statistical significance was assessed by Mann-Whitney unpaired test: ***$p < 0.001$ very highly significant.

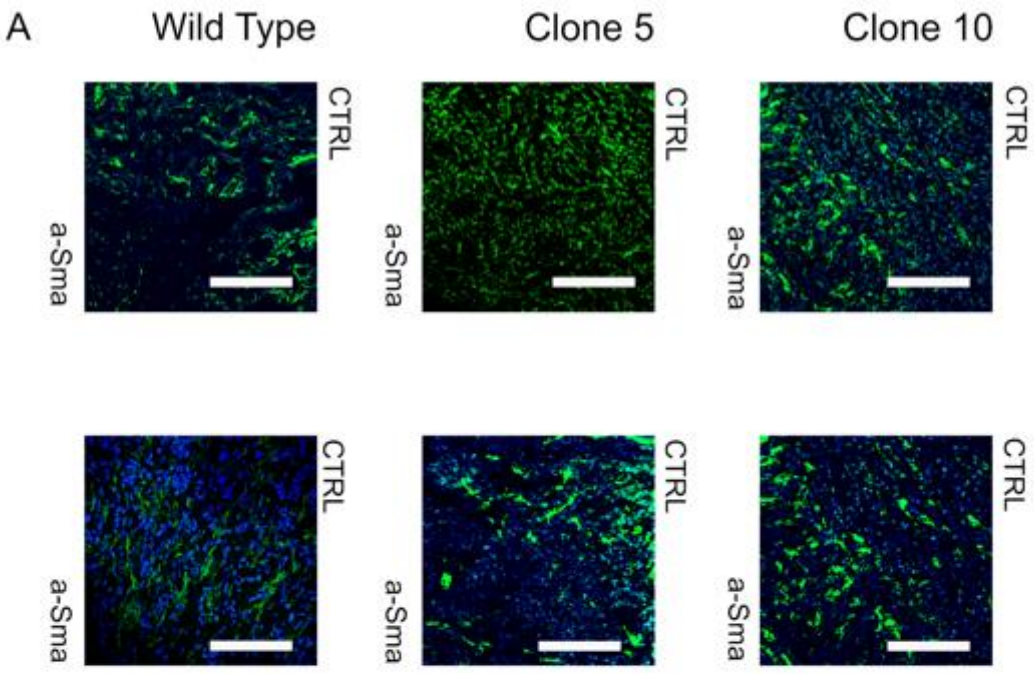
A
Wild Type
Clone 5
Clone 10
CTRL
a-Sma

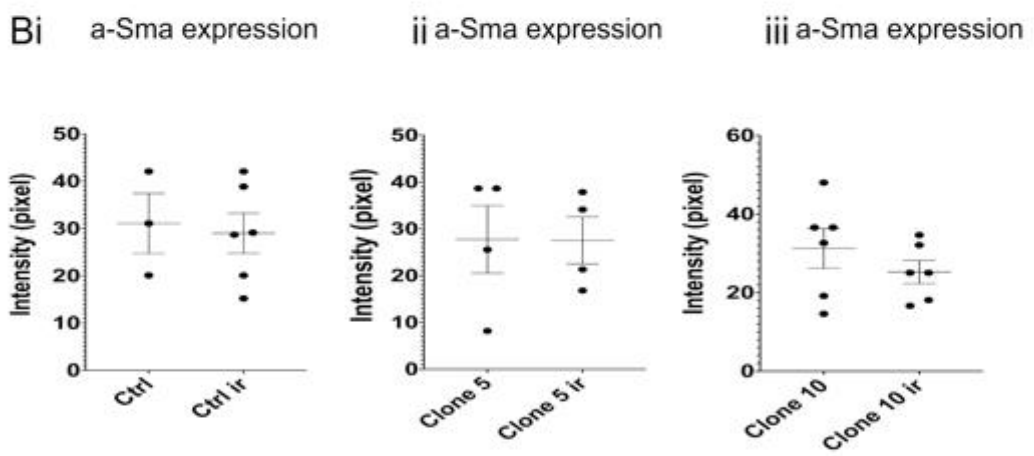
Bi a-Sma expression
ii a-Sma expression
iii a-Sma expression
Intensity (pixel)
Ctrl
Ctrl ir
Clone 5
Clone 5 ir
Clone 10
Clone 10 ir

Figure 19: α-sma expression does not significantly change in *COL5a1* KO clones after irradiation

A) Representative images of α-sma immunofluorescence staining in *COL5a1* KO KPC subcutaneous tumour samples. α-sma is shown in green. (scale bar=2mm).

B) Quantification of α-sma expression in *COL5a1* KO KPC tumour samples. Images were quantified using ImageJ. Statistical significance was assessed by Mann-Whitney unpaired test (ns= non significant)

4.2.6 *Col5a1 KO* affected collagen fibre formation

We next examined the effects of *Col5a1* KO on collagen deposition through Picrosirius Red Staining assay and Second Harmonic Generation. As shown in **Figure 10,** irradiation did not affect overall collagen deposition as revealed by Picrosirius Red Staining of WT KPC tumour samples although the structure of the ECM fibres was clearly different. **(Figure 20A-B)**. Strikingly, irradiation seemed to have the opposite effect on *Col5a1* KO tumours. The percentage of positive stained area in unirradiated Clone 5 and Clone 10 tumours was similar to the WT tumours, around 40% **(Figure 20B-D-F)**. Irradiation led to an increase of red signal, suggesting that irradiation results in an increase in collagen deposition in the Col*5a1* KO tumours **(Figure 20D-F**) noting that these tumours paradoxically contain more Col5a1 than WT as judged by immunofluorescence. The red signal was given by Picrosirius red, an acidic dye molecule that efficiently aligns and binds parallel to collagen fibres[164].

To more reliably characterize changes in collagen fibres, we determined quantitative parameters of the collagen fibres using SHG imaging. SHG microscopy is a powerful modality for imaging fibrillar collagen, due to its optical underlying physical origin, it is highly sensitive to the collagen fibril/fibre structure, and, importantly, to changes that occurs in collagen organisation during diseases such as cancer or fibrosis[121]. Using the open-source software CT-FIRE, we analysed width, length, alignment (angle) and fibre number, in *Col5a1*KO KPC subcutaneous tumours and their WT counterparts **(Figure 21B-C-D-E)**. As expected, irradiation disrupted collagen organisation in WT samples, showing a decrease in width, length and fibre number compared to the images from the unirradiated tumours, but with the alignment unchanged **(Figure 21)**. SHG

imaging showed a very weak signal in unirradiated Clone 5 and 10 tumours, suggesting that lack of *Col5a1* had a deleterious effect on collagen fibre formation **(Figure 21A)**. Collagen fibre number, width and length in tumours from KO *Col5a1* clones were significantly lower than in the WT counterpart **(Figure 21B-C-D-E)**. Unexpectedly, irradiation seemed to reverse the effect of *Col5a1* KO resulting in an increase of fibre number, collagen fibre length and width **(Figure 21)** consistent with the increased amount of COL5a1 seen in immunohistochemistry. Fibres number almost doubled after irradiation compared with the irradiated WT **(Figure 21E)**, whilst width and length increased by 20% and 10% respectively **(Figure 21B-C)**.

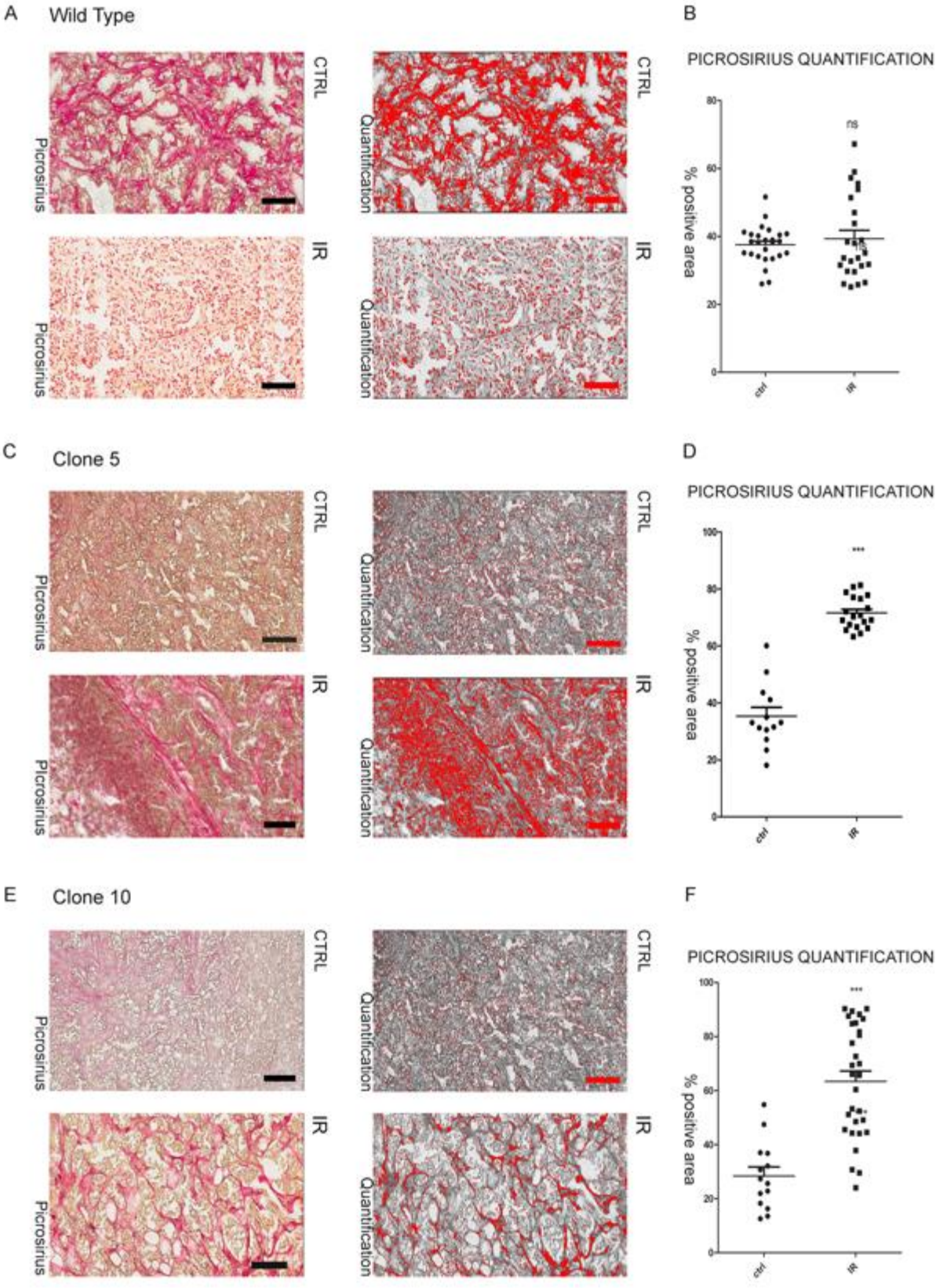
A
Wild Type
CTRL
IR
Picrosirius
Quantification
B
PICROSIRIUS QUANTIFICATION
% positive area
ns
ctrl
IR
C
Clone 5
D
PICROSIRIUS QUANTIFICATION
% positive area
***
E
Clone 10
F
PICROSIRIUS QUANTIFICATION
% positive area
***

Figure 20: *Col5a1* KO affects collagen deposition A) Representative images of WT KPC tumour samples stained with Picrosirius Red Staining. From the left: 100x magnification detail (Scale bar=100um), and an example of collagen quantification. **B)** Picrosirius signal quantification. Statistical Whitney Mann-test has been performed, differences are not significative. **C)** Representative images of *Col5a1* Clone 5 KO KPC tumour samples stained with Picrosirius Red. From the left: 100x magnification detail (Scale bar=100um), and an example of collagen quantification. **D)** Picrosirius signal quantification. Statistical Whitney Mann-test has been performed (***p<0.001). **E)** Representative images of *Col5a1* Clone 10 KO KPC tumour samples stained with Picrosirius Red. From the left: 100x magnification detail (Scale bar=100um), and an example of collagen quantification. **F)** Picrosirius signal quantification. Statistical Mann-Whitney test has been performed (***p<0.001)

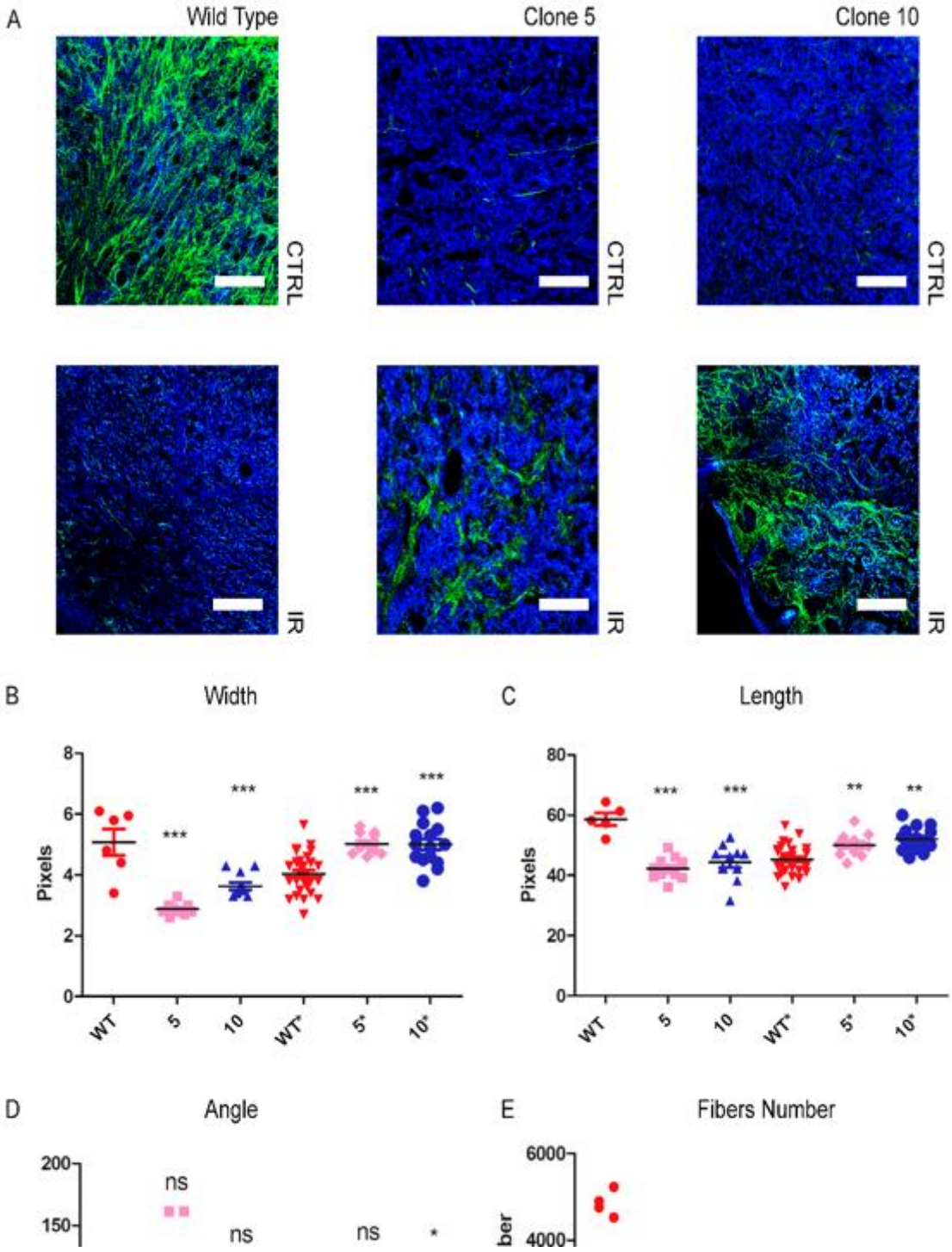
A
Wild Type
Clone 5
Clone 10
CTRL
IR
B
Width
Pixels
WT
5
10
WT*
5*
10*
C
Length
D
Angle
ns
E
Fibers Number
6000
4000

Figure 21: Second Harmonic Generation (SHG) Imaging and quantitative analysis of Collagen Fibres. A) Second harmonic generation microscopy of KPC WT and *Col5a1* KO subcutaneous tumours. Collagen fibres are shown in green. **B-E)** Collagen fibres were automatically extracted for analysis using the open-source software CT-FIRE. Quantitative parameters including width, length, alignment and fibres number were calculated basing on SHG images. Statistical Whitney Mann test has been performed (n=3, *p<0.05, **p<0.01, ***p<0.001). (WT,5 and 10 stand for untreated samples, WT*, 5* and 10* stand for irradiated samples)

4.3 Discussion

4.3.1 Summary of findings in current study

The present study showed that *Col5a1* has a role in tumour growth and radiation response. The reduction or ablation of this protein inhibited cell migration, cell proliferation, increased radiosensitivity *in vitro*, and inhibited tumour growth *in vivo*. We also showed that radiation had a different effect on WT and *Col5a1*KO KPC cells *in vivo* and *in vitro*, suggesting that the role of *Col5a1* in the radiation response needs to be further investigated. Therefore, despite the potential of Col5a1 as a therapeutic target in colorectal and pancreatic cancer, its correlation with radiotherapy needs to be better understood.

4.3.2 KD and KO of Col5a1 affect migration in 3D cell culture

A decrease (KD) or a complete lack (KO) of *Col5a1* gene expression seemed to reduce migration (3D migration assay), proliferation (MTT) and tumour growth (spheroids assay). These findings suggest that *Col5a1* is important in tumour migration and proliferation both in 2D and in 3D.

Recently *Feng et al*[165], showed similar findings in a ccRcc Caki-1 cell model. The KD of *COL5A1* led to cell growth inhibition in a time dependent manner as assessed by MTT essay, a decrease in migration and invasion as assessed by Matrigel invasion and wound healing assay and a significant increase in apoptosis[165]. These data support our hypothesis of a role for Col5a1 in tumour growth and migration.

Irradiation added a level of complexity to it. In the migration assay, the seven *Col5a1*KO clones did not respond consistently to radiation doses. As showed in figure 16, the lack of *Col5a1* reduced migration in all the clones, except for clone 5, whereas radiation led to an unexpected increase in migration in the majority of the KO clones after a dose of 10 Gy, and to a discrepant reaction after a dose of 2 Gy. There are no clear interpretations about this result. However, a possible explanation could be connected with the activation of TGF-ß signalling pathway. It has been shown that radiation activates TGF-ß signalling pathway in cancer progression[166] and that this activation induce collagen 1 production[167]. *Kahai et al* showed that *in vitro Col5a1* is a target of beta signalling pathway in osteoblasts[157]. In addition, it is known that the gene *Col5a1* is fundamental for Col1a1 fibres assembly in fibrils. After these considerations, we hypothesized that the increase of TGF-ß re-activated the expression of *Col5a1* in KO tumour cells.

To validate this hypothesis further experiments are needed, starting from investigating changes in TGF-ß and *Col5a1* expression in *Col5a1*KO samples after irradiation. Unfortunately, short term effects of radiation on ECM proteins, including Col5a1 are not well investigated.

4.3.3 **Lack of *Col5a1* increases radiosensitivity**

It is known that radiation sensitivity mechanisms in cancer are regulated by intracellular factors and interactions of cells with ECM or adjacent cells as well as with the tumour microenvironment. At the same time, Col5a1 is a member of collagen family and is known that collagens are overexpressed in the majority of cancers. Our data indicated that Col5a1 is involved in radiosensitivity, but the mechanism of how Col5a1 plays a role was not investigated here. In addition, the KO of the gene had a stronger effect than the KD. Gene KO and KD genes often give different results given issues of dosage and potential compensation. Some scientists maintain that both of these methods should be performed in order to understand the role of the protein[168].

Feng et al[165] recently showed that *Col5a1* KD caused significant decrease in colony numbers formed by Caki-1 cells. *Liu et al*[169] used CFA to investigate the role in radiosensitivity of COL1A1 showing that sh-RNA KD of this protein enhanced cells radiosensitivity whereas COL1A1 activation increased radioresistance[169].

In order to boost our findings we should test the effect of radiation on other *Col5a1* KO cell lines.

4.3.4 *Col5a1* KO inhibits tumour growth *in vivo*

It is known that COL5a1 is overexpressed in different tumours[114]. COL5a1 overexpression has been associated with increased malignancy in different cancer types[72,114,170]. To investigate the contribution of Col5a1 to tumour growth we established a subcutaneous tumour *in vivo* model from the pancreatic adenocarcinoma cell line *Col5a1*KO KPC or WT-KPC. The lack of Col5a1 resulted in notable slowing of the tumour growth. Tumours reached the culling point an average of 8 days earlier in WT compared to *COL5a1*KO animals suggesting that *Col5a1* has the ability to modulate tumour growth.

This hypothesis is supported by a recent study published by *Feng et al*[165]. They showed that COL5A1 expression increased together with the tumour diameter and stage in ccRCC tissue compared to adjacent normal tissue, suggesting a role for COL5A1 in tumour growth. They confirmed this data using a nude xenograft mice model of ccRCC CAKI-1 cell line and injecting *COL5A1*-siRNA or *COL5A1*-ntsiRNA intratumourally. Consistently with our results they saw that the group receiving the *COL5A1*-siRNA show a decrease in tumour growth along with a decrease in *COL5A1* expression, compared to control.

4.3.5 **Col5a1 is produced by tumour cells**

In our experiment, we found that in untreated tumours, Col5a1 was not expressed in KO tumours unlike the WT specimens, suggesting that mouse host cells did not compensate with increased production of Col5a1. Thus in these untreated tumours, our data suggested that the main source for Col5a1 in our model were tumour cells and not host cells such as fibroblasts. These findings agree with *Hynes*[28] and *Feng*[171] studies which showed that tumour cells also produce ECM proteins although collagen type I is usually mainly derived from fibroblasts. In particular, *Feng* group showed that in the multi cancer associated gene expression signature they identified, the majority of the genes, including α-sma were expressed in some xenografted human cells but not in the host mouse cells[171]. Together with the microarray study done by *Casey et al*[30], these papers show that cancer cells are also major producers of ECM proteins and suggested a more complicated mechanism in tumour cell/microenvironment cross-talk. Nonetheless little is still known about the mechanisms governing the production of ECM proteins by cancer cells.

In order to extend our data and confirm our hypothesis, further experiments focused on understanding which kind of cells, either cancer cells or fibroblasts are stimulated to produce Col5a1 and in which conditions should be performed.

4.3.6 **Irradiation starts a compensatory mechanism of Col5a1**

Fibrosis is a frequent and deleterious consequence of radiation therapy. Irradiation can initiate an anti-inflammatory response that leads to an abnormal production of ECM proteins by CAFs[79] called fibrosis. In previous studies fibrosis is observed after a minimum of 3 weeks after a high radiation dose[101], or 6 weeks after a lower dose[102], therefore we assumed that fibrosis had not developed in our samples. We collected tumours 20 days after the end of the treatment. In figure 21 we used SHG to show that irradiation provoked an increase in Col1 fibres number of 75% in clone 10 and 95% in clone 5 tumours. This result confirmed our previous findings that showed how irradiation mediated decrease of Col5a1 was then connected with a decrease in collagen fibres as quantified by SHG. What was more interesting and surprising is that irradiation showed an increase in fibres number as well as an increase in Col5a1 expression in the KO tumours but not in the WT tumours. Based on our observation it seems that radiation induced a compensatory mechanism in the *Col5a1*KO tumours which led to an increased host deposition of Col5a1.

One hypothesis to explain the increased deposition of Col5a1 is that it is a consequence of fibroblast activation. Many different studies have shown that irradiation of tissues results in activation of fibroblast (as identified by α-sma) and that in addition to activation there may also be an increase in numbers of fibroblasts. However, this hypothesis, that the increase of collagen deposition is connected with increase in fibroblast activation, does not fully explain why Col5a1 expression increases after irradiation in KO tumours but not in unirradiated tumours. This observation might suggest that as a response to radiation, the tumour needs to produce Col5a1 due to its pivotal role in forming and assembling

new bundles of collagen I fibres[116]. Based on our data we could speculate that Col5a1 is not necessary for the tumour to survive but it becomes indispensable when the tumour need to repair and grow after radiation damage[116].

The role of Col5a1 overall in cancer is not yet well investigated. Its role in the Ehlers Danlos Syndrome, which is the result of a mutation in *COL5A1,* is more understood. In a study using dermal fibroblasts, *Wenstrup et al*[70] suggested that Col5a1 may control the utilization of type I collagen during initiation of collagen fibril formation in some tissues. This would explain why the presence of Col5a1 is needed to start a compensatory effect when there is an increase in collagen deposition, and therefore an increase in collagen I assembly after irradiation, but not in untreated tumours.

These hypotheses await further experimentation.

5 General Discussion and Conclusion:

Over the past 20 years, different studies have revealed the importance of collagen and ECM in regulating fundamental physiological processes such as cell migration, proliferation and fibrosis[172,173]. As a consequence, cancer is no longer considered to be simply a disease of uncontrolled cell proliferation, but also that of dysregulation of the microenvironment.

In the last years a group of ECM molecules have emerged as valuable targets for disease prognosis and treatment. Hence, it is of great importance to unravel the mechanism underlying the ECM remodelling and its involvement in disease. Of great interest is the study of the dynamic changes of ECM biomechanisms associated with tumour progression. With the developing appreciation that biochemical forces are crucial determinants for tissue development, cell differentiation and homeostasis, it is reasonable to assume that losing the ability to sense, respond and adapt properly to such biochemical forces, by either tumour cells or stromal cells, contributes to tumour progression[29]. Hence, collagen, being the most important player within the ECM that generates these biochemical forces is no longer considered to be an inert and passive background.

One of the tools which advanced the knowledge of the ECM is proteomics. Proteomics has been used to study the ECM signature for different cancers such as lung cancer[174], pancreatic ductal adenocarcinoma[175,176], colorectal cancer[177,178] and breast cancer[179,180] in the last decade. In 2012, *Hynes et al*[28] developed a new method which connected proteomics-based methods with a bioinformatic definition of the 'matrisome' (a term that identifies the ECM and ECM-associated proteins) to analyse the protein composition of the tissue ECM.

This project contributed fundamentally to our understanding of the ECM , creating a comprehensible and complete inventory of ECM proteins and their associated modifiers that can be used as a basis for analyses of tissue specific ECM composition and that of changes which occur during physiological or pathological conditions, such as cancer. Once identified, ECM signatures can be further analysed with pathway or interaction analysis tools such as *MatrixDB*[181]. The *MatrixDB* was created in 2009 to enable the interrogation of data reporting interactions between ECM components, often neglected in general protein databases. The characterisation of the protein composition of the ECM by mass spectrometry depends on the availability of methods that enrich for ECM proteins. *Hynes et al*[28] also proposed a new method to extract ECM proteins. Analysis of the protein composition of the extracellular matrix presents challenges due to the diversity, large size, insolubility and cross-linking of these proteins. By contrast, most other cellular components are soluble even at relatively low concentrations of salt or detergents. The proposed protocol involved the depletion of intracellular proteins and the enrichment of insoluble ECM proteins and associated-proteins. In this thesis we used this method to obtain ECM protein fractions that could be analysed by western blotting.

Thanks to proteomics different collagens have been identified as tumour signature and possible tumour markers. For example, *Naba et al.* identified a series of different collagen molecules, including COL1A1, COL5A1, COL3A1, COL2A1, COL5A2 COL4A1 and COL6A1 as overexpressed during the angiogenic switch in pancreatic tumour islets[176]. In another study they found COL22A1 to be absent in normal colon and normal liver tissues but overexpressed in both colorectal cancer and liver metastasis[177]. COL1A1

expression was also shown to change during CRC tumour development from stages I to IV in a separate study conducted by Yang et al[182].

COL5A1 is present in the majority of connective tissue matrices where it plays a functional role in maintaining tissue integrity. During the malignant transformation COL5A1 is overexpressed and a study in pancreatic ductal adenocarcinoma showed that, via activation of FAK signalling, COL5A1 affects cancer cells viability, proliferation, migration and formation of metastases[72].

Our molecule of interest, COL5A1 is overexpressed in different cancer types such as breast cancer[108], pancreatic ductal adenocarcinoma[72],oral squamous cell carcinoma[109], thyroid carcinoma[110], ovarian cancer[111], gastric cancer[112], papillary thyroid carcinoma[75] and lung cancer[113]. In particular, COL5A1 has been identified as a detection factor in breast cancer diagnosis, due to there being a strict correlation between a high protein expression and an aggressive cancer phenotype and relation with a poor prognosis[114,115]. Despite the growing interest for COL5A1's role in cancer progression its function in radiation response is still elusive. This thesis confirmed the importance of COL5A1 in tumour development and suggested a role for COL5A1 in radiation response.

Our results indicated that Col5a1 is present in colorectal and pancreatic cancer and that it is downregulated following irradiation. The three *in vivo* experiments, which involve both murine and human cell lines, suggested that the decrease of Col5a1 expression happen as shortly as one week after the radiation treatment. It was surprising that we were able to observe substantial changes in collagen expression and collagen deposition as soon as 6 days following radiation treatment, considering that effects of radiation on the extracellular matrix are usually considered as long-term side effects on the extracellular matrix

and connected with the fibrotic process[89]. COL5A1 is a minor fibril collagen. Its role is not completely understood, but it is known to regulate fibrillogenesis and matrix organization[116]. Therefore our suggestion is that the downregulation of COL5A1 leads to alterations in the organisation of collagen fibres resulting in a decrease of ECM stiffness. *Miller et al.* show that ionizing radiation reduces the stiffness of both non-cellularised collagen scaffolds and *ex vivo* mammary tumours from transgenic mice[88]. Cell adhesion, cell spreading and cell migration all decrease in irradiated matrices, in line with what is known about cells interacting with a less stiff matrix[88]. In our study, the KD and the KO of *Col5a1* showed an inhibitory effect on cell migration and an increase in radio sensitivity, confirming our hypothesis that the lack of Col5a1 contributed to create a softer matrix. However, given the contradicting effects that radiation had on KO *Col5a1* tumours, this hypothesis needs further evaluation. As shown in Chapter 4, KO of *Col5a1* seemed to activate a compensatory effect after radiation stimulation that led to an increase in Col5a1 expression and less radiosensitivity. In order to confirm these data, further experiments are needed, including knocking-out *Col5a1* in an expanded panel of cell lines.

We also showed that the reduction in Col5a1 protein levels following irradiation was due to gene downregulation. The activity of MMP2 and MM9, two of the enzymes which are known to degrade Col5a1, did not change after irradiation, suggesting that protein degradation was not involved. The well described collagen degradation pathways were activated when there was an excess in collagen deposition with the goal of preventing the development of cancer fibrosis[172]. Our results showed that *Col5a1* gene expression was downregulated before any increase in Col1a1 expression or collagen deposition,

suggesting that Col5a1 could have an active role in inititating the radiation response that leads to ECM remodelling. We did not investigate which pathway regulates Col5a1 expression, however future studies should be directed to elucidate the role of TGF-ß signalling in Col5a1 radiation response as discussed in chapter 3.

The contribution of cancer cells to the ECM radiation response is still poorly understood. Our study strongly suggest that CoL5a1 was produced by cancer cells as well as by fibroblasts, and our *in vitro* study shows how KO and KD of Col5a1 expression led to changes in phenotype, including a decrease in cell migration and a change in radiosensitivity. Further studies need to be done in order to understand the exact contribution of fibroblasts and cancer cells to Col5a1 production and radiation response.

In addition we investigated the effects of radiation and Col5a1 depletion in collagen deposition. Our results confirmed that an increase in collagen fibres width and length are correlated with a tumourigenic condition as previously established[29]. Irradiation led to a decrease in collagen fibres width and length. Considering that irradiation is the main cause of RIF, this could sound controversial. Nonetheless the *in vivo* samples we analysed were collected at a relatively early time point, before the fibrotic process could take get started. This is interesting in light of the fact that irradiation affects the ECM before the inflammatory process that lead fibrosis start. This observation could lead to novel approaches on how to improve radiotherapy efficiency in order to make it effective before the occurrence of fibrosis. We also showed that *Col5a1* KO affected collagen deposition, resulting in a similar condition as irradiation. However, the combination of *Col5a1* KO and IR treatment unexpectedly showed a promotion

of collagen production. Our hypothesis is that in the absence of Col5a1, a compensatory effect takes place, probably driven by host cells..

To conclude, our results suggest that irradiation affects the tumour microenvironment, and the ECM in particular, through the downregulation of *CoL5a1* expression. We also showed that cancer cells seems to contribute to this process in a more substantial manner than fibroblasts. In addition, we demonstrated that Col5a1 has a role in collagen deposition.

Col5a1 knockdown and knockout reduced cell proliferation, inhibited cell migration and invasion *in vitro*, and inhibited tumour growth *in vivo*. Therefore, Col5a1 may be a novel prognostic biomarker and a promising therapeutic target for colorectal and pancreatic cancer. In this light, we suggest further elucidation of the molecular mechanisms underlying Col5a1 function following radiation as well as translation of our findings to human cells and specimens should be regarded as important fields of research.

6 Abbreviations

ECM	Extracellular Matrix
Col5a1	Collagen 5a1 (murine gene)
COL5A1	Collagen 5a1 (human gene)
Col5a1	Collagen 5a1 (murine protein)
COL5A1	Collagen 5a1 (human protein)
DDRs	Discoidin Domain Receptors
GFs	Growth Factors
TGF-ß	Tumour Growth factor-beta
MYC	MYC proto oncogene – bHLH transcription factor
EMT	Epithelial Mesenchymal Transition
TME	Tissue Microenvironment
CAFs	Cancer Associated Fibroblasts
LOX	Lysin Oxidase
CAFs	Cancer Associated Fibroblasts
PDAC	Pancreatic Ductal Adenocarcinoma
SHH	Sonic Hedgehog
α-sma	alpha-smooth muscle actin
COL	Collagen
LAIR-1	Leukocyte associated immunoglobulin like receptor 1
ER	Endoplasmic Retilicum
MMPs	Matrix metalloproteinases
CRC	Colorectal cancer
FAK	Focal adhesion kinase
RNA	Ribonucleic acid

IR	Irradiation
RT	Radiotherapy
DNA	Deoxyribonucleic acid
ROS	Reactive oxygen species
CAM	Chicken embryo chorio allantoic membrane model of angiogenesis
IPF	Idiophatic pulmonary fibrosis
RIF	Radiation induced fibrosis
Gy	Gray
siRNA	Small Interference RiboNucleic Acid
SHG	Second Harmonic Imaging
CFA	Colony Formation Assay
KD	Knock Down
KO	Knock Out
gRNA	guide RiboNucleic Acid
RT-PCR	Real Time Polymerase Chain Reaction
cDNA	complementary DNA
Ct	cycle treshold
CNMCS	Compartmental Protein Extraction Kit
BSA	Bovine Serum Albumin
PBS	Phosphate-buffered saline
HRP	Horseradish Peroxidase
MTT	Colorimetric assay with dye 3-(4,5-Dimethylthiazol-2-yl)-2,5-diphenyltetrazolium bromidefor

PE	Plating efficiency
SF	Surviving fraction
OCT	Optical Cutting Temperature compound
TACS	Tumour Associated Collagen Signature
WT	Wild type
CNS	Centreal Nervous System
OS	Overall Survival
TMA	Tissue Micro Array
miR-29	microRNA-29
PI3K-AKT	Phosphatidylinositol-3-kinase/Protein Kinase B
ccRcc	clear cell Renal cell carcinoma
nt-RNA	Non targeting RiboNucleic Acid
F	Fraction
MT1-MMP/TIMP-1	Membrane type-1 Matrix Metalloproteinase/tissue Inhibitor of Matrix Metalloproteinase-2
BC	Breast Cancer

7 Bibliography:

1. Theocharis AD, Skandalis SS, Gialeli C, Karamanos NK. Extracellular matrix structure. *Adv Drug Deliv Rev*. 2016;97:4-27. doi:10.1016/j.addr.2015.11.001
2. Frantz C, Stewart KM, Weaver VM. The extracellular matrix at a glance. *J Cell Sci*. 2010;123(24):4195-4200. doi:10.1242/jcs.023820
3. King MW. Extracellular Matrix: Glycosaminoglycans and Proteoglycans. *Integr Med Biochem - McGraw-Hill Educ*. www.accesspharmacy.com.
4. Schlie-Wolter S, Ngezahayo A, Chichkov BN. The selective role of ECM components on cell adhesion, morphology, proliferation and communication in vitro. *Exp Cell Res*. 2013;319(10):1553-1561. doi:10.1016/j.yexcr.2013.03.016
5. Rozario T, DeSimone DW. The extracellular matrix in development and morphogenesis: A dynamic view. *Dev Biol*. 2010;341(1):126-140. doi:10.1016/j.ydbio.2009.10.026
6. Giannandrea M, Parks WC. Diverse functions of matrix metalloproteinases during fibrosis. *Dis Model Mech*. 2014;7(2):193-203. doi:10.1242/dmm.012062
7. Theocharis AD, Manou D, Karamanos NK. The extracellular matrix as a multitasking player in disease. *FEBS J*. 2019:1-40. doi:10.1111/febs.14818
8. Castro NE, Kato M, Park JT, Natarajan R. Transforming growth factorβ1 (TGF-β1) enhances expression of profibrotic genes through a novel signaling cascade and MicroRNAs in renal mesangial cells. *J Biol Chem*. 2014;289(42):29001-29013. doi:10.1074/jbc.M114.600783
9. Roberts AB, McCune BK, Sporn MB. TGF-β: Regulation of extracellular matrix. *Kidney Int*. 1992;41(3):557-559. doi:10.1038/ki.1992.81
10. Todorovic V, Rifkin DB. LTBPs, more than just an escort service. *J Cell Biochem*. 2012;113(2):410-418. doi:10.1002/jcb.23385
11. Cichon MA, Radisky DC. Extracellular matrix as a contextual determinant of transforming growth factor-b signaling in epithelial-mesenchymal transition and in cancer http://www.tandfonline.com/doi/pdf/10.4161/19336918.2014.972788. *Cell Adhes Migr*. 2014;8(6):588-594. doi:10.4161/19336918.2014.972788
12. Furler RL, Nixon DF, Brantner CA, Popratiloff A, Uittenbogaart CH. TGF-β sustains tumor progression through biochemical and mechanical signal transduction. *Cancers (Basel)*. 2018;10(6):1-18. doi:10.3390/cancers10060199
13. Principe DR, Doll JA, Bauer J, et al. TGF-β: Duality of function between tumor prevention and carcinogenesis. *J Natl Cancer Inst*. 2014;106(2):1-16. doi:10.1093/jnci/djt369
14. Pickup M, Novitskiy S, Moses HL. The roles of TGFβ in the tumour microenvironment. *Nat Rev Cancer*. 2013;13:788. https://doi.org/10.1038/nrc3603.
15. Walker RA, Dearing SJ, Gallacher B. Relationship of transforming growth factor β1 to extracellular matrix and stromal infiltrates in invasive breast carcinoma. *Br J Cancer*. 1994;69(6):1160-1165. doi:10.1038/bjc.1994.228
16. Hazelbag S, Gorter A, Kenter GG, Den Broek L Van, Fleuren G. Transforming growth factor-β1 induces tumor stroma and reduces tumor infiltrate in cervical cancer. *Hum Pathol*. 2002;33(12):1193-1199. doi:10.1053/hupa.2002.130109

17. Roberts AB, Wakefield LM. The two faces of transforming growth factor β in carcinogenesis. *Proc Natl Acad Sci U S A*. 2003;100(15):8621-8623. doi:10.1073/pnas.1633291100
18. Ihn H. Pathogenesis of fibrosis : role of TGF-β and CTGF : Current Opinion i ... Current Opinion in Rheumatology : Pathogenesis of fibrosis : role of TGF-β and CTGF. *Curr Opin Rheumatol*. 2002;14:681-685.
19. Verona E V., Elkahloun AG, Yang J, Bandyopadhyay A, Yeh IT, Sun LZ. Transforming growth factor-β signaling in prostate stromal cells supports prostate carcinoma growth by up-regulating stromal genes related to tissue remodeling. *Cancer Res*. 2007;67(12):5737-5746. doi:10.1158/0008-5472.CAN-07-0444
20. LEASK A, ABRAHAM DJ. TGF-β signaling and the fibrotic response. *FASEB J*. 2004;18(7):816-827. doi:10.1096/fj.03-1273rev
21. Luong VH, Chino T, Oyama N, et al. Blockade of TGF-β/Smad signaling by the small compound HPH-15 ameliorates experimental skin fibrosis. *Arthritis Res Ther*. 2018;20(1):1-13. doi:10.1186/s13075-018-1534-y
22. Sime PJ, Xing Z, Graham FL, Csaky KG, Gauldie J. Adenovector-mediated gene transfer to activate transforming growth factor beta1 induces prolonged severe fibrosis in lung. *J Clin Invest*. 1997;100(4):768-776.
23. Vallance BA, Gunawan MI, Hewlett B, et al. TGF-β1 gene transfer to the mouse colon leads to intestinal fibrosis. *Am J Physiol - Gastrointest Liver Physiol*. 2005;289(1 52-1):116-128. doi:10.1152/ajpgi.00051.2005
24. Hinz B. The extracellular matrix and transforming growth factor-β1: Tale of a strained relationship. *Matrix Biol*. 2015;47:54-65. doi:10.1016/j.matbio.2015.05.006
25. ALEXAKIS C, GUETTOUFI A, MESTRIES P, et al. Heparan mimetic regulates collagen expression and TGF-β1 distribution in gamma-irradiated human intestinal smooth muscle cells. *FASEB J*. 2001;15(9):1546-1554. doi:10.1096/fj.00-0756com
26. Lu P, Weaver VM, Werb Z. The extracellular matrix: A dynamic niche in cancer progression. *J Cell Biol*. 2012;196(4):395-406. doi:10.1083/jcb.201102147
27. Adair-Kirk T, Senior RM. Fragments of extracellular matrix as mediators of inflammation. *Int J Biochem cell biol*. 2008:1101-1110. https://www.ncbi.nlm.nih.gov/pmc/articles/PMC2478752/pdf/nihms52307.pdf.
28. Naba A, Clauser KR, Hoersch S, Liu H, Carr SA, Hynes RO. The Matrisome: In Silico Definition and In Vivo Characterization by Proteomics of Normal and Tumor Extracellular Matrices. *Mol Cell Proteomics*. 2012;11(4):M111.014647-M111.014647. doi:10.1074/mcp.M111.014647
29. Fang M, Yuan J, Peng C, Li Y. Collagen as a double-edged sword in tumor progression. *Tumor Biol*. 2014;35(4):2871-2882. doi:10.1007/s13277-013-1511-7
30. Casey T, Bond J, Tighe S, et al. Molecular signatures suggest a major role for stromal cells in development of invasive breast cancer. *Breast Cancer Res Treat*. 2009;114(1):47-62. doi:10.1007/s10549-008-9982-8
31. Denko NC, Fontana LA, Hudson KM, et al. Investigating hypoxic tumor physiology through gene expression patterns. *Oncogene*. 2003;22(37):5907-5914. doi:10.1038/sj.onc.1206703

32. Kumar S, Chan CJ, Coussens LM. Inflammation and Cancer. *Encycl Immunobiol*. 2016;4(December):406-415. doi:10.1016/B978-0-12-374279-7.17002-X
33. Pickup MW, Mouw JK, Weaver VM. The extracellular matrix modulates the hallmarks of cancer. *EMBO Rep*. 2014;15(12):1243-1253. doi:10.15252/embr.201439246
34. Siegel RL, Miller KD, Fedewa SA, et al. Colorectal cancer statistics, 2017. *CA Cancer J Clin*. 2017;67(3):177-193. doi:10.3322/caac.21395
35. Conti J, Thomas G. The role of tumour stroma in colorectal cancer invasion and metastasis. *Cancers (Basel)*. 2011;3(2):2160-2168. doi:10.3390/cancers3022160
36. Caporale A, Benvenuto E, Cosenza UM, et al. Is desmoplasia a protective factor for survival in patients with colorectal carcinoma? *Clin Gastroenterol Hepatol*. 2005;3(4):370-375. doi:10.1016/S1542-3565(04)00674-3
37. Adur J, Carvalho HF, Cesar CL, Casco VH. Nonlinear optical microscopy signal processing strategies in cancer. *Cancer Inform*. 2014;13:67-76. doi:10.4137/CIN.S12419
38. Birk JW, Tadros M, Moezardalan K, et al. Second harmonic generation imaging distinguishes both high-grade dysplasia and cancer from normal colonic mucosa. *Dig Dis Sci*. 2014;59(7):1529-1534. doi:10.1007/s10620-014-3121-7
39. Rahib L, Smith BD, Aizenberg R, Rosenzweig AB, Fleshman JM, Matrisian LM. Projecting cancer incidence and deaths to 2030: The unexpected burden of thyroid, liver, and pancreas cancers in the united states. *Cancer Res*. 2014;74(11):2913-2921. doi:10.1158/0008-5472.CAN-14-0155
40. Olive KP, Jacobetz MA, Davidson CJ, et al. Inhibition of Hedgehog Signaling Enhances Delivery of Chemotherapy in a Mouse Model of Pancreatic Cancer. *Science (80-)*. 2009;324(5933):1457-1461. doi:10.1126/science.1171362
41. Rosow DE, Liss AS, Strobel O, et al. Sonic Hedgehog in pancreatic cancer: From bench to bedside, then back to the bench. *Surgery*. 2012;152(3):S19-S32. doi:10.1016/j.surg.2012.05.030
42. Sugimoto H, Mundel TM, Kieran MW, Kalluri R. Identification of fibroblast heterogeneity in the tumor microenvironment. *Cancer Biol Ther*. 2006;5(12):1640-1646. doi:10.4161/cbt.5.12.3354
43. Laklai H, Miroshnikova YA, Pickup MW, et al. Genotype tunes pancreatic ductal adenocarcinoma tissue tension to induce matricellular fibrosis and tumor progression. *Nat Med*. 2016;22(5):497-505. doi:10.1038/nm.4082
44. Ricard-Blum S. The Collagen Family. *Cold Spring Harb Perspect Biol*. 2011;3(1):1-19. doi:10.1101/cshperspect.a004978
45. An B, Lin YS, Brodsky B. Collagen interactions: Drug design and delivery. *Adv Drug Deliv Rev*. 2016;97:69-84. doi:10.1016/j.addr.2015.11.013
46. Heino J. The collagen family members as cell adhesion proteins. *BioEssays*. 2007;29(10):1001-1010. doi:10.1002/bies.20636
47. Xu H, Raynal N, Stathopoulos S, Myllyharju J, Farndale RW, Leitinger B. Collagen binding specificity of the discoidin domain receptors: Binding sites on collagens II and III and molecular determinants for collagen IV recognition by DDR1. *Matrix Biol*. 2011;30(1):16-26. doi:10.1016/j.matbio.2010.10.004
48. Fiorucci S, Mencarelli A, Palazzetti B, et al. Importance of innate immunity and collagen binding

integrin α1β1 in TNBS-induced colitis. *Immunity*. 2002;17(6):769-780. doi:10.1016/S1074-7613(02)00476-4

49. Zeltz C, Gullberg D. The integrin–collagen connection – a glue for tissue repair? *J Cell Sci*. 2016;129(6):1284-1284. doi:10.1242/jcs.188672
50. Coelho NM, Wang A, McCulloch CA. Discoidin domain receptor 1 interactions with myosin motors contribute to collagen remodeling and tissue fibrosis. *Biochim Biophys Acta - Mol Cell Res*. 2019;(June):118510. doi:10.1016/j.bbamcr.2019.07.005
51. Kehrel B, Wierwille S, Clemetson KJ, et al. Glycoprotein VI is a major collagen receptor for platelet activation: It recognizes the platelet-activating quaternary structure of collagen, whereas CD36, glycoprotein IIb/IIIa, and von Willebrand factor do not. *Blood*. 1998;91(2):491-499.
52. Lebbink RJ, de Ruiter T, Adelmeijer J, et al. Collagens are functional, high affinity ligands for the inhibitory immune receptor LAIR-1. *J Exp Med*. 2006;203(6):1419-1425. doi:10.1084/jem.20052554
53. Lebbink RJ, van den Berg MCW, de Ruiter T, et al. The Soluble Leukocyte-Associated Ig-Like Receptor (LAIR)-2 Antagonizes the Collagen/LAIR-1 Inhibitory Immune Interaction. *J Immunol*. 2008;180(3):1662-1669. doi:10.4049/jimmunol.180.3.1662
54. Lodish H, Berk A, Zipursky SL et al. Collagen: The Fibrous Proteins of the Matrix. *Mol Cell Biol*. 2000. https://www.ncbi.nlm.nih.gov/books/NBK21582/.
55. De Wever O, Demetter P, Mareel M, Bracke M. Stromal myofibroblasts are drivers of invasive cancer growth. *Int J Cancer*. 2008;123(10):2229-2238. doi:10.1002/ijc.23925
56. Pittayapruek P, Meephansan J, Prapapan O, Komine M, Ohtsuki M. Role of matrix metalloproteinases in Photoaging and photocarcinogenesis. *Int J Mol Sci*. 2016;17(6). doi:10.3390/ijms17060868
57. Veidal SS, Larsen DV, Chen X, et al. MMP mediated type V collagen degradation (C5M) is elevated in ankylosing spondylitis. *Clin Biochem*. 2012;45(7-8):541-546. doi:10.1016/J.CLINBIOCHEM.2012.02.007
58. Shi M, Yu B, Gao H, Mu J, Ji C. Matrix metalloproteinase 2 overexpression and prognosis in colorectal cancer: a meta-analysis. *Mol Biol Rep*. 2013;40(1):617-623. doi:10.1007/s11033-012-2100-3
59. Zhang Q, Li J, Liu F, Li Z. "A systematic review of matrix metalloproteinase 9 as a biomarker of survival in patients with osteosarcoma." *Tumor Biol*. 2014;36(1):5-6. doi:10.1007/s13277-014-2857-1
60. Ambekar R, Lau T-Y, Walsh M, Bhargava R, Toussaint KC. Quantifying collagen structure in breast biopsies using second-harmonic generation imaging. *Biomed Opt Express*. 2012;3(9):2021. doi:10.1364/boe.3.002021
61. Natal RA, Vassallo J, Paiva GR, et al. Collagen analysis by second-harmonic generation microscopy predicts outcome of luminal breast cancer. *Tumor Biol*. 2018;40(4):1-12. doi:10.1177/1010428318770953
62. Wyckoff JB, Wang Y, Lin EY, et al. Direct visualization of macrophage-assisted tumor cell intravasation in mammary tumors. *Cancer Res*. 2007;67(6):2649-2656. doi:10.1158/0008-

5472.CAN-06-1823

63. Xiao Q, Jiang Y, Liu Q, et al. Minor Type IV Collagen α5 Chain Promotes Cancer Progression through Discoidin Domain Receptor-1. *PLoS Genet*. 2015;11(5):1-19. doi:10.1371/journal.pgen.1005249
64. Mak KM, Png CYM, Lee DJ. Type V Collagen in Health, Disease, and Fibrosis. *Anat Rec*. 2016;299(5):613-629. doi:10.1002/ar.23330
65. Wenstrup RJ, Florer JB, Brunskill EW, Bell SM, Chervoneva I, Birk DE. Type V collagen controls the initiation of collagen fibril assembly. *J Biol Chem*. 2004;279(51):53331-53337. doi:10.1074/jbc.M409622200
66. Sun M, Chen S, Adams SM, et al. Collagen V is a dominant regulator of collagen fibrillogenesis: dysfunctional regulation of structure and function in a corneal-stroma-specific Col5a1-null mouse model. *J Cell Sci*. 2011;124(23):4096-4105. doi:10.1242/jcs.091363
67. Sun M, Connizzo BK, Adams SM, et al. Targeted deletion of collagen V in tendons and ligaments results in a classic Ehlers-Danlos syndrome joint phenotype. *Am J Pathol*. 2015;185(5):1436-1447. doi:10.1016/j.ajpath.2015.01.031
68. Birk DE, Fitch JM, Babiarz JP, Doane KJ, Linsenmayer TF. Collagen fibrillogenesis in vitro: interaction of types I and V collagen regulates fibril diameter. *J Cell Sci*. 1990;95 (Pt 4):649-657. http://www.ncbi.nlm.nih.gov/pubmed/2384532.
69. Makuszewska M, Bonda T, Cieślińska M, et al. Expression of collagens type I and V in healing rat's tympanic membrane. *Int J Pediatr Otorhinolaryngol*. 2019;118:79-83. doi:10.1016/j.ijporl.2018.12.020
70. Wenstrup RJ, Florer JB, Cole WG, Willing MC, Birk DE. Reduced type I collagen utilization: A pathogenic mechanism in COL5A1 haplo-insufficient Ehlers-Danlos syndrome. *J Cell Biochem*. 2004;92(1):113-124. doi:10.1002/jcb.20024
71. Marian B, Danner MW. skin tumour promotion is associated with increased type V collagen content in the dermis. *Carcinogenesis*. 1987;8:151-154. https://doi.org/10.1093/carcin/8.1.151.
72. Berchtold S, Grünwald B, Krüger A, et al. Collagen type V promotes the malignant phenotype of pancreatic ductal adenocarcinoma. *Cancer Lett*. 2015;356(2):721-732. doi:10.1016/j.canlet.2014.10.020
73. Coulson-Thomas VJ, Coulson-Thomas YM, Gesteira TF, et al. Colorectal cancer desmoplastic reaction up-regulates collagen synthesis and restricts cancer cell invasion. *Cell Tissue Res*. 2011;346(2):223-236. doi:10.1007/s00441-011-1254-y
74. Sun H. Identification of key genes associated with gastric cancer based on DNA microarray data. *Oncol Lett*. 2016;11(1):525-530. doi:10.3892/ol.2015.3929
75. Qiu J, Zhang W, Xia Q, et al. RNA sequencing identifies crucial genes in papillary thyroid carcinoma (PTC) progression. *Exp Mol Pathol*. 2016;100(1):151-159. doi:10.1016/j.yexmp.2015.12.011
76. Guan X. Cancer metastases: Challenges and opportunities. *Acta Pharm Sin B*. 2015;5(5):402-418. doi:10.1016/j.apsb.2015.07.005
77. Ciccia A, Elledge SJ. ScienceDirect - Molecular Cell : The DNA Damage Response: Making It

Safe to Play with Knives. *Mol Cell*. 2011;40(2):179-204. doi:10.1016/j.molcel.2010.09.019.The

78. Menon H, Ramapriyan R, Cushman TR, et al. Role of radiation therapy in modulation of the tumor stroma and microenvironment. *Front Immunol*. 2019;10(FEB):1-13. doi:10.3389/fimmu.2019.00193
79. Straub JM, New J, Hamilton CD, Lominska C, Shnayder Y, Thomas SM. Radiation-induced fibrosis: mechanisms and implications for therapy. *J Cancer Res Clin Oncol*. 2015;141(11):1985-1994. doi:10.1007/s00432-015-1974-6
80. Gerashchenko BI, Howell RW. Bystander cell proliferation is modulated by the number of adjacent cells that were exposed to ionizing radiation. *Cytom Part A*. 2005;66(1):62-70. doi:10.1002/cyto.a.20150
81. Belyakov O V., Mitchell SA, Parikh D, et al. From The Cover: Biological effects in unirradiated human tissue induced by radiation damage up to 1 mm away. *Proc Natl Acad Sci*. 2005;102(40):14203-14208. doi:10.1073/pnas.0505020102
82. C M, Seymour R, SEymour C. Bystander effects in repair-deficient cell lines. *Radiat Res*. 2004;3:256-263. https://www.ncbi.nlm.nih.gov/pubmed/14982489?dopt=Abstract.
83. Giannopoulou E, Katsoris P, Hatziapostolou M, et al. X-rays modulate extracellular matrix in vivo. *Int J Cancer*. 2001;94(5):690-698. doi:10.1002/ijc.1535
84. Zhao, Y. O'Malley, S. Wei, M. E. C. W. Irradiation of rat tubule epithelial cells alters the expression of gene products associated with the synthesis and degradation of extracellular matrix. *Int J Radiat Biol*. 2002;76(3):391-402. doi:10.1080/095530000138736
85. Abdollahi A, Griggs DW, Zieher H, et al. Inhibition of αvβ3 integrin survival signaling enhances antiangiogenic and antitumor effects of radiotherapy. *Clin Cancer Res*. 2005;11(17):6270-6279. doi:10.1158/1078-0432.CCR-04-1223
86. Eke I, Dickreuter E, Cordes N. Enhanced radiosensitivity of head and neck squamous cell carcinoma cells by β1 integrin inhibition. *Radiother Oncol*. 2012;104(2):235-242. doi:10.1016/j.radonc.2012.05.009
87. Monnier Y, Farmer P, Bieler G, et al. CYR61 and αVβ5 integrin cooperate to promote invasion and metastasis of tumors growing in preirradiated stroma. *Cancer Res*. 2008;68(18):7323-7331. doi:10.1158/0008-5472.CAN-08-0841
88. Miller JP, Borde BH, Bordeleau F, et al. Clinical doses of radiation reduce collagen matrix stiffness. *APL Bioeng*. 2018;2(3):031901. doi:10.1063/1.5018327
89. Straub JM, New J, Hamilton CD, Lominska C, Shnayder Y, Thomas SM. Radiation-induced fibrosis: mechanisms and implications for therapy. *J Cancer Res Clin Oncol*. 2015;141(11):1985-1994. doi:10.1007/s00432-015-1974-6
90. Boyd NF, Martin LJ, Yaff MJ, Minkin S. Mammographic density and breast cancer risk: current understanding and future prospec. 2011:1-12.
91. Parker MW, Larsson O, Bitterman PB, et al. Fibrotic extracellular matrix activates a profibrotic positive feedback loop Find the latest version : Fibrotic extracellular matrix activates a profibrotic positive feedback loop. 2014;124(4):1622-1635. doi:10.1172/JCI71386.1622
92. Wei J, Meng L, Hou X, et al. Radiation-induced skin reactions: Mechanism and treatment. *Cancer*

Manag Res. 2019;11:167-177. doi:10.2147/CMAR.S188655

93. Bronova I, Smith B, Aydogan B, et al. Protection from radiation-induced pulmonary fibrosis by peripheral targeting of cannabinoid receptor-1. *Am J Respir Cell Mol Biol*. 2015;53(4):555-562. doi:10.1165/rcmb.2014-0331OC
94. Williams JP, Jackson IL, Shah JR, Czarniecki CW, Maidment BW, DiCarlo AL. Animal Models and Medical Countermeasures Development for Radiation-Induced Lung Damage: Report from an NIAID Workshop. *Radiat Res*. 2012;177(5):e0025-e0039. doi:10.1667/rrol04.1
95. Chen Z, Wu Z, Ning W. Advances in Molecular Mechanisms and Treatment of Radiation-Induced Pulmonary Fibrosis. *Transl Oncol*. 2019;12(1):162-169. doi:10.1016/j.tranon.2018.09.009
96. Takemura N, Kurashima Y, Mori Y, et al. Eosinophil depletion suppresses radiation-induced small intestinal fibrosis. *Sci Transl Med*. 2018;10(429):1-8. doi:10.1126/scitranslmed.aan0333
97. Stacey R, Green JT. Radiation-induced small bowel disease: Latest developments and clinical guidance. *Ther Adv Chronic Dis*. 2014;5(1):15-29. doi:10.1177/2040622313510730
98. Rieder F, Kessler S, Sans M, Fiocchi C. Animal models of intestinal fibrosis: New tools for the understanding of pathogenesis and therapy of human disease. *Am J Physiol - Gastrointest Liver Physiol*. 2012;303(7):786-801. doi:10.1152/ajpgi.00059.2012
99. Bentzen SM. Preventing or reducing late side effects of radiation therapy: radiobiology meets molecular pathology. *Nat Rev Cancer*. 2006;6(9):702-713. doi:10.1038/nrc1950
100. McKelvey KJ, Hudson AL, Back M, Eade T, Diakos CI. Radiation, inflammation and the immune response in cancer. *Mamm Genome*. 2018;29(11-12):843-865. doi:10.1007/s00335-018-9777-0
101. Pan J, Li D, Xu Y, et al. Inhibition of Bcl-2/xl With ABT-263 Selectively Kills Senescent Type II Pneumocytes and Reverses Persistent Pulmonary Fibrosis Induced by Ionizing Radiation in Mice. *Int J Radiat Oncol*. 2017;99(2):353-361. doi:10.1016/j.ijrobp.2017.02.216
102. Groves AM, Johnston CJ, Williams JP, Finkelstein JN. Role of Infiltrating Monocytes in the Development of Radiation-Induced Pulmonary Fibrosis. *Radiat Res*. 2018;189(3):300-311. https://doi.org/10.1667/RR14874.1.
103. Bull C, Malipatlolla D, Kalm M, et al. A novel mouse model of radiation-induced cancer survivorship diseases of the gut. *Am J Physiol - Gastrointest Liver Physiol*. 2017;313(5):G456-G466. doi:10.1152/ajpgi.00113.2017
104. Cong L, Zhang F. Genome engineering using crispr-cas9 system. *Chromosom Mutagen Second Ed*. 2014;8(11):197-217. doi:10.1007/978-1-4939-1862-1_10
105. Bredfeldt JS, Liu Y, Pehlke CA, et al. Computational segmentation of collagen fibers from second-harmonic generation images of breast cancer. *J Biomed Opt*. 2014;19(1):016007. doi:10.1117/1.JBO.19.1.016007
106. Rhodes DR, Yu J, Shanker K, et al. ONCOMINE: A Cancer Microarray Database and Integrated Data-Mining Platform. *Neoplasia*. 2004;6(1):1-6.
107. Rhodes DR, Kalyana-Sundaram S, Mahavisno V, et al. Oncomine 3.0: Genes, pathways, and networks in a collection of 18,000 cancer gene expression profiles. *Neoplasia*. 2007;9(2):166-180. doi:10.1593/neo.07112
108. Chai F, Liang Y, Zhang F, Wang M, Zhong L, Jiang J. Systematically identify key genes in

inflammatory and non-inflammatory breast cancer. *Gene*. 2016;575(2):600-614. doi:10.1016/j.gene.2015.09.025

109. Li G, Li X, Yang M, Xu L, Deng S, Ran L. Prediction of biomarkers of oral squamous cell carcinoma using microarray technology. *Sci Rep*. 2017;7(February):1-8. doi:10.1038/srep42105
110. Huang Y, Tao Y, Li X, et al. Bioinformatics analysis of key genes and latent pathway interactions based on the anaplastic thyroid carcinoma gene expression profile. *Oncol Lett*. 2017;13(1):167-176. doi:10.3892/ol.2016.5447
111. Sun Q, Zhao H, Zhang C, et al. Gene co-expression network reveals shared modules predictive of stage and grade in serous ovarian cancers. *Oncotarget*. 2017;8(26):42983-42996. doi:10.18632/oncotarget.17785
112. Zhao X, Cai H, Wang X, Ma L. Discovery of signature genes in gastric cancer associated with prognosis. *Neoplasma*. 2016;63(2):239-245. doi:10.4149/209_150531N303
113. Liu W, Wei H, Gao Z, et al. COL5A1 may contribute the metastasis of lung adenocarcinoma. *Gene*. 2018;665:57-66. doi:10.1016/j.gene.2018.04.066
114. Wu M, Sun Q, Mo CH, et al. Prospective molecular mechanism of COL5A1 in breast cancer based on a microarray, RNA sequencing and immunohistochemistry. *Oncol Rep*. 2019;42(1):151-175. doi:10.3892/or.2019.7147
115. Ren W, Zhang Y, Zhang L, Lin Q, Zhang J, Xu G. Overexpression of collagen type V α1 chain in human breast invasive ductal carcinoma is mediated by TGF-β1. *Int J Oncol*. March 2018. doi:10.3892/ijo.2018.4317
116. Wenstrup RJ, Florer JB, Brunskill EW, Bell SM, Chervoneva I, Birk DE. Type V collagen controls the initiation of collagen fibril assembly. *J Biol Chem*. 2004;279(51):53331-53337. doi:10.1074/jbc.M409622200
117. Kadler KE, Hill A, Canty-Laird EG. Collagen fibrillogenesis: fibronectin, integrins, and minor collagens as organizers and nucleators. *Curr Opin Cell Biol*. 2008;20(5):495-501. doi:10.1016/j.ceb.2008.06.008
118. Walker C, Mojares E, Del Río Hernández A. *Role of Extracellular Matrix in Development and Cancer Progression*. Vol 19.; 2018. doi:10.3390/ijms19103028
119. Chen X, Nadiarynkh O, Plotnikov S, Campagnola PJ. Second harmonic generation microscopy for quantitative analysis of collagen fibrillar structure. *Nat Protoc*. 2012;7(4):654-669. doi:10.1038/nprot.2012.009
120. Perry SW, Burke RM, Brown EB. Two-Photon and Second Harmonic Microscopy in Clinical and Translational Cancer Research. *Ann Biomed Eng*. 2012;40(2):277-291. doi:10.1007/s10439-012-0512-9
121. Hompland T, Erikson A, Lindgren M, Lindmo T, de Lange Davies C. Second-harmonic generation in collagen as a potential cancer diagnostic parameter. *J Biomed Opt*. 2008;13(5):054050. doi:10.1117/1.2983664
122. LaComb R, Nadiarnykh O, Townsend SS, Campagnola PJ. Phase matching considerations in second harmonic generation from tissues: Effects on emission directionality, conversion efficiency and observed morphology. *Opt Commun*. 2008;281(7):1823-1832.

doi:10.1016/j.optcom.2007.10.040

123. Williams RM, Zipfel WR, Webb WW. Interpreting second-harmonic generation images of collagen I fibrils. *Biophys J*. 2005;88(2):1377-1386. doi:10.1529/biophysj.104.047308

124. Pfeffer CP, Olsen BR, Ganikhanov F, Légaré F. Multimodal nonlinear optical imaging of collagen arrays. *J Struct Biol*. 2008;164(1):140-145. doi:10.1016/j.jsb.2008.07.002

125. Lin S-J, Jee S-H, Kuo C-J, et al. Discrimination of basal cell carcinoma from normal dermal stroma by quantitative multiphoton imaging. *Opt Lett*. 2006;31(18):2756. doi:10.1364/OL.31.002756

126. Conklin MW, Eickhoff JC, Riching KM, et al. Aligned collagen is a prognostic signature for survival in human breast carcinoma. *Am J Pathol*. 2011;178(3):1221-1232. doi:10.1016/j.ajpath.2010.11.076

127. Zhou ZH, Ji CD, Xiao HL, Zhao H Bin, Cui YH, Bian XW. Reorganized collagen in the tumor microenvironment of gastric cancer and its association with prognosis. *J Cancer*. 2017;8(8):1466-1476. doi:10.7150/JCA.18466

128. Drifka CR, Tod J, Loeffler AG, et al. Periductal stromal collagen topology of pancreatic ductal adenocarcinoma differs from that of normal and chronic pancreatitis. 2015;28(11):1470-1480. doi:10.1038/modpathol.2015.97

129. Hanley CJ, Noble F, Ward M, et al. A subset of myofibroblastic cancer-associated fibroblasts regulate collagen fiber elongation, which is prognostic in multiple cancers. *Oncotarget*. 2016;7(5):6159-6174. doi:10.18632/oncotarget.6740

130. Nadiarnykh O, LaComb RB, Brewer MA, Campagnola PJ. Alterations of the ECM in ovarian carcinogenesis studied by second harmonic generation imaging microscopy. *2009 Asia Commun Photonics Conf Exhib ACP 2009*. 2009.

131. Zhang K, Corsa CA, Ponik SM, et al. The collagen receptor discoidin domain receptor 2 stabilizes SNAIL1 to facilitate breast cancer metastasis. *Nat Cell Biol*. 2013;15:677. https://doi.org/10.1038/ncb2743.

132. Provenzano PP, Inman DR, Eliceiri KW, et al. Collagen density promotes mammary tumor initiation and progression. *BMC Med*. 2008;6:1-15. doi:10.1186/1741-7015-6-11

133. Wu PC, Hsieh TY, Tsai ZU, Liu TM. In vivo Quantification of the Structural Changes of Collagens in a Melanoma Microenvironment with Second and Third Harmonic Generation Microscopy. *Sci Rep*. 2015;5:34-38. doi:10.1038/srep08879

134. Lyons TR, O'Brien J, Borges VF, et al. Postpartum mammary gland involution drives progression of ductal carcinoma in situ through collagen and COX-2. *Nat Med*. 2011;17(9):1109-1115. doi:10.1038/nm.2416

135. Gilkes DM, Chaturvedi P, Bajpai S, et al. Collagen Prolyl Hydroxylases Are Essential for Breast Cancer Metastasis. *Cancer Res*. 2013;73(11):3285-3296. doi:10.1158/0008-5472.CAN-12-3963

136. Barretina J, Caponigro G, Stransky N, et al. The Cancer Cell Line Encyclopedia enables predictive modelling of anticancer drug sensitivity. *Nature*. 2012;483(7391):603-607. doi:10.1038/nature11003

137. Okada Y, Naka K, Kawamura K, et al. Localization of matrix metalloproteinase 9 (92-kilodalton gelatinase/type IV collagenase = gelatinase B) in osteoclasts: implications for bone resorption. *Lab*

Invest. 1995;72(3):311-322. https://www.ncbi.nlm.nih.gov/pubmed/7898050.

138. Symoens S, Renard M, Bonod-Bidaud C, et al. Identification of binding partners interacting with the α1-N-propeptide of type V collagen. *Biochem J*. 2011;433(2):371-381. doi:10.1042/bj20101061
139. Ratnikov BI, Deryugina EI, Strongin AY. Gelatin zymography and substrate cleavage assays of matrix metalloproteinase-2 in breast carcinoma cells overexpressing membrane type-1 matrix metalloproteinase. *Lab Investig*. 2002;82(11):1583-1590. doi:10.1097/01.LAB.0000038555.67772.DB
140. Skrzypczak M, Goryca K, Rubel T, et al. Modeling oncogenic signaling in colon tumors by multidirectional analyses of microarray data directed for maximization of analytical reliability. *PLoS One*. 2010;5(10). doi:10.1371/journal.pone.0013091
141. Segara D, Biankin A V., Kench JG, et al. Expression of HOXB2, a retinoic acid signaling target in pancreatic cancer and pancreatic intraepithelial neoplasia. *Clin Cancer Res*. 2005;11(9):3587-3596. doi:10.1158/1078-0432.CCR-04-1813
142. Drifka CR, Loeffler AG, Mathewson K, et al. Comparison of Picrosirius Red Staining With Second Harmonic Generation Imaging for the Quantification of Clinically Relevant Collagen Fiber Features in Histopathology Samples. *J Histochem Cytochem*. 2016;64(9):519-529. doi:10.1369/0022155416659249
143. Junqueira LC, Bignolas G, Brentani RR. Picrosirius staining plus polarization microscopy, a specific method for collagen detection in tissue sections. *Histochem J*. 1979;11(4):447-455. https://www.ncbi.nlm.nih.gov/pubmed/91593.
144. Kirkpatrick ND, Brewer MA, Utzinger U. Endogenous optical biomarkers of ovarian cancer evaluated with multiphoton microscopy. *Cancer Epidemiol Biomarkers Prev*. 2007;16(10):2048-2057. doi:10.1158/1055-9965.EPI-07-0009
145. Natal RDA, Paiva GR, Pelegati VB, et al. Exploring Collagen Parameters in Pure Special Types of Invasive Breast Cancer. 2019;(May):1-11. doi:10.1038/s41598-019-44156-9
146. Best SL, Liu Y, Keikhosravi A, et al. Collagen organization of renal cell carcinoma differs between low and high grade tumors. 2019:1-8.
147. Marian B, Danner MW. Skin tumor promotion is associated with increased type V collagen content in the dermis. *Carcinogenesis*. 1987;8(1):151-154. doi:10.1093/carcin/8.1.151
148. Lei GS, Kline HL, Lee CH, Wilkes DS, Zhang C. Regulation of Collagen V Expression and Epithelial-Mesenchymal Transition by miR-185 and miR-186 during Idiopathic Pulmonary Fibrosis. *Am J Pathol*. 2016;186(9):2310-2316. doi:10.1016/j.ajpath.2016.04.015
149. Zhao W, Wang X, Sun KH, Zhou L. A-Smooth Muscle Actin Is Not a Marker of Fibrogenic Cell Activity in Skeletal Muscle Fibrosis. *PLoS One*. 2018;13(1):1-16. doi:10.1371/journal.pone.0191031
150. Duffield JS, Duffield JS. Cellular and molecular mechanisms in kidney fibrosis Find the latest version : Review series Cellular and molecular mechanisms in kidney fibrosis. 2014;124(6):2299-2306. doi:10.1172/JCI72267.a
151. Illsley MC, Peacock JH, McAnulty RJ, Yarnold JR. Increased collagen production in fibroblasts

cultured from irradiated skin and effect of TGF β1– clinical study. *Br J Cancer*. 2000;83(5):650-654. doi:10.1054/bjoc.2000.1321

152. Sakata-Takatani K, Matsuo N, Sumiyoshi H, Tsuda T, Yoshioka H. Identification of a functional CBF-binding CCAAT-like motif in the core promoter of the mouse pro-α1(V) collagen gene (Col5a1). *Matrix Biol*. 2004;23(2):87-99. doi:10.1016/j.matbio.2004.03.003
153. Wu YF, Matsuo N, Sumiyoshi H, Yoshioka H. Sp7/Osterix is involved in the up-regulation of the mouse pro-α1(V) collagen gene (Col5a1) in osteoblastic cells. *Matrix Biol*. 2010;29(8):701-706. doi:10.1016/j.matbio.2010.09.002
154. Yang T, Liang Y, Lin Q, et al. MiR-29 mediates TGFβ1-induced extracellular matrix synthesis through activation of PI3K-AKT pathway in human lung fibroblasts. *J Cell Biochem*. 2013;114(6):1336-1342. doi:10.1002/jcb.24474
155. Liu GX, Li YQ, Huang XR, et al. Disruption of Smad7 Promotes ANG II-Mediated Renal Inflammation and Fibrosis via Sp1-TGF-β/Smad3-NF.κB-Dependent Mechanisms in Mice. *PLoS One*. 2013;8(1):19-23. doi:10.1371/journal.pone.0053573
156. Zhang JJ, Yano H, Sasaki T, Matsuo N, Yoshioka H. The pro-α1(V) collagen gene (Col5a1) is coordinately regulated by miR-29b with core promoter in cultured cells. *Connect Tissue Res*. 2018;59(3):263-273. doi:10.1080/03008207.2017.1370465
157. Kahai S, Vary CPH, Gao Y, Seth A. Collagen, type V, α1 (COL5A1) is regulated by TGF-β in osteoblasts. *Matrix Biol*. 2004;23(7):445-455. doi:10.1016/j.matbio.2004.09.004
158. Anscher MS. Targeting the TGF- 1 Pathway to Prevent Normal Tissue Injury After Cancer Therapy. *Oncologist*. 2010;15(4):350-359. doi:10.1634/theoncologist.2009-s101
159. Maslennikova A, Kochueva M, Ignatieva N, et al. Effects of gamma irradiation on collagen damage and remodeling. *Int J Radiat Biol*. 2015;91(3):240-247. doi:10.3109/09553002.2014.969848
160. Schiller J, Huster D. New methods to study the composition and structure of the extracellular matrix in natural and bioengineered tissues. *Biomatter*. 2012;2(3):115-131. doi:10.4161/biom.20866
161. Berkeley L. Biology ' s new dimension. 2003;424(August).
162. Nederman, T., Norling, B., Gimelius, B., Carlsson, J., and Brunk U. Demonstration of an extracellular matrix in MCTSs. *Cancer Res*. 1984;44(July):3090–‒3097.
163. Eke I, Cordes N. Radiobiology goes 3D: How ECM and cell morphology impact on cell survival after irradiation. *Radiother Oncol*. 2011;99(3):271-278. doi:10.1016/j.radonc.2011.06.007
164. Vogel B, Siebert H, Hofmann U, Frantz S. Determination of collagen content within picrosirius red stained paraffin-embedded tissue sections using fluorescence microscopy. *MethodsX*. 2015. doi:10.1016/j.mex.2015.02.007
165. Feng G, Ma HM, Huang HB, et al. Overexpression of col5a1 promotes tumor progression and metastasis and correlates with poor survival of patients with clear cell renal cell carcinoma. *Cancer Manag Res*. 2019;11:1263-1274. doi:10.2147/CMAR.S188216
166. Dancea HC, Shareef MM, Ahmed MM. Role of radiation-induced TGF-beta signaling in cancer therapy. *Mol Cell Pharmacol*. 2009;1(1):44-56. doi:10.4255/mcpharmacol.09.06
167. Yano H, Hamanaka R, Nakamura M, Sumiyoshi H, Matsuo N, Yoshioka H. Smad, but not MAPK, pathway mediates the expression of type I collagen in radiation induced fibrosis. *Biochem Biophys*

Res Commun. 2012;418(3):457-463. doi:10.1016/j.bbrc.2012.01.039

168. El-Brolosy MA, Stainier DYR. Genetic compensation: A phenomenon in search of mechanisms. *PLoS Genet*. 2017;13(7):1-17. doi:10.1371/journal.pgen.1006780
169. Liu S, Liao G, Li G. Regulatory effects of COL1A1 on apoptosis induced by radiation in cervical cancer cells. *Cancer Cell Int*. 2017;17(1):1-9. doi:10.1186/s12935-017-0443-5
170. Barsky SH, Rao CN, Grotendorst GR, Liotta LA. Increased Content of Type V Collagen in Desmoplasia of Human Breast Carcinoma. *Am J Pathol*. 1982;108(3):276-283.
171. Cheng WY, Kandel JJ, Yamashiro DJ, Canoll P, Anastassiou D. A multi-cancer mesenchymal transition gene expression signature is associated with prolonged time to recurrence in glioblastoma. *PLoS One*. 2012;7(4):1-8. doi:10.1371/journal.pone.0034705
172. McKleroy W, Lee T-H, Atabai K. Always cleave up your mess: targeting collagen degradation to treat tissue fibrosis. *AJP Lung Cell Mol Physiol*. 2013;304(11):L709-L721. doi:10.1152/ajplung.00418.2012
173. Venning FA, Wullkopf L, Erler JT. Targeting ECM Disrupts Cancer Progression. *Front Oncol*. 2015;5(October):1-15. doi:10.3389/fonc.2015.00224
174. Gocheva V, Naba A, Bhutkar A, et al. Quantitative proteomics identify Tenascin-C as a promoter of lung cancer progression and contributor to a signature prognostic of patient survival. *Proc Natl Acad Sci U S A*. 2017;114(28):E5625-E5634. doi:10.1073/pnas.1707054114
175. Tian C, Clauser KR, Öhlund D, et al. Proteomic analyses of ECM during pancreatic ductal adenocarcinoma progression reveal different contributions by tumor and stromal cells. *Proc Natl Acad Sci*. September 2019:201908626. doi:10.1073/pnas.1908626116
176. Naba A, Clauser KR, Mani DR, Carr SA, Hynes RO. Quantitative proteomic profiling of the extracellular matrix of pancreatic islets during the angiogenic switch and insulinoma progression. *Sci Rep*. 2017;7(September 2016):40495. doi:10.1038/srep40495
177. Naba A, Clauser KR, Whittaker CA, Carr SA, Tanabe KK, Hynes RO. Extracellular matrix signatures of human primary metastatic colon cancers and their metastases to liver. *BMCCancer*. 2014;14:518-.
178. Wang LF, Liu YS, Yang B, et al. The extracellular matrix protein mindin attenuates colon cancer progression by blocking angiogenesis via Egr-1-mediated regulation. *Oncogene*. 2018;37(5):601-615. doi:10.1038/onc.2017.359
179. Naba A, Clauser KR, Lamar JM, Carr SA, Hynes RO. Extracellular matrix signatures of human mammary carcinoma identify novel metastasis promoters. *Elife*. 2014;3:1-23. doi:10.7554/elife.01308
180. Naba A, Pearce OMT, Del Rosario A, et al. Characterization of the Extracellular Matrix of Normal and Diseased Tissues Using Proteomics. *J Proteome Res*. 2017;16(8):3083-3091. doi:10.1021/acs.jproteome.7b00191
181. Launay G, Salza R, Multedo D, Thierry-Mieg N, Ricard-Blum S. MatrixDB, the extracellular matrix interaction database: Updated content, a new navigator and expanded functionalities. *Nucleic Acids Res*. 2015;43(D1):D321-D327. doi:10.1093/nar/gku1091
182. Zou X, Feng B, Dong T, et al. Up-regulation of type I collagen during tumorigenesis of colorectal

cancer revealed by quantitative proteomic analysis. *J Proteomics*. 2013;94:473-485. doi:10.1016/j.jprot.2013.10.020